U.S. Geological Survey Award Nos.
G18AP00015 and G18AP00016

Final Technical Report

ASSESSMENT OF THE CONTRIBUTION OF INPUT MOTION SELECTION PROCEDURES TO UNCERTAINTY IN GROUND MOTION INTENSITY MEASURES:

COLLABORATIVE RESEARCH WITH NORTH CAROLINA STATE UNIVERSITY AND MERRIMACK COLLEGE

Principal Investigators:

Ashly Cabas[1] (G18AP00015)

James Kaklamanos[2] (G18AP00016)

Authoring Panel Member:

Albert Kottke[3]

Graduate Research Assistant:

Ishika Nawrin Chowdhury[4]

Project Start Date: 1 January 2018

Project End Date: 31 December 2018

[1] Assistant Professor
North Carolina State University
Civil, Construction, and Environmental Engineering
425A Mann Hall, 2501 Stinson Drive
Raleigh, NC 27695-7908
Tel: (919) 515-7338
Fax: (919) 515-7908
Email: amcabasm@ncsu.edu

[2] Associate Professor
Department of Civil Engineering
Merrimack College
315 Turnpike Street, North Andover, MA 01845
Tel: (978) 837-3401
Fax: (978) 837-5029
Email: kaklamanosj@merrimack.edu

[3] Consultant
Albany, CA 94706
Email: albert.kottke@gmail.com

[4] Ph.D. Student
North Carolina State University
Civil, Construction, and Environmental Engineering
208 Mann Hall, 2501 Stinson Drive
Raleigh, NC 27695-7908
Email: ichowdh@ncsu.edu

Acknowledgment of support and disclaimer: This material is based upon work supported by the U.S. Geological Survey under Grant Nos. G18AP00015 and G18AP00016. The views and conclusions contained in this document are those of the authors and should not be interpreted as representing the opinions or policies of the U.S. Geological Survey. Mention of trade names or commercial products does not constitute their endorsement by the U.S. Geological Survey.

Abstract

The importance of properly characterizing ground motion intensity measures for seismic hazard assessment is unequivocally large. However, only a few studies have investigated the degree to which the uncertainty resulting from traditional input motion selection protocols introduces errors in the estimation of ground-motion intensity measures at the surface. This study compares current practices for input motion selection, identifies shortcomings in these practices, and investigates their impact on the uncertainties in ground-motion intensity measures. The assessment of the effects of input motion selection protocols has been performed in the context of two study sites with different tectonic and geologic settings: Seattle, Washington, and Boston, Massachusetts. Seattle is located in an active tectonic region in the western United States (WUS) and has seismic sources associated with crustal earthquakes, as well as interface and intraslab earthquakes from the Cascadia subduction zone. Conversely, Boston is located in the Central and Eastern U.S. (CEUS) stable continental region with lower relative seismic activity than the WUS. Boston's seismic hazard is mostly associated with background seismicity.

This collaborative effort between North Carolina State University and Merrimack College involves a probabilistic seismic hazard assessment conducted at each study site; the definition of multiple target spectra including the uniform hazard spectrum (UHS), the risk-targeted maximum considered earthquake spectrum (MCE_R), and the conditional spectrum (CS); equivalent-linear and fully nonlinear site response analyses; and an assessment of the resulting ground-motion intensity measures from site response model predictions. Target spectra are also constructed to represent various hazard levels (i.e., 2% and 10% probability of exceedance in 50 years), dominant earthquake scenarios for different tectonic regimes (e.g., shallow crustal versus subduction events), and different conditioning spectral periods of interest (from short to long spectral periods). As a result, 25 sets of input ground motions are generated to be used in seismic site response analyses at the study sites.

A geotechnical profile was developed for each location to be representative of typical conditions in the center of each city. Large portions of both Boston and Seattle are underlain by layers of artificial fill, and typical profiles are characterized by sharp impedance contrasts at depth (corresponding to the interface between post-glacial and pre-glacial materials). The assumed reference rock conditions for Seattle and Boston are prevalent throughout the WUS and CEUS regions, respectively. In this report, we focus upon softer sites in each city where site response is expected to be more substantial, and engineering ground motions are more challenging to predict. The variability in resulting ground motion intensity measures at the surface of the study sites was evaluated across the 25 sets of input ground motions. We observe an excessive amount of nonlinearity for design-level ground motions in Seattle, leading to significant deamplifications and excessive dissipations of seismic energy within the profile. The influence of the input motion selection protocol seems to have a greater influence in Boston (where the level of nonlinear soil behavior is smaller) compared to Seattle. Due to the excessive nonlinear soil behavior in Seattle, the effects of the site response modeling assumptions and parameters outweigh the effects of the input motion selection protocols at short spectral periods, while the differences in input motion selection are more pronounced at longer periods. This study illustrates how input motion selection protocols offer varying contributions to uncertainty for different ground-motion intensity measures in different tectonic environments.

Table of Contents

1 Introduction

Earthquake ground motions are greatly influenced by near-surface geologic materials as seismic waves propagate from depth to the ground surface. Site response analyses (SRA) are used to estimate site-specific ground motions as a function of the properties of the soil profile, the assumed constitutive models to represent dynamic soil behavior, and the input motion at the base of the soil profile. In addition to their frequent usage in dynamic analyses of critical infrastructure (e.g., bridges, earth dams, and power plants), SRA are also used in liquefaction and seismic slope stability assessments.

Furthermore, the estimation of site response constitutes a primary component of the stochastic method for simulating ground motions, and the evaluation of site-specific seismic hazards in probabilistic seismic hazard analyses. Despite their broad usage in engineering practice, site response models are burdened with significant uncertainties (Figure 1.1). Recent research into site response analysis uncertainty has largely focused on the assumed site response model type, such as linear, equivalent-linear, or nonlinear (e.g., Kaklamanos et al., 2013, 2015; Kaklamanos and Bradley, 2018a; Kim et al., 2016; Chandra et al., 2016; Stewart et al., 2014; Regnier et al., 2013). To a lesser degree, research has addressed the influence of soil profile uncertainty on site response estimates (e.g., Kaklamanos and Bradley, 2018a, 2018b; Rathje et al., 2010; Li and Assimaki, 2010; Kwok et al., 2008; Bazzurro and Cornell, 2004; Toro, 1995). To this date, however, very little research has focused on the specification of the input motion and the uncertainties associated with different input motion selection protocols (e.g., Bradley, 2010; Rathje et al., 2010; Cabas and Rodriguez-Marek, 2017) used in geotechnical engineering applications. By selecting appropriate input motions using pertinent selection procedures, we can improve the estimation of ground motion intensity measures, which in turn will advance the state of the art and practice in site-specific seismic hazard assessment.

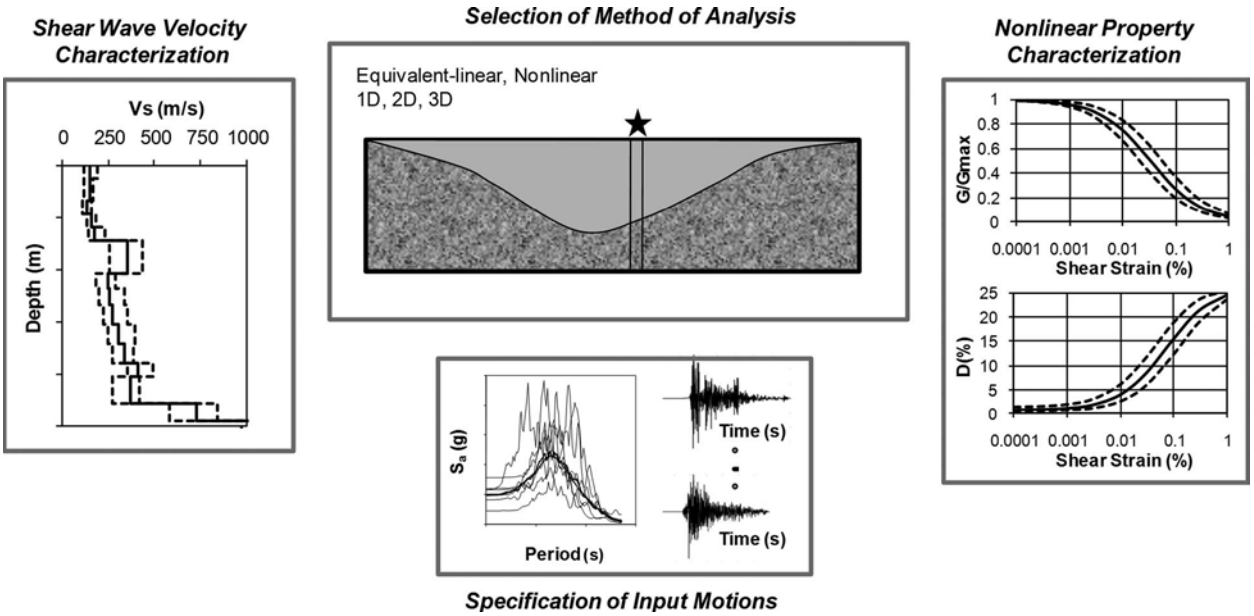

Figure 1.1. Sources of uncertainty in seismic site response analysis (after Rathje et al., 2010).

The selection of input motions varies with the application (Rathje et al., 2010). Multiple protocols populate the literature concerning ground motion selection for: (a) building seismic design (e.g., Chapter 16 of the ASCE/SEI 7-16 Standard, 2016), (b) performing response-history analysis of low and medium rise buildings (NEHRP Consultants Joint Venture, 2011), (c) nonlinear response history analysis of buildings within the performance-based design framework (Kwong and Chopra, 2015), and (d) nuclear power plants (McGuire et al., 2001). However, none of these guidelines has a particular focus on ground motions required for geotechnical engineering analyses (e.g., site response analysis, liquefaction assessment, or seismic slope stability analyses). The existing protocols also fail to provide insights on the impact of the selection of input motions on the uncertainty of ground motion intensity measures, such as peak ground acceleration (PGA), maximum shear strain (γ_{max}), cumulative absolute velocity (CAV), and Arias intensity (I_a). The important role of these (and other) ground motion intensity measures in geotechnical engineering analyses demands an improvement on our understanding of the most relevant sources of uncertainty, and how they propagate through the different steps involved in design. Differences in tectonic regimes and geologic conditions between sites located in the western US (WUS) and in the central and eastern US (CEUS) impose yet another challenge. The infrequent seismic events in stable continental regions, such as the CEUS, along with the lack of recorded ground motions at hard rock sites constitute major limitations when selecting appropriate ground motions for design.

The effects of input motion selection procedures on ground motion intensity measures relevant to a variety of geotechnical engineering applications have not been thoroughly assessed. This project addresses the aforementioned issues, namely the need for a ground motion selection framework for different geotechnical engineering analyses, and the investigation of the propagation of uncertainty from the input motion selection protocols to different ground motion intensity measures used in current practice. Parallels can be drawn to previous studies with a focus on structural engineering (e.g., Baker, 2007, 2011; Baker and Cornell, 2006; Bommer and Acevedo, 2004) or to previous studies that incorporate ground motion intensity measures in the algorithm for selecting the input motions (e.g., Bradley, 2010, 2012). The novelty of this study lies precisely on providing geotechnical engineering analyses with a similar or even more robust and systematic framework for input ground motion selection.

The objective of this study is to investigate the impact of input motion selection protocols on ground motion intensity measures that are most significant for geotechnical analyses such as site response analysis. This study compares current practices for input motion selection, identifies shortcomings in these practices, and investigates their impact on the uncertainty in critical ground -motion intensity measures. Recommendations for input motion selection are proposed, and insights on the controlling aspects of input motion selection for various ground-motion intensity measures are provided.

2 Project Framework

In engineering practice, design ground motions are selected and then often modified (e.g., through linear scaling or spectral matching) to match a target response spectrum. The latter can result from (a) the uniform hazard spectrum from probabilistic seismic hazard analyses (PSHA), (b) the design response spectrum from seismic codes, (c) the response spectrum corresponding to a single hazard scenario (from deaggregation or from deterministic seismic hazard analysis), or (d) the response spectrum conditioned on a spectral period (fundamental period of the structure or any other period of interest). In general, the target is associated with an annual probability of exceeding a specific limit for a given ground motion intensity measure. Such a performance goal can then be used to define the uniform hazard response spectrum (UHS) with a given annual probability of exceedance (or alternatively a return period) of interest. This hazard level depends on the type of structure and associated design requirements. For instance, a 2% in 50-year probability of exceedance is typically prescribed for new buildings, while seismic bridge design as performed by the California Department of Transportation (Caltrans) requires a 5% in 50-yr probability of exceedance as their design-basis hazard level (Stewart et al. 2014). In some instances, the UHS is used directly as a target spectrum to select input ground motions for site response analysis. However, the spectral shape of the UHS includes contributions from multiple events, and more realistic seismic demands may be computed by partitioning the UHS in scenarios based on the deaggregation of the hazard (i.e., considering multiple hazard levels).

In this study, we systematically analyze the influence of various definitions of the target spectrum on multiple ground motion intensity measures. The holistic approach implemented herein is illustrated in Figure 2.1, where a fundamental understanding of the seismic hazards at the site of interest is an essential first step to define meaningful target spectrum for input motion selection. Then, we consider the state-of-the-art and practice in ground motion selection to evaluate different procedures to construct target spectra. We evaluate scaling and spectral matching procedures, as well as the availability of ground motion recordings from different tectonic regimes in terms of their influence on obtaining appropriate input motions for seismic site response analyses. Lastly, we quantify the effect of different input motion selection protocols on ground motion intensity measures estimated at the ground surface of two study sites by means of seismic site response analysis. The resulting variability in peak amplitude parameters, cumulative absolute velocity, Arias intensity, significant duration, and spectral shape at the surface of two study sites is evaluated and discussed in future sections.

At each site, two uniform hazard spectra (UHS) are developed at return periods of 475 and 2500 years in the study presented herein. These spectra are representative of design levels that would be considered for typical and critical infrastructure (corresponding to a 10% probability of exceedance in 50 years and a 2% probability of exceedance in 50 years), respectively. The UHS is also used to consider different scenarios based on the conditional mean spectrum (CMS) approach (Baker and Cornell, 2006; Baker, 2011). The CMS approach is gaining popularity with structural engineers, but is not commonly applied to geotechnical engineering applications. However, in recent years, researchers have shown its potential in assessing seismic performance of a slope during cyclic loading (Petermann and Rathje 2017) and in evaluating liquefaction and lateral spreading (Hashash et al. 2015). The risk-targeted maximum considered earthquake spectrum (MCE_R; Haselton et al. 2017) is also considered in this study. It is derived from the ASCE 7-16

code and it corresponds to 1.5 times the design spectrum. After defining the aforementioned types of target spectra, input ground motions matching those spectra are selected.

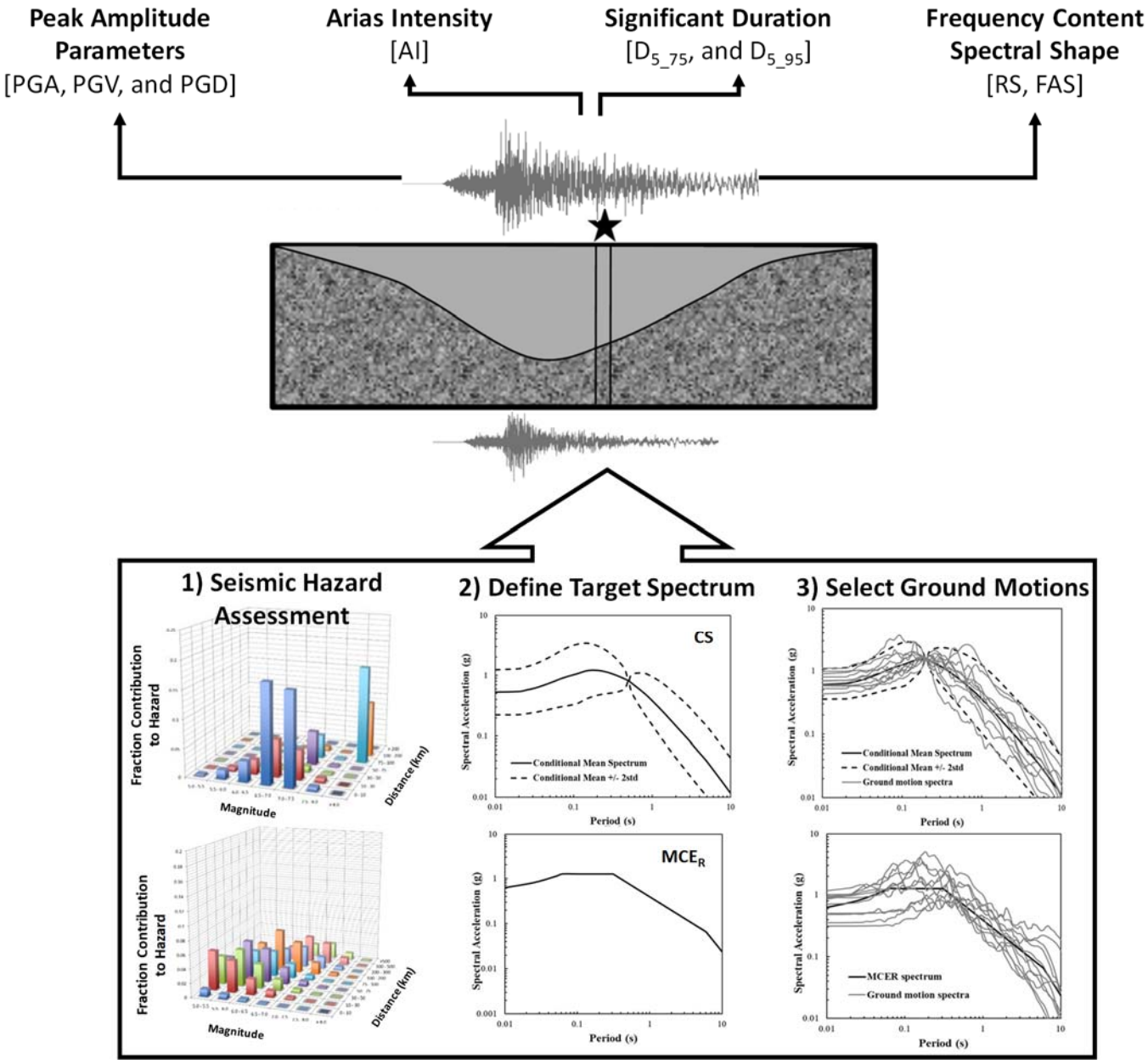

Figure 2.1. Overview of the framework used in this project to assess the influence of the input motion selection process on ground motion intensity measures relevant for geotechnical engineering analyses.

Technical hurdles associated with differences in tectonic regimes and geologic conditions between sites in WUS and CEUS are also addressed in this study. Comprehensive site response analyses are performed at two representative sites, one in the WUS, and the other in the CEUS. These sites not only represent different geologic, and geotechnical conditions, but different types of seismicity. Many WUS sites are in a region of high seismicity in which a small number of faults dominates the hazard, whereas many CEUS sites are in a region of low-to-moderate seismicity in which the sources of hazard are much more diffuse. The infrequent seismic events in stable continental regions, such as the CEUS, along with the lack of recorded ground motions at hard rock sites constitute major limitations when selecting appropriate ground motions for design. The variability in the estimated ground motion intensity measures at the ground surface of the study sites is assessed when using different subsets of input ground motions resulting from multiple target spectra. Recommendations for ground motion selection are proposed, and we investigate the controlling aspects of input motion selection on site response analyses.

3 Selected Sites

One site from the WUS and another from the CEUS have been selected in this study to explore the differences in input motion selection for various tectonic, geologic and geotechnical conditions. Considering their high population density, presence of critical civil infrastructure (from bridges to high-rise buildings), and challenging seismicity (from diverse to stable tectonic environments), Seattle, Washington, and Boston, Massachusetts, are used as study sites.

The Seattle site is located in the active tectonic region of the Western U.S. and has seismic sources associated with crustal earthquakes (i.e., both in terms of defined faults and gridded background seismic events), and interface and intraslab earthquakes from the Cascadia subduction zone located off the coast in the Pacific Northwest region (Figure 3.1). Conversely, the Boston site location in CEUS is located in a stable continental region (SCR) with lower relative seismic activity than the WUS. Apart from the effect of distant seismic zones at long spectral periods, Boston's seismic hazard is mostly associated with background seismicity. Recent earthquakes, such as the 2011 **M** 5.8 Mineral, Virginia event, have focused attention on seismic hazards and risk in regions with moderate seismic activity and high population density (e.g., Hough, 2012). In the CEUS, bedrock is harder and less fractured than in the Western U.S., strong bedrock/soil seismic impedance contrasts are common, and the resulting soil amplification can greatly influence damage patterns over large areas (even due to a moderate sized event). Seismic hazard analyses in the CEUS are further burdened by the fact that there exists a limited database of recorded ground motions in this region; therefore, the input motion selection protocols implemented in the WUS are often not possible in the CEUS.

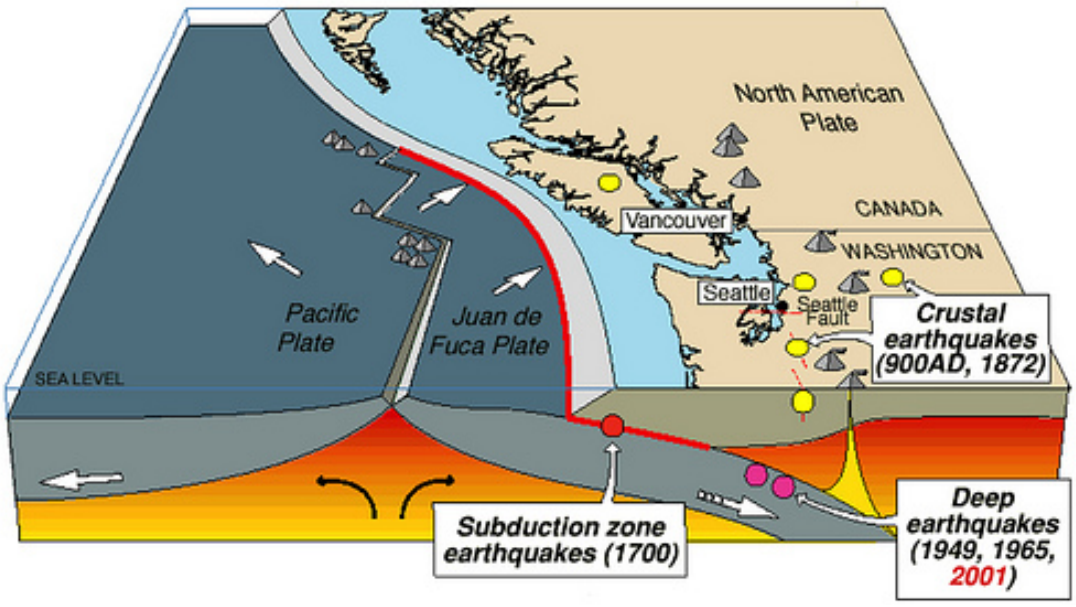

Figure 3.1. Sketch depicting types of earthquakes that control seismic hazards in the Pacific Northwest (including Seattle): (1) shallow crustal earthquakes near the earth's surface, (2) deep [intraslab] earthquakes that occur within the oceanic plate, and (3) subduction-zone [interface] earthquakes that occur along the boundary between the continental and oceanic plate (University of Washington, 2018).

The two selected sites are also different in terms of geologic settings. The reference bedrock horizon in Seattle sites often has soft rock conditions (i.e., with an average shear wave velocity in the top 30 m of the subsurface, V_{s30}, approximately equal to 760 m/s). On the contrary, Boston has predominantly crystalline hard rock (with an assumed V_{s30} of 2830 m/s). These differences in weathering conditions of the bedrock between sites in WUS and CEUS can influence the attenuation of ground motions and their frequency content (Cabas and Rodriguez-Marek 2017). The assessment of the aforementioned differences will allow for comparisons of the influence of input motion selection protocols in these environments.

4 Probabilistic Seismic Hazard Analysis

A probabilistic seismic hazard analysis (PSHA) study was performed following a standard state-of-the-practice methodology for both the site locations: Seattle and Boston. These two sites represent different tectonic environments and hence are modeled with different seismic source characterization (SSC) models and ground motion characterization (GMC) models.

4.1 Seismic Source Characterization (SSC) Models

The Seattle site is located in a region of active tectonics. It can be characterized as having earthquakes associated with crustal faults or background seismic sources and earthquakes associated with the Cascadia subduction zone located off of the coast of Oregon, Washington, and British Columbia. Both shallow large-magnitude interface earthquakes and the deeper intraslab events are characterized in this region for the subduction zone. For the PSHA calculations, the U.S. Geological Survey [USGS] (2014) seismic source characterization (SSC) model was used. Specifically, for the crustal earthquakes, defined planar crustal faults were modeled or gridded seismicity data files were used to represent the observed historical seismicity not directly associated with a mapped crustal fault. For the Seattle site, only those crustal faults within about 300 km were considered. An exact distance cutoff was not used, because some faults in western Oregon that are less than 300 km from Seattle were excluded due to their defined low slip rates, large distance to the Seattle site, and expected lack of significant contribution to the total hazard at the site.

The closest crustal fault to the site is the Seattle Fault, which is a south dipping reverse fault. The mean recurrence interval for this fault is 1,667 years (USGS, 2014). Based on its activity rate and close proximity to the site, the Seattle fault is a significant contributor to the total hazard at the site, especially for the low to moderate spectral periods.

For the gridded seismicity data files, a southern boundary at a latitude of 43°N was selected. The northern extent as provided within the USGS (2014) SSC model is along the United States – Canadian border. This geographical limit on the gridded seismicity data files should be large enough to capture any significant contribution to the hazard from the gridded seismicity source.

For the interface events associated with the Cascadia subduction zone, the USGS (2014) SSC model is based on the observed historical segmentation and geographical extent of the defined planar fault. The surface projection of the eastern down-dip extent of the interface seismic source is taken from Figure 61 of USGS (2014). There are grouped eastern down-dip edges for the interface zone, and these were modeled as part of the epistemic uncertainty in the USGS (2014) SSC model. For the deeper intraslab events, a staircase of flat seismic sources was used to model the increasing depth of the subducting slab, representing earthquake sources from west to east (taken from Figure 54 of USGS, 2014).

For the Boston site location, the EPRI (2012) SSC model was implemented. This SSC model was developed for the entire CEUS and includes areal seismic source zones based on the observed historical seismicity and planar faults classified as repeated-large magnitude earthquakes (RLME).

For the PSHA of the Boston site, only significantly contributing areal seismic sources were included. Although the RLME seismic sources can contribute at large distances depending on the hazard level and relative activity of the more local areal sources, no RLME sources were included in the PSHA for the Boston site based on the range of interest in hazard (i.e., 72 year to 5,000 year) and the large closest distance of any of the RLME sources defined in the EPRI (2012) SSC model. The closest RLME is the Charlevoix seismic source, located greater than 500 km north of the Boston site.

The EPRI (2012) SSC model is based on a fully developed logic tree approach with different branches for different seismic source parameter models. The full description of this logic tree for the EPRI (2012) SSC model is documented in EPRI (2012). For the Central and Eastern U.S., an example of the areal sources based on one branch of the logic tree is presented in Figure 4.1. The four closest regions to the Boston site are the Extended Continental Crust – Atlantic Margin (ECC-AM), Northern Appalachians (NAP), Paleozoic Extended Zone – Narrow (PEZ-N), and Saint Lawrence Rift (SLR); these are the four primary areal source zones used in this PSHA study. For the other branches of the EPRI (2012) logic tree, slight geographical variations are defined for the seismic sources, but these differences are not in the immediate region around the Boston site location.

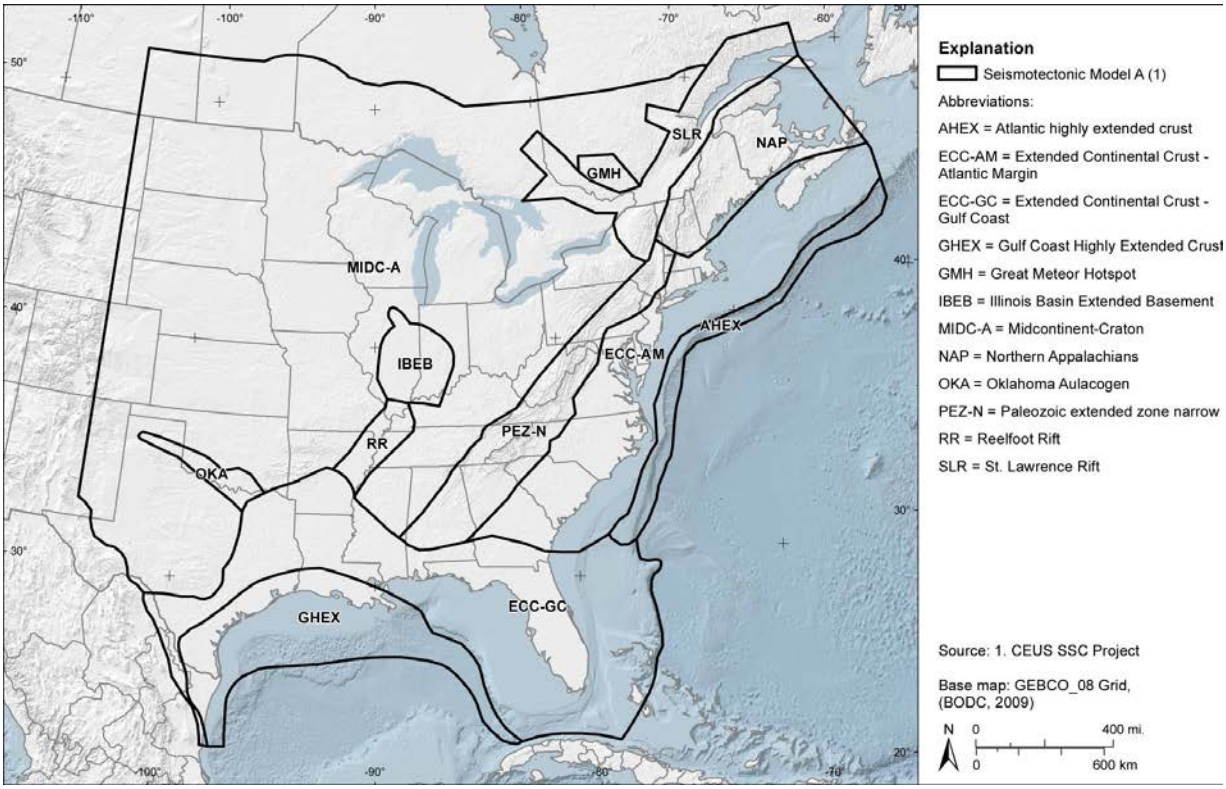

Figure 4.1. EPRI (2012) SSC model for the CEUS seismotectonic zone based on one branch of the logic tree (taken from Figure 4.2.4-2 of EPRI, 2012).

4.2 Ground Motion Characterization (GMC) Models

Similar to the two separate SSC models, the locations of the two sites in an active tectonic region and a stable continental crust region, respectively, requires the development of two separate GMC models. In addition, for the Seattle site, ground motion prediction equations (GMPEs) will need to be defined for crustal earthquakes and as well the two types of subduction zone earthquakes.

For the Seattle site GMC model, four equally-weighted Enhancement of Next Generation Attenuation for Western U.S. (NGA-West2) GMPEs (Bozorgnia et al., 2014) were used to predict the ground motions in the PSHA. These GMPEs are: Abrahamson et al. (2014) (referred to as ASK14), Boore et al. (2014) (referred to as BSSA14), Campbell and Bozorgnia (2014) (referred to as CB14), and Chiou and Youngs (2014) (referred to as CY14). An average shear-wave velocity (V_{S30}) of 760 m/s assigned for the PSHA in Seattle. We note that the Idriss (2014) model was not used in this study because its observed extrapolation to short distances for moderate to large earthquakes, as would be expected from the Seattle Fault, are not consistent with the predictions from the other GMPE models.

For the ASK14 and CY14 models, the functional form of the models based on an "estimated V_{S30}" value was implemented in this study. Note that the differences between the estimated and measured V_{S30} values only impact the uncertainty of each GMPE model but does not impact the median ground motion estimates. The sediment depths (Z_1 for ASK14 and CY14; $Z_{2.5}$ for CB14) used in this study are default values suggested by the GMPE developers based on the V_{S30} values in California. Note that for the BSSA14 model, the analysis was performed assuming no basin effects. Because the NGA-West2 GMPEs were developed in a collaborative effort with interactions and exchange of ideas among the developers, the NGA-West2 developers indicated that additional epistemic uncertainty needs to be incorporated into the median ground-motion estimation from their GMPEs. The additional epistemic uncertainty model of Al Atik and Youngs (2014) developed as part of the NGA-West2 project was used in the PSHA study for this study. The epistemic uncertainty in the median ground-motion prediction (σ_μ) of Al Atik and Youngs (2014) is distance-independent but depends on magnitude, style-of-faulting (SOF), and spectral period (T). The final ground motion logic tree for the ground motion models assigned to the crustal seismic sources is shown in Figure 4.2. The aleatory variability models of the four NGA-West2 GMPEs used in this study were used along with the corresponding median model for each GMPE.

For the subduction ground-motion model, the recent Abrahamson et al. (2016) model was used for the PSHA. This model was developed as part of the BC Hydro (2012) PSHA study and included a GMPE for both interface and intraslab events. In addition, for the intraslab events, a branch of the logic tree was developed for Cascadia specific earthquakes based on the limited empirical data which indicated a potential difference in the ground motions than those from the global dataset. A similar adjustment was not developed for the interface events based on the lack of empirical data from interface earthquakes in Cascadia. The full logic tree from the BC Hydro (2012) PSHA study is shown in Figure 4.3. As shown on the logic tree additional branches are included to account for the epistemic uncertainty for the model.

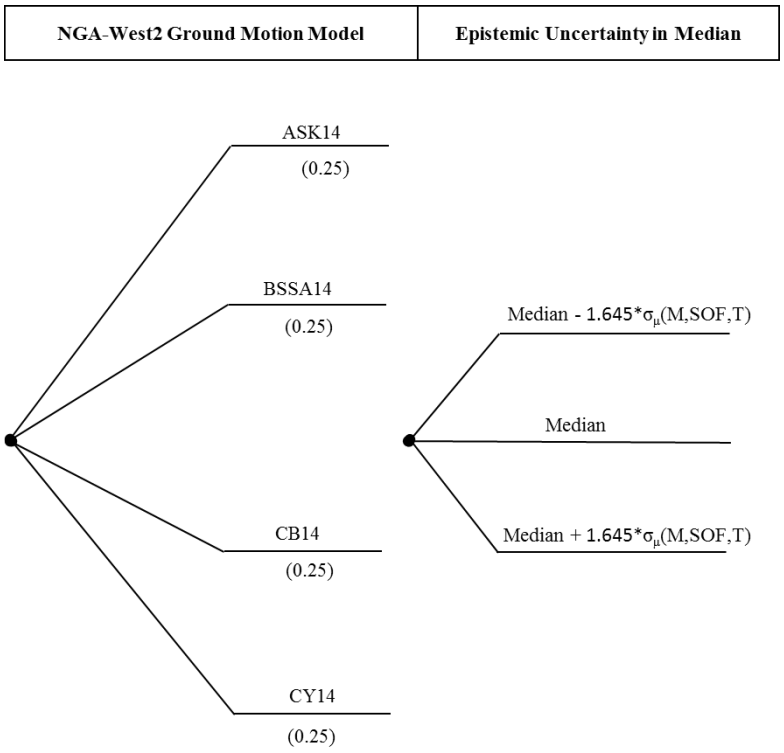

Figure 4.2. Median ground motion logic tree for the crustal seismic sources used in the PSHA study.

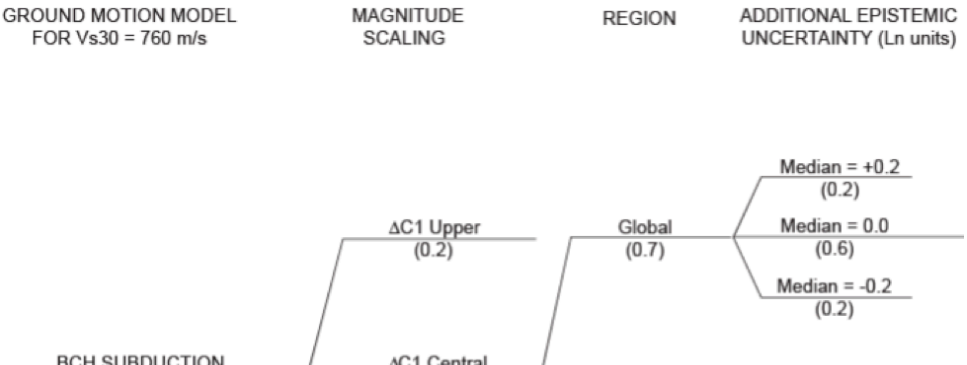

Period	ΔC1		
(s)	Lower	Central	Upper
0.01	0	0.2	0.4
0.30	0	0.2	0.4
0.50	-0.1	0.1	0.3
1.00	-0.2	0	0.2
2.00	-0.3	-0.1	0.1
3.0 - 10.0	-0.4	-0.2	0

Figure 4.3. BC Hydro (2012) logic tree for the subduction ground motion models (taken from Figure 3-50 of BC Hydro, 2012).

For the Boston site, a different suite of GMPEs was required due to differences in the tectonic environments between the WUS and CEUS. Unlike active tectonic regions like the WUS, stable continental regions such as the CEUS tend to have fewer empirical data from earthquakes in which empirically based GMPE models can be developed. In lieu of empirical data, several GMPE models have been developed based on numerical simulations and or adjustments of empirically based GMPE model to the CEUS region (e.g., see EPRI [2004] and PEER [2015] for a presentation of several GMPE models applicable for the CEUS). Most of the GMPE models developed for the CEUS region are defined for a reference hard rock site condition of V_{S30} of 2.8 km/sec. This reference hard rock site condition is assumed based on the properties of the crystalline hard rock pervasive throughout the CEUS.

For the PSHA study performed for the Boston site, the suite of GMPE models used was based on the set of models developed by Silva et al. (2002). This set of 11 individual GMPE models are listed in Table 4.1. Unlike other GMPE models developed for the CEUS, these models are defined for the full broadband spectral period range of 0.01 to 10 sec. The assigned site condition is for the reference hard rock conditions (i.e., V_{S30} of 2.8 km/sec). These models are based on a point source numerical modeling of ground motions and the methodology has been validated against previously recorded earthquakes. To account for epistemic uncertainty, both a single corner and double corner seismic source model are used in the development of the GMPE models. In addition, ground motion models for both a constant and variable stress parameter are developed. Finally, for the constant stress parameter models two versions of the models are developed in which the near field ground motions are modeled with and without a saturation effect.

The assigned weights listed in Table 4.1 for the suite of 11 GMPE models are based on the following logic tree branch weights:

- Single corner model = 0.80, Double Corner = 0.20
- Mean stress parameter = 0.63, High and Low stress parameter = 0.185
- Single corner constant = 0.213, Single corner constant with saturation = 0.164, Single corner variable = 0.622
- Double corner constant = 0.538, Double corner variable = 0.462

Table 4.1. GMPE models used in the PSHA study for the Boston site along with the assigned weights.

GMPE Model	Weight
Double Corner	0.1077
Double Corner-Saturation	0.0923
Single Corner-Variable-High	0.0921
Single Corner-Variable-Median	0.3136
Single Corner-Variable-Low	0.0921
Single Corner-Constant-High	0.0316
Single Corner-Constant-Median	0.1075
Single Corner-Constant-Low	0.0316
Single Corner-Constant-Sat-High	0.0243
Single Corner-Constant-Sat-Median	0.0829
Single Corner-Constant-Sat-Low	0.0243

These assigned weights are consistent with the weights developed and assigned in EPRI (2004). As a suite, these 11 GMPE models and their assigned weights provide a satisfactory range to capture the expected epistemic uncertainty and no additional models, scaling or weights were required for the PSHA.

4.3 Methodology and Results

Probabilistic seismic hazard calculations were carried out using the computer program HAZ46 (Abrahamson and Gregor, 2018). This version of PSHA program follows a standard state-of-the-practice approach for probabilistic seismic hazard analysis. A sigma truncation value of 6.0 was used for the PSHA. The minimum magnitude used in the analysis was 5.0. Mean hazard curves were computed for the two site locations along with the individual hazard curves for each seismic source. Based on the mean hazard curves, the UHS is computed for the two hazard levels of 475 and 2500 years. Mean magnitude, distance and epsilon results for these hazard levels are also computed, along with the binned deaggregation results.

The PSHA for the Seattle site is based on a longitude of 122.330833°W and a latitude of 47.598601°N. The results are presented for a V_{S30} value of 760 m/sec. The mean hazard curves for PGA are shown in Figure 4.4. Based on this plot, the intraslab, crustal background, Cascadia subduction zone, and Seattle fault are the most important contributors to the total hazard at the site. For longer spectral periods, the relative importance of the Seattle and Cascadia seismic sources increases, whereas the contribution from the intraslab seismic source decreases. Figure 4.5 provides the mean UHS for return periods of 475 and 2500 years for the Seattle site.

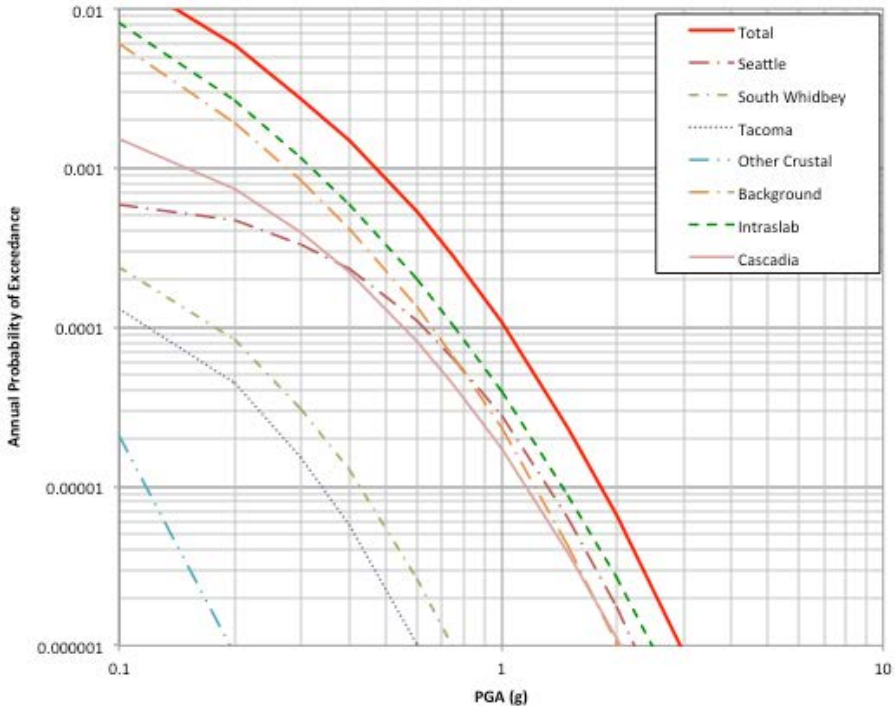

Figure 4.4. Mean total hazard curve and individual seismic source hazard curves for PGA at the Seattle site.

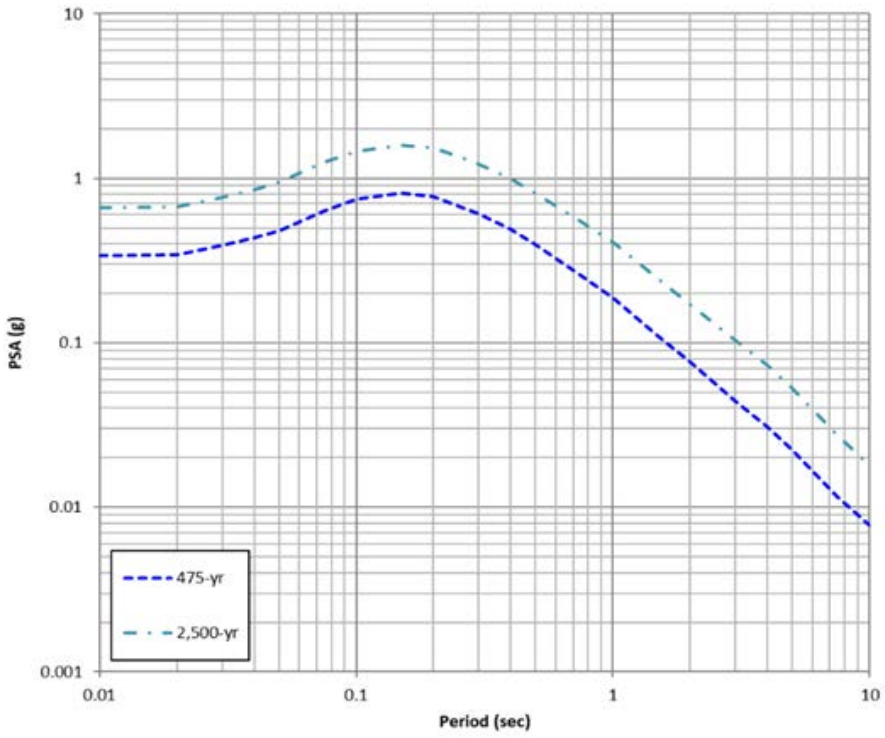

Figure 4.5. Mean UHS for return periods of 475 and 2500 years for the Seattle site, with reference site conditions characterized by V_{s30} = 760 m/s.

The PSHA for the Boston site is based on a longitude of 71.0897°W and a latitude of 42.3379°N. The results are presented for a V_{S30} value of 2.8 km/sec. The mean hazard curves for PGA are shown in Figure 4.6; based on this plot for PGA, the Extended Continental Crust – Atlantic Margin (ECC-AM) dominates the hazard, although the Saint Lawrence Rift (SLR) is the largest contributor for low levels of ground motion. For longer spectral periods, the relative importance of the Saint Lawrence Rift (SLR) seismic source increases. Figure 4.7 provides the mean UHS for return periods of 475 and 2500 years for the Boston site.

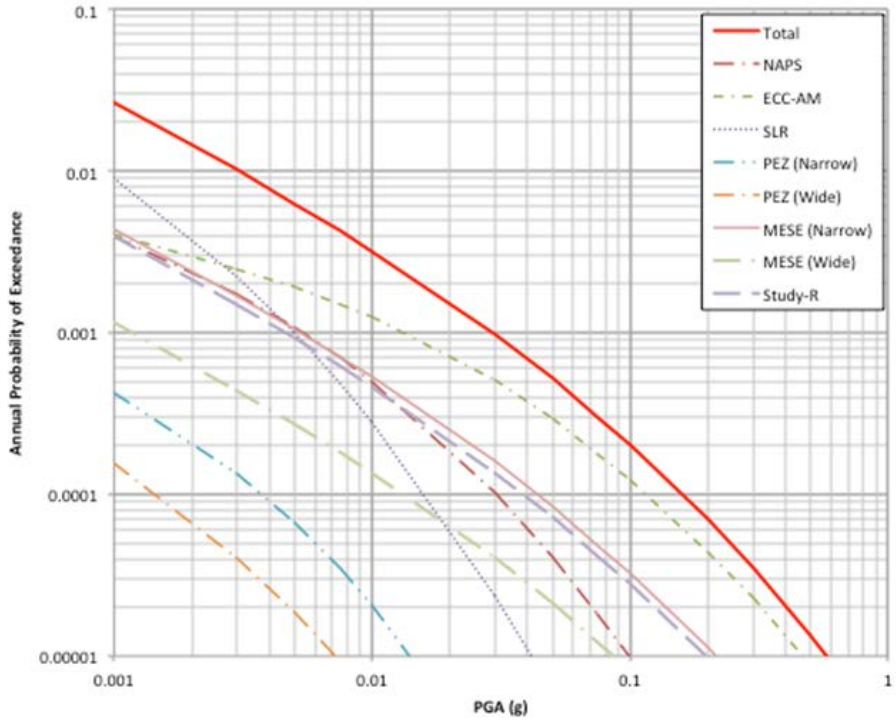

Figure 4.6. Mean total hazard curve and individual seismic source hazard curves for PGA at the Boston site.

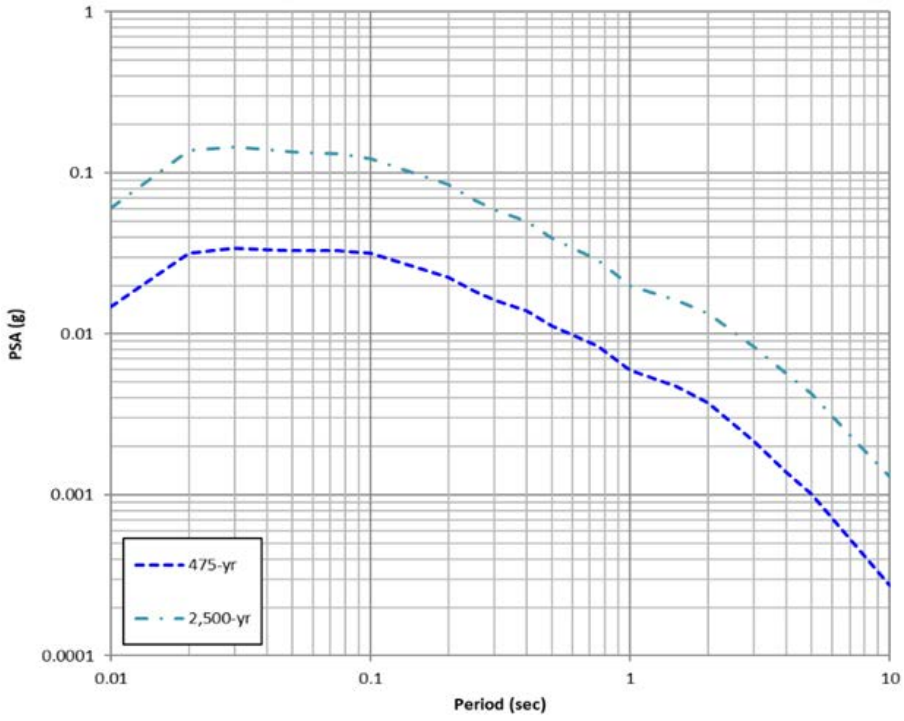

Figure 4.7. Mean UHS return periods of 475 and 2500 years for the Boston site, with reference site conditions characterized by V_{s30} = 2830 m/s.

5 Input Motion Selection

5.1 Target Spectra

This study considers three target spectra recommended by the American Society of Civil Engineers [ASCE] 7-16 design standards (ASCE, 2016) and used in practice. These include the uniform hazard spectrum (UHS), the conditional spectrum (CS), and the risk-targeted maximum considered earthquake (MCE_R) spectrum.

Uniform Hazard Spectrum (UHS)

The uniform hazard spectrum (UHS) is a target spectrum developed from probabilistic seismic hazard analyses (PSHA). The UHS envelopes spectral acceleration values at different periods corresponding to the same hazard level or probability of exceedance. Details corresponding to the calculation of UHS for Seattle and Boston were presented in Chapter 4. Hazard results were computed for the two study sites and a suite of 22 spectral periods over the period range of 0.01 sec (PGA) to 10.0 seconds. The uniform hazard spectra were plotted in Figures 4.5 and 4.7 for two return periods, 475 years and 2500 years, based on the suite of mean hazard curves. The UHS, however, is a conservative target spectrum because spectral values are unlikely to all occur in a single ground motion realization. Therefore, UHS is not representative of the spectrum corresponding to a single recorded ground motion.

Conditional Mean Spectra (CMS)

To bridge the gap between PSHA and deterministic analysis, and to be able to select site-specific ground motions, the conditional mean spectrum (CMS) was proposed by Baker and Cornell (2006) and Baker (2011). The computation of a CMS requires the determination of a conditioning period (based on knowledge of the fundamental period of the structure of interest), selection of a single or multiple ground motion prediction equations (GMPEs) deemed representative of the tectonic environment, selection of inter-period correlation coefficients, and selection of a dominant magnitude-distance (M-R) scenario from deaggregation results. The CMS can be more representative of the spectrum from a single ground motion which has the same spectral acceleration (Sa) as the UHS at the conditioning period, T^*. The spectral accelerations at all other periods of CMS are conditional on the spectral acceleration at the conditioning period, Sa(T^*). Figure 5.1 shows an example of a CMS conditioned at different periods.

For the computation of CMS, given a specific M-R combination, the mean natural logarithmic spectral value $\mu(T)$ and natural logarithmic standard deviation $\sigma(T)$ are calculated at all periods using a GMPE. $\varepsilon(T^*)$ is the number of standard deviation difference between the $\mu(T^*)$ and the natural logarithm of the UHS value at the conditioning period T^*. The CMS in natural logarithmic units at a period T_i conditioned at a period of T^* is then computed as follows:

$$CMS_{T^*}(T_i) = \mu(T_i) + \varepsilon(T^*) \times \sigma(T_i) \times \rho(T_i, T^*) \quad (5.1)$$

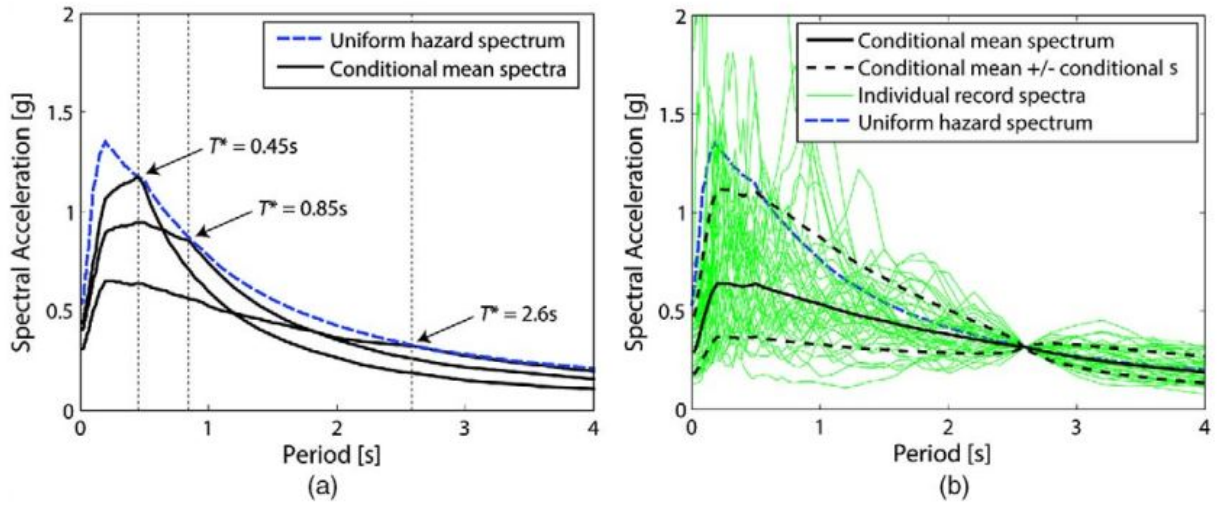

Figure 5.1 (a) Example Uniform Hazard Spectrum and Conditional Mean Spectra for an example site in Palo Alto, California, for a 2% in 50-year exceedance probability and with conditioning periods of T* = 0.45 s, 0.85 s, and 2.6 s. (b) Conditional spectra for the same example with a conditioning period of T = 2.6 s. [Haselton et al. (2017) in NIST (2011).]

Here, $\rho(T_i, T^*)$ is the correlation between ε at T^* and ε at different periods. In this study, we have used the inter-period correlation proposed by Baker and Jayaram (2008) for the NGA West 1 database (Chiou et al., 2008).

Deaggregation corresponding to different spectral periods provide the contributions to the hazard at a given site of multiple magnitude-distance-epsilon combinations. For Seattle, short periods (e.g., 0.01 s (PGA), 0.2 s, 0.5 s), and long periods (e.g., 1.0 s and 3.0 s) are selected because the hazard at short and long periods is dominated by different seismic sources. Figure 5.2a shows the deaggregation of the 5%-damped pseudo-acceleration response spectrum (PSA) at 0.01 seconds for Seattle corresponding to a 2% probability of exceedance in 50 years. The deaggregation plot for Seattle (Figure 5.2a) shows the contribution to seismic hazard from three distinct seismic sources: (1) shallow crustal earthquakes on faults within the North American plate (e.g. the Seattle Fault) at less than 30 km distance, (2) deep earthquakes originating along the subducting oceanic plate (intraslab earthquakes) at 50-100 km distance, and (3) large magnitude thrust events along the Cascadia subduction zone (interface earthquakes) at 75-200 km. Deaggregation plots for other selected spectral periods are shown in Figure 5.2b-e.

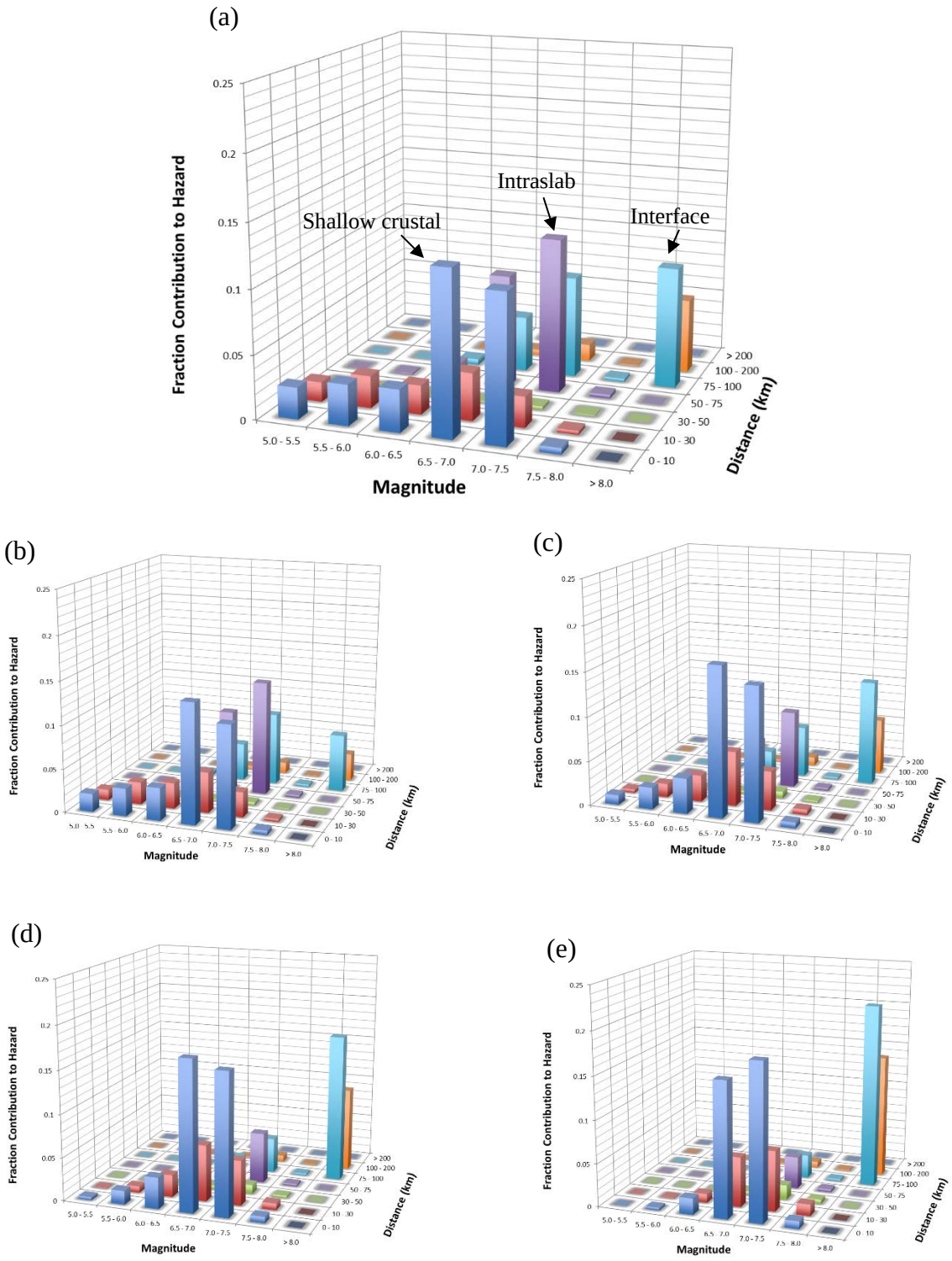

Figure 5.2. PSHA deaggregation results for Seattle at periods of (a) 0.01 s, (b) 0.2 s, (c) 0.5 s, (d) 1.0 s, and (e) 3.0 s.

At shorter periods (e.g., Figure 5.2a for T = 0.01 s and Figure 5.2b for T = 0.2 s), the highest contribution to the hazard comes from shallow crustal earthquakes and intraslab earthquakes. At longer periods (Figure 5.2d for T = 1.0 s and Figure 5.2e for T = 3.0 s), the contribution from the shallow crustal earthquakes and subduction-zone interface earthquakes are dominant. Therefore, instead of using the mean M-R combination from the deaggregation (which does not represent any physical seismic source), we have selected three different dominant M-R scenarios corresponding to the three different seismic sources for Seattle. Moreover, when a diverse tectonic setting results in multiple types of GMPEs being used for PSHA (as is the case for Seattle), choosing a single type of GMPE to calculate CMS using a M-R value poses a challenge. Therefore, for Seattle, we have selected three different dominant M-R scenarios corresponding to crustal, intraslab, and interface earthquakes, we and computed the CMS using crustal GMPEs, subduction intraslab, and subduction interface GMPEs, respectively.

Figure 5.3 provides the deaggregation of the 5%-damped PSA at 0.01 seconds and 1.0 seconds for Boston corresponding to a 2% probability of exceedance in 50 years. The deaggregation plots of Boston corresponding to long spectral periods (Figure 5.3b) do not show any predominant contribution to the hazard associated with a particular seismic source. However, for short periods (Figure 5.3a), we observe higher contributions coming from nearby areal sources at distances of 10-50 km. We can also observe from Figure 5.3 that the mean M-R (i.e., M = 5.77, R = 58.1 km for short periods, and M = 6.22, R = 149.21 km for long periods) combination is not the highest contributor to the hazard. Computing the CMS using these mean values may provide us with lower target spectra than the expected possible hazard in the site. Therefore, we also select causal parameters corresponding to apparent dominant scenarios of moderate-magnitude, near-source earthquakes (i.e. M = 5.5, R = 30 km for T = 0.01 s, and M = 6.0, R = 30 km for T = 1.0 s).

Table 5.1 shows the mean and selected dominant M-R scenarios for the CMS computations at the study sites in Seattle and Boston for spectral periods of T = 0.01 s and T = 1 s. For Seattle, we compute the CMS for three dominant scenarios (each representing a physical type of earthquake source); for Boston, we compute the CMS using the mean M-R combination from the deaggregation in addition to the dominant scenario of a moderate-magnitude, near-source earthquake.

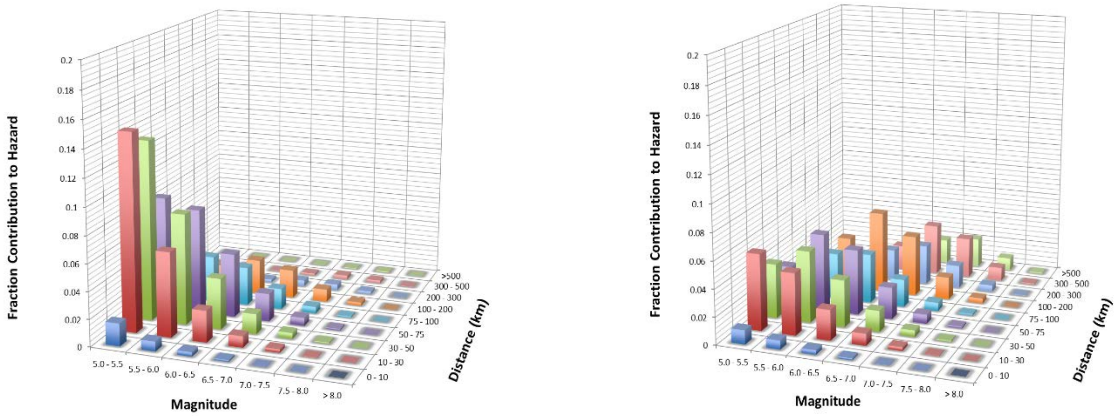

Figure 5.3. PSHA deaggregation results for Boston at periods of (a) 0.01 s and (b) 1.0 s.

Table 5.1. Magnitude-distance combinations for mean and selected dominant scenarios (DS) from deaggregation

	T = 0.01 s		T = 1.0 s	
	M	R_{rup} (km)	**M**	R_{rup} (km)
Seattle:				
Shallow crustal DS	7.0	5	7.0	5
Subduction intraslab DS	7.0	50	7.0	50
Subduction interface DS	9.0	100	9.0	100
Boston:				
Mean from deaggregation	5.77	58.1	6.22	149.21
Moderate-magnitude, near-source DS	5.5	30	6.0	30

The calculation of the CMS when considering stable tectonic regions or subduction events imposes additional challenges. The NGA West 2 (Ancheta et al. 2013) database consists of shallow crustal earthquakes, as does the NGA West 1 database (Chiou et al., 2008). Therefore, the use of the same correlation coefficients (in Equation 5.1) for shallow crustal GMPEs and NGA West 2 database is justified. However, different correlation coefficients may be required for calculating the subduction zone CMS (for Seattle) and stable continental zone CMS (for Boston). The Baker and Jayaram (2008) correlation was developed for shallow crustal seismicity, but the model has been applied to subduction zones such as Japan. Jayaram et al. (2011) calculated correlation coefficients based on the Japanese ground-motion databases K-net and KiK-net (which have both crustal and subduction earthquakes), and suggested the use of the Baker and Jayaram (2008) model to obtain approximate correlation predictions. Moreover, Carlton and Abrahamson (2014) showed the similarity of correlation coefficients between the BC Hydro GMPE (Abrahamson et al., 2016) for subduction zone events, and the Abrahamson and Silva (2008) GMPE for shallow crustal earthquakes. Hence, they suggested that any variation in correlation coefficients comes from spectral shape rather than the tectonic region, and that generic correlation models are robust and can be used in determination of CMS regardless of the GMPEs considered. There is currently no correlation study involving the NGA-East database. Therefore, we decided to apply the generic correlation model proposed by Baker and Jayaram (2008) for Boston.

The calculation of the conditional mean spectrum (CMS) considers only the mean spectral values, and does not consider the spectral variability in the recorded ground motion spectra. Therefore, an alternative to the CMS is the conditional spectra (CS), which considers the mean and the spectral variability. Figure 5.4 shows the CS (mean +/- 2 standard deviations) for Seattle at a conditioning period of T* = 0.5 s. Ground motions are matched to only the mean spectrum when considering the CMS. However, for the CS, the ground motions are matched to the mean +/- 2 standard deviations (std).

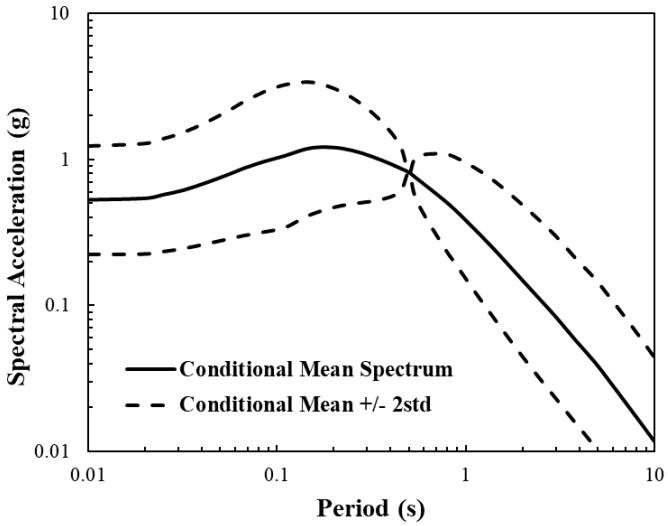

Figure 5.4. Conditional spectrum for Seattle at conditioning period of T* = 0.5 s.

MCE_R Spectrum

The risk-targeted maximum considered earthquake spectrum (MCE_R Spectrum) results from the most severe earthquake effects considered by the ASCE 7-16 design standards (ASCE, 2016). It is determined for the orientation that results in the largest maximum response to horizontal ground motions and with adjustment for targeted risk. The MCE_R Spectrum corresponding to a 1% collapse risk in 50 years is generally modified from the UHS using a risk coefficient. Zimmerman et al. (2017) provide examples for developing MCE_R spectra according to the ASCE 7-16 code. The MCE_R Spectrum for Seattle and Boston are calculated using the ASCE 7 Hazard Tool (see Data and Resources section) and are presented in Figure 5.5.

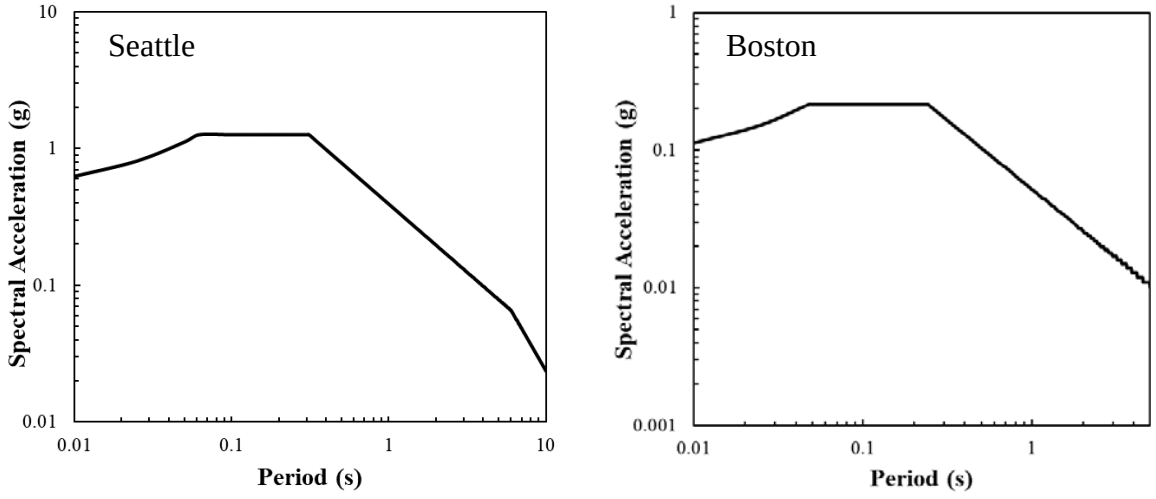

Figure 5.5. MCE_R design spectra for Seattle and Boston.

5.2 Ground Motion Selection Procedure

There are generally two approaches for modifying the time series to be consistent with the design response spectrum: scaling and spectral matching. As summarized by Al Atik and Abrahamson (2010), "Scaling involves multiplying the initial time series by a constant factor so that the spectrum of the scaled time series is equal to or exceeds the design spectrum over a specified period range. Spectral matching involves modifying the frequency content of the time series to match the design spectrum at all spectral periods." However, the smooth spectrum derived from spectral matching is not representative of a real ground motion. A recorded ground motion will not match the UHS or design spectrum over a wide range of periods and it often has peaks and troughs. There are two types of spectral matching techniques: frequency domain and time domain. "For spectrum-matching methods, one of the chief concerns is the modification of the frequency content that can distort the nonstationary characteristics of the time series. Other concerns include the uncertain effects of leveling or flattening all the peaks and troughs of the spectrum on the computed structural response" (Heo et al., 2011). Moreover, spectral matching has not been recommended as part of hazard-consistent site response analysis preferred practices (Stewart et al., 2014). In this study, we have used the scaling method only.

Various tools are available for ground motion selection and scaling. However, most of these tools select ground motions based on their fit or match to a single target spectrum. The conditional spectrum (CS) considers the variability in the target spectra along with the mean spectrum. As a result, this procedure does not have a single target spectrum to match the ground motion with. Baker and Lee (2017) have improved a ground motion selection algorithm previously proposed by Jayaram et al. (2011) to select ground motions matching the CS. The algorithm samples data from a multivariate normal distribution with the target conditional (or unconditional) mean and the corresponding covariance matrix to simulate realizations of response spectra. Then, ground motions that best match each of the statistically simulated spectra are selected from the specified database using either the sum of squared errors (SSE) or the Kolmogorov-Smirnov goodness of fit test (KS test).

The input motion selection and scaling protocol proposed by Baker and Lee (2017) is used to select ground motions matching all the target spectra in this study. When selecting motions matching the UHS and MCE_R spectra, we kept the variance to be zero, so that the motions are matched directly to the target spectrum. However, for selecting motions matching the CS, the algorithm statistically simulates response spectra from a target distribution, finds motions whose spectra match each statistically simulated response spectrum, and then performs an optimization to further improve the consistency of the selected motions with the target distribution. The simulated spectra accounts for the variability in spectral values at periods other than the conditioning period, while the CMS considers the mean spectral values only. To find the error between each statistically simulated spectrum and candidate ground motion, the *d* statistic from a Kolmogorov-Smirnov goodness-of-fit test (KS test) is used as the metric.

Eleven pairs of ground motions are selected as per the ASCE 7-16 design standards (ASCE, 2016). Eleven input motions are also recommended by FEMA (2012), which showed that this number of motions provides mean response parameters within 30% of the targets at a 70% confidence level (Stewart et al. 2014).

5.3 Ground Motion Databases

An important step in the input motion selection process is to identify appropriate databases with representative ground motion recordings from the seismic sources that contribute to the hazard at a site. The NGA-West2 database (Ancheta et al. 2013) is used in this study to select shallow crustal earthquake motions for Seattle. This database has 21,539 records from shallow crustal earthquakes around the globe. The U.S. subduction database for the NGA-Sub project is still being developed and is currently not available for use. Therefore, we have identified the Japanese Kiban-Kyoshin network (KiK-net) database (Okada et al. 2004, Dawood et al. 2016) as a suitable option to select records from subduction events. From this database, we have incorporated 568 subduction interface earthquake records and 19,943 subduction intraslab earthquake records in the selection algorithm. The KiK-net database of vertical seismometer arrays has both surface and borehole records. However, for this study, we have only used surface records.

In the case of Boston, we have used the NGA-East database (Goulet et al. 2014) with 9,382 records. Even with the crystalline hard rock conditions found in CEUS, it is nearly impossible to find ground motions recorded at sites with a V_{S30} of 2830 m/s (i.e., the reference site conditions identified as appropriate for Boston hazard calculations, as detailed in Chapter 4) within the NGA-East database. Causal parameters (i.e., magnitude, distance, V_{S30}) are often kept within a reasonable bound to screen the database and find appropriate ground motions for scaling and matching to the target spectra. However, Tarbali and Bradley (2016) showed that keeping this bound wide can help to select ground motions with a better representation of the target intensity measure distribution. Hence, we kept the causal parameter bound wide while selecting ground motions matching CS. For the scaling of ground motions, Haselton et al. (2017) indicated that a factor of 0.25-4.0 is not uncommon. However, for both the NGA-East database and the KiK-net database, it was difficult to find appropriate number of ground motions maintaining this range. The maximum scaling factor was relaxed up to 20 for selecting motions from the NGA-East and KiK-net database.

5.4 Selected Input Motion Sets

The following is an outline of the input motion suites that are considered in this study:

- Boston:
  - 1: Uniform Hazard Spectrum
    - 1a: UHS, 2% in 50 years
    - 1b: UHS, 10% in 50 years
  - 2a: Conditional Spectra, 2% in 50 years, T = 0.01 s
    - 2a(i): Dominant scenario, near-source moderate-magnitude earthquake
    - 2a(ii): Mean M, R from deaggregation
  - 2b: Conditional Spectra, 2% in 50 years, T = 1 s
    - 2b(i): Dominant scenario, near-source moderate-magnitude earthquake
    - 2b(ii): Mean M, R from deaggregation
  - 3: Risk-targeted Maximum Considered Earthquake
    - 3a: MCE_R, ASCE 7-16 design response spectrum multiplied by 1.5

- Seattle
  - 1: Uniform Hazard Spectrum
    - 1a: UHS, 2% in 50 years
    - 1b: UHS, 10% in 50 years
  - 2a: Conditional Spectra, 2% in 50 years, T = 0.01 s
    - 2a(i): Shallow crustal earthquakes
    - 2a(ii): Intraslab earthquakes
    - 2a(iii): Interface earthquakes
  - 2b: Conditional Spectra, 2% in 50 years, T = 0.2 s
    - 2b(i): Shallow crustal earthquakes
    - 2b(ii): Intraslab earthquakes
    - 2b(iii): Interface earthquakes
  - 2c: Conditional Spectra, 2% in 50 years, T = 0.5 s
    - 2c(i): Shallow crustal earthquakes
    - 2c(ii): Intraslab earthquakes
    - 2c(iii): Interface earthquakes
  - 2d: Conditional Spectra, 2% in 50 years, T = 1 s
    - 2d(i): Shallow crustal earthquakes
    - 2d(ii): Intraslab earthquakes
    - 2d(iii): Interface earthquakes
  - 2e: Conditional Spectra, 2% in 50 years, T = 3 s
    - 2e(i): Shallow crustal earthquakes
    - 2e(ii): Intraslab earthquakes
    - 2e(iii): Interface earthquakes
  - 3: Risk-targeted Maximum Considered Earthquake
    - 3a: MCE_R, ASCE 7-16 design response spectrum multiplied by 1.5

Several of the target spectra and the selected motions are shown in Figures 5.6-5.11 as examples. Each figure provides the original target spectrum with the selected and scaled ground motion records, along with the comparison between such target spectrum and the median spectral values from the selected ground motions (labeled as "Selection" in the plots). Details of the selected ground motions for all suites (magnitude, distance, Vs_{30}, etc.) are presented Table S1 in the Appendix.

A reasonable match to the UHS is often achieved for the Seattle site, as observed in Figure 5.6, where the spectral shapes of the target and the mean from the 11 selected records are almost the same across all periods. One of the strengths of utilizing the CS spectra is also depicted in Figure 5.7, where the variability in the target spectrum is explicitly considered. This results in an even better match between the target spectrum and the mean spectral values from selected and scaled motions. Fitting the spectral shape of the design spectrum provides the poorest match among all target spectra considered in Seattle (e.g., Figure 5.8), which is expected given the difficulty of real ground motions to be compatible with this representative spectral shape. In the case of Boston, achieving a reasonable agreement with defined target spectra proves more difficult. As seen in Figures 5.9, 5.10, and 5.11, a good match is often only maintained for a given range of periods. Note that the mismatch is especially severe for short periods when matching the CS (Figure 5.10) and the MCE_R (Figure 11). These details will be further discussed in Chapter 7.

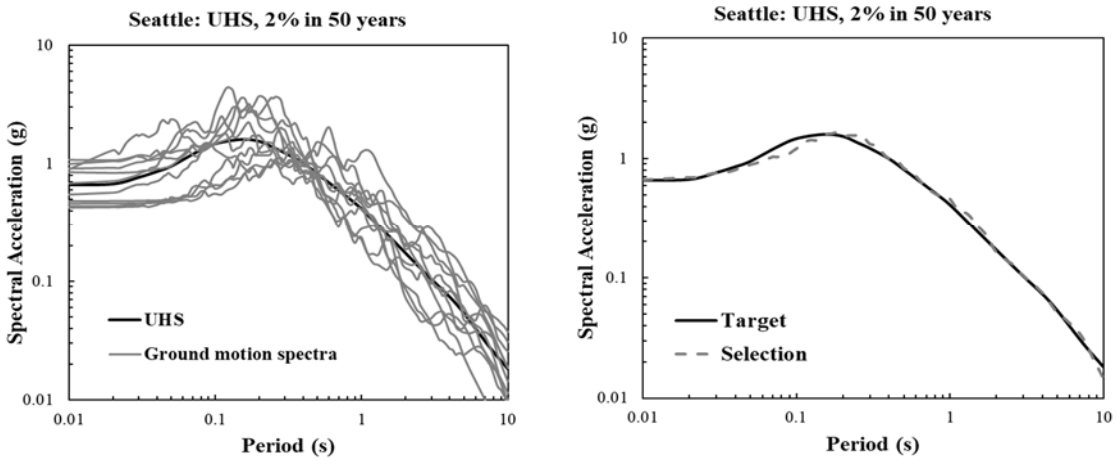

Figure 5.6. Selected suite of motions matching the UHS (2% in 50 years) for Seattle.

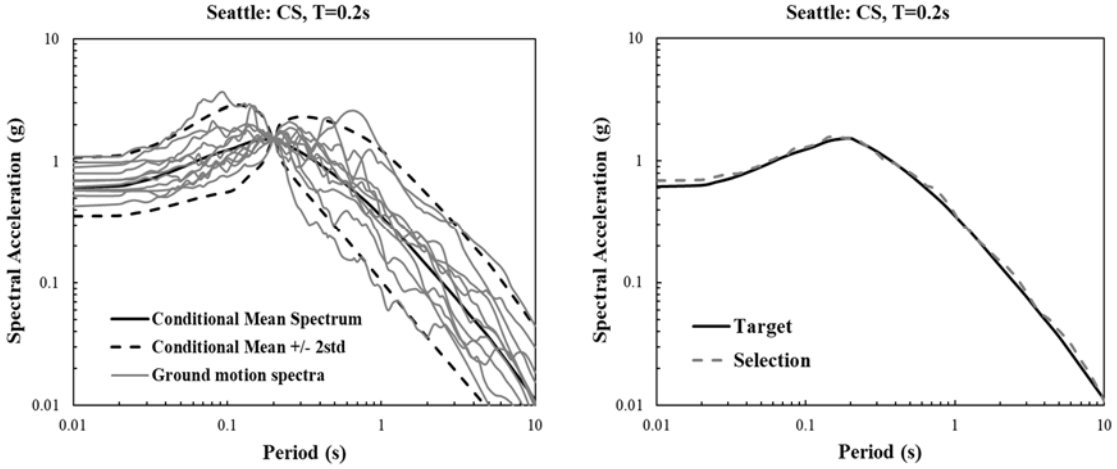

Figure 5.7. Selected suite of motions matching the CS at a spectral period of T = 0.2 s for Seattle.

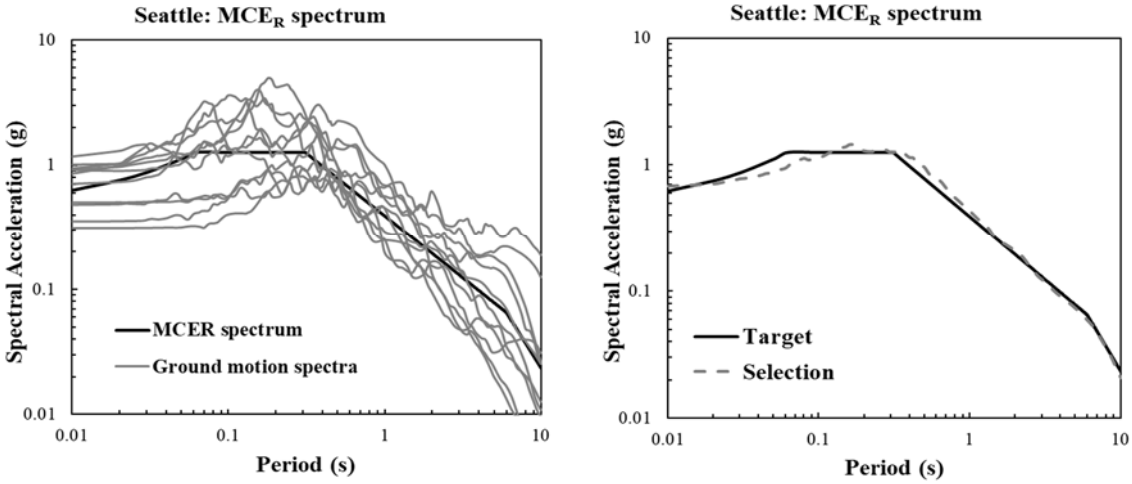

Figure 5.8. Selected suite of motions matching the MCE_R spectrum for Seattle.

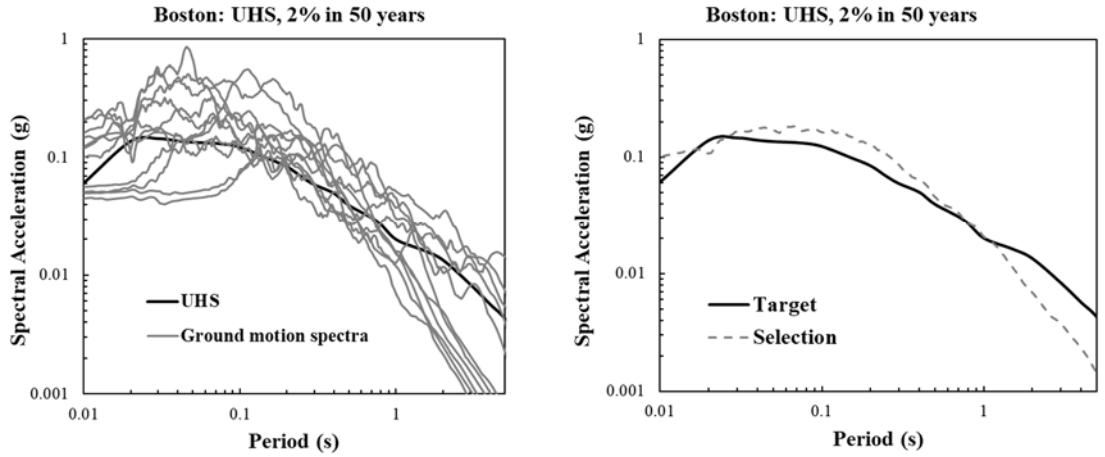

Figure 5.9. Selected suite of motions matching UHS (2% in 50 years) for Boston.

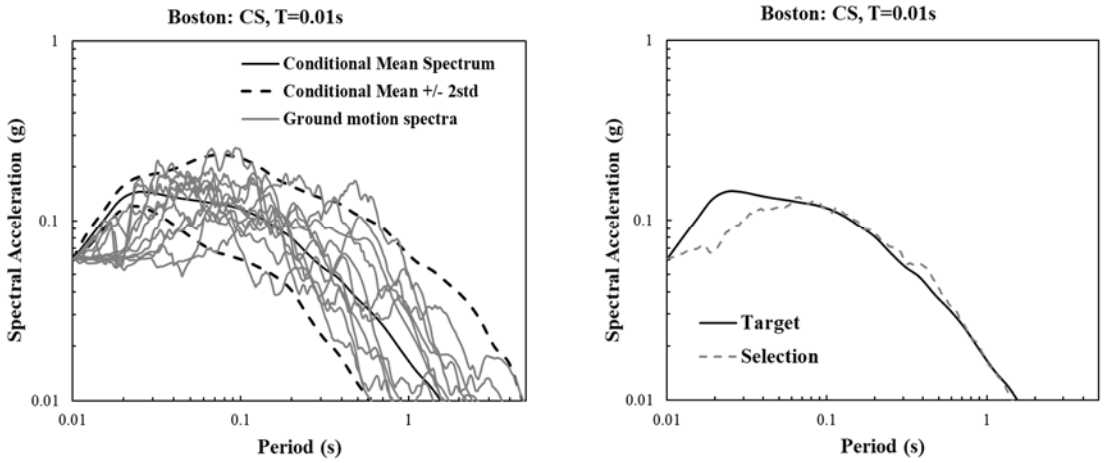

Figure 5.10. Selected suite of motions matching the CS at a spectral period of T = 0.01 s for Boston.

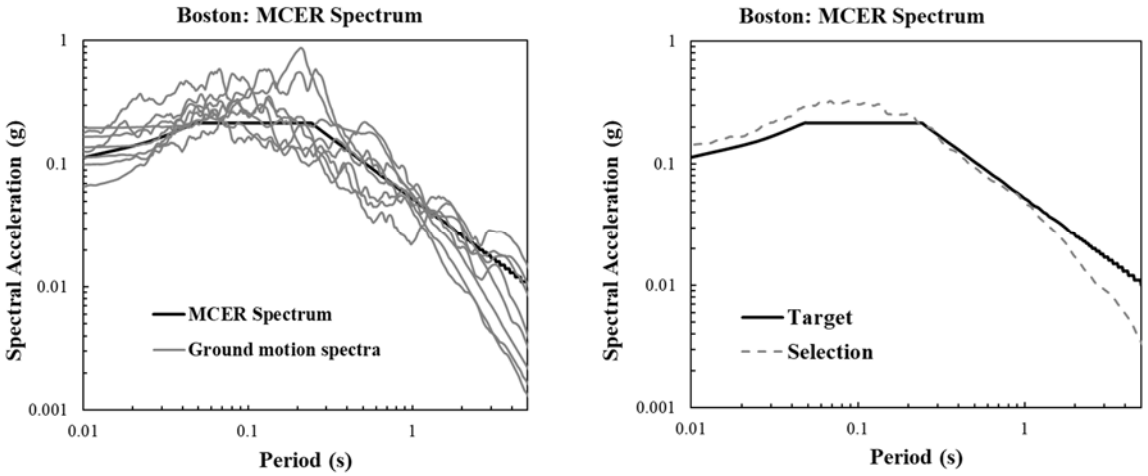

Figure 5.11. Selected suite of motions matching the MCE_R spectrum for Boston.

6 Site Response Analyses

6.1 Overview

A large contribution to the level of ground motion experienced during an earthquake is the influence of the site-specific geology as seismic waves propagate from depth to the ground surface. An important tool in seismic hazard analysis is a site response model, which is a computational model used to predict the ground motion at the surface of a site, as a function of (1) the input motion at the base of the site, and (2) the material properties and dynamic behavior of the soil profile. As illustrated in Figure 6.1, the input ground motion is numerically applied at the base of the profile, and a site response analysis is performed by propagating the seismic waves through the soil profile in order to predict the ground motion at the surface (and potentially throughout the soil profile). These predicted ground motions may then be used to design structures or to perform subsequent geotechnical engineering analyses (such as liquefaction and/or slope stability).

In engineering practice, site response analyses are burdened with significant uncertainties both in terms of the input (rock) motions and the soil profile. The two sites we selected (Boston and Seattle) were relatively well-characterized in terms of geotechnical information. Therefore, we hypothesized that the most significant source of site response uncertainty is the input motion. The input motions described in Chapter 5 were propagated through the two profiles described in this chapter, and we evaluated the predicted ground motions at these locations from the various suites of input motions.

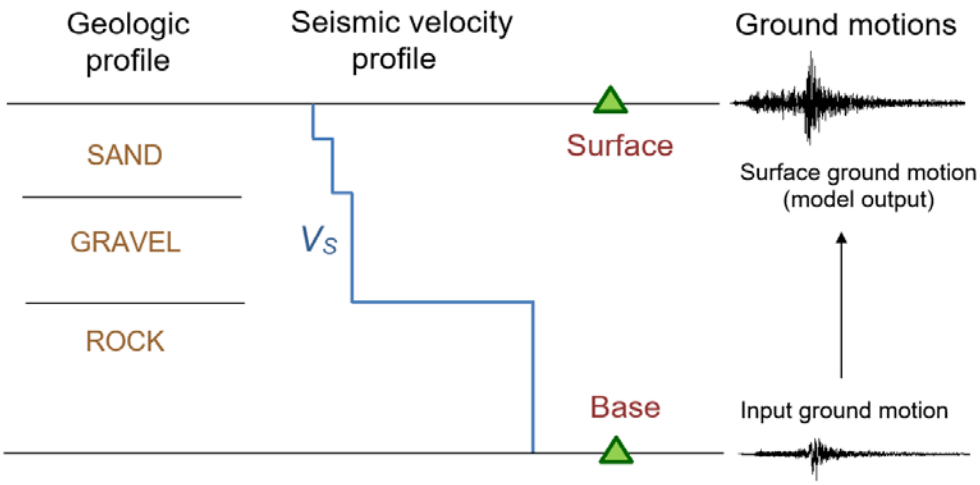

Figure 6.1. Schematic of an earthquake site response model: the input ground motion (representing bedrock conditions) is applied at the base of the site, and is propagated upward through the soil profile to predict the ground motion at the surface. An example geologic profile and V_S profile are shown for a hypothetical site.

6.2 Geotechnical Profiles

A geotechnical profile was developed for each location to be representative of typical conditions in the center of each city. Large portions of both Boston and Seattle are underlain by layers of artificial fill, and typical profiles are characterized by sharp impedance contrasts at depth

(corresponding to the interface between post-glacial and pre-glacial materials). The geotechnical conditions in both locations have been heavily influenced by glaciation during the last Ice Age. The assumed reference rock conditions for Seattle and Boston are prevalent throughout the Western United States (WUS) and Central and Eastern United States (CEUS) regions, respectively.

Within each city, there are significant variations in typical geotechnical conditions in Boston and Seattle. Predominant types of surficial geology in Boston include artificial fill, glaciofluvial, and glacial till / bedrock (Brankman and Baise, 2008), each of which has distinct geotechnical characteristics (Woodhouse and Barosh, 2011/2012; Baise et al., 2016). Sites predominantly characterized by artificial fill versus bedrock represent the end members of the spectrum of site-response behavior, with glaciofluvial deposits representing a middle ground. In Seattle, typical surficial geotechnical conditions tend to bifurcate into two categories: postglacial deposits (alluvium and artificial fill) and glacial till / bedrock (Galster and Laprade, 1991). River valleys tend to be characterized by extremely soft sites, and areas of greater topography are much stiffer. In this report, we focus upon softer sites in each city where site response is expected to be more substantial, and engineering ground motion predictions are likely more challenging to predict. Furthermore, each city has critical infrastructure in these areas (including ports, oil and gas storage facilities, and airports). Future work may assess the influence of input motion selection on other typical sites in these cities. The assumed shear-wave velocity and geotechnical profiles are provided graphically in Figure 6.2 for both sites.

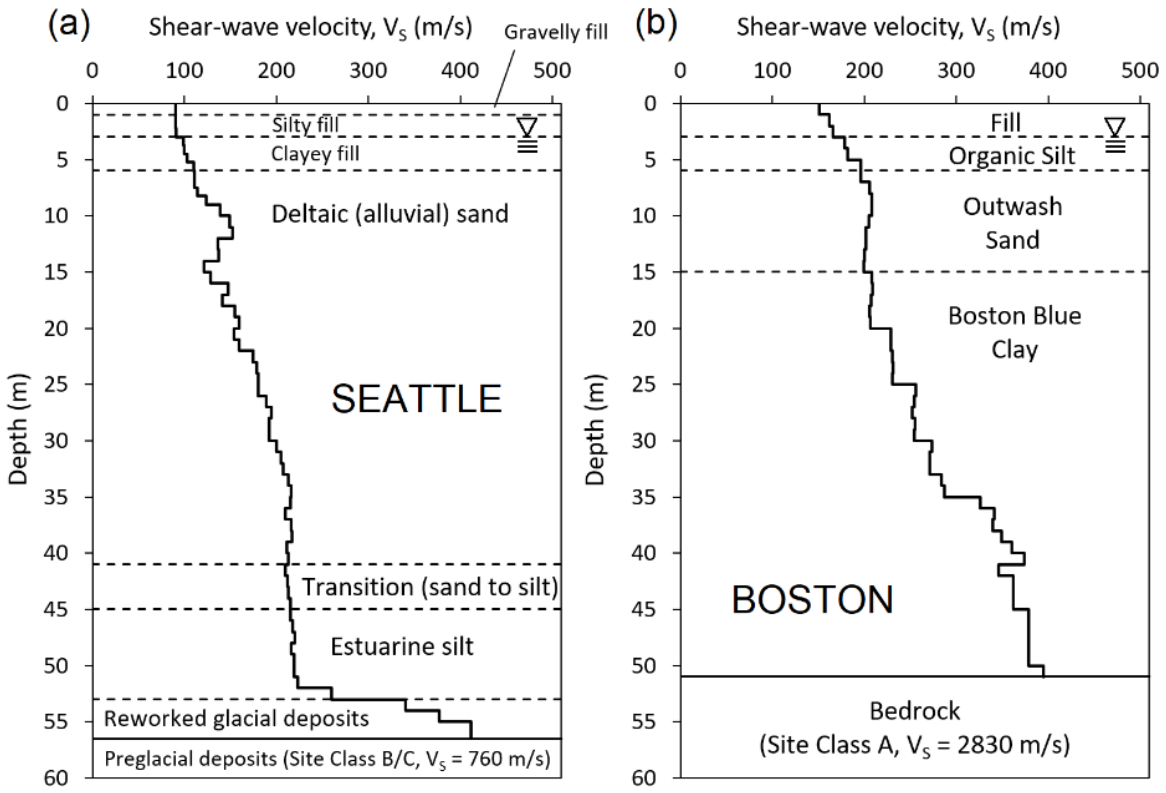

Figure 6.2. Shear-wave velocity profiles and geotechnical profiles used in the analyses for (a) Seattle and (b) Boston. The groundwater table was assumed to occur at a depth of 3 m at each site.

Boston, Massachusetts

The Boston site consists of artificial fill, organic silt, glacial outwash (sand), and a thick layer of Boston Blue Clay overlying dense glacial till / bedrock (modeled as crystalline hard rock [V_{Sb} = 2830 m/s] for engineering purposes) at a depth *H* of 51 m. The 51 m depth is representative of the varying depth to bedrock throughout the city, and it is consistent with the location of the Northeastern University downhole array (Yegian, 2004). The assumed shear-wave velocity profile was developed by Baise et al. (2016) from multiple spectral analysis of surface waves (SASW) measurements throughout the Boston basin (Thompson et al., 2014). Relative to the Baise et al. (2016) V_S profile, we smoothed out the profile in the vicinity of 45-51 m depth to reduce a potentially unrealistic V_S reversal that was based on measurements at a single site. The soil profile from Baise et al. (2016) was used as the basis for the soil layer types and thicknesses. The groundwater table was assumed to be 3 m, a typical depth for the Boston area and consistent with Yegian (2004) for the vicinity of the downhole array at Northeastern University. Unit weights of soils were derived from median values of Woodhouse and Barosh (2011/2012) for typical soils in the Boston profile. The plasticity index (PI) of Boston Blue Clay is assumed from Woodhouse and Barosh (2011/2012); the plasticity index of the organic silt was assumed to be 15 (generic value for silt). The upper 3 m of the clay consists of an overconsolidated crust, and an overconsolidation ratio (OCR) of 2 was assumed here. For all other points in the profile, an OCR of 1 was used. The at-rest lateral earth-pressure coefficient was assumed to be 0.5 in all layers.

The time-averaged shear-wave velocity over the top 30 m of the subsurface (V_{S30}) is 207.1 m/s, making this a NEHRP Class D site. The bedrock is assumed to represent Site Class A (2830 m/s) and is modeled as an elastic halfspace with 2% damping (for time domain analyses, the damping of the elastic halfspace does not enter the calculation and has no impact on the results). The time-averaged shear-wave velocity over the entire 51-m-thick soil profile is 246.3 m/s, meaning that the fundamental site frequency (based on average shear-wave velocity) is $V_{S,avg}$ / (4H) = 1.2 Hz. The corresponding fundamental site period based on $V_{S,avg}$ is therefore 1 / (1.2 Hz) = 0.83 s. The one-dimensional (1D) linear theoretical surface/outcrop amplification spectrum for the Boston location is plotted in Figure 6.3. The fundamental peak of the 1D amplification spectrum occurs at 1.42 Hz, corresponding to a fundamental site period of 0.7 s, in agreement with the fundamental site period measured from $V_{S,avg}$. Horizontal-to-vertical (H/V) spectral ratios of ambient noise data collected by Yilar et al. (2017) collected at the Northeastern University downhole array show agreement with our computed fundamental site periods (0.7 to 0.8 s), and further confirm that the site response at this location is largely governed by the impedance contrast at the soil-bedrock interface.

A simplified geotechnical profile for Boston is shown in Table 6.1. The minimum shear-wave velocity ($V_{S,min}$) is 151 m/s at the top of the profile; therefore, a sublayer thickness (*h*) of 1 m was used throughout the soil profile. The maximum frequency of transmission at the top of the profile (the critical point) for nonlinear calculations is therefore $V_{S,min}$ / (4*h*) = 38 Hz. A table of the full geotechnical and shear-wave velocity profile (with entries for each sublayer) is provided in Table 6.2.

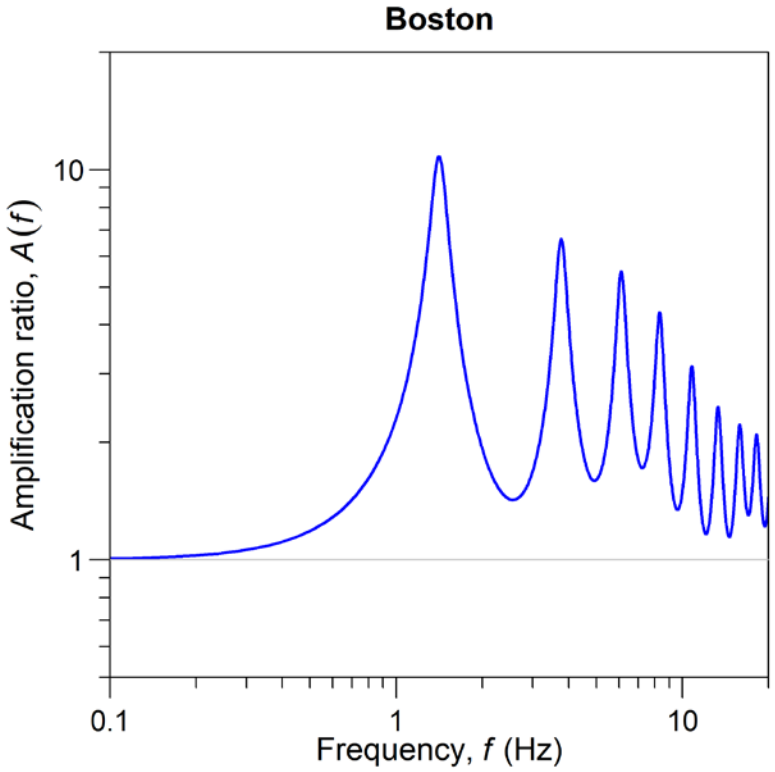

Figure 6.3. One-dimensional linear theoretical surface/outcrop amplification spectrum for Boston.

Table 6.1. Simplified geotechnical profile for Boston, Massachusetts

Layer name	Predominant soil type	Depth of layer top (m)	Thickness (m)	Unit weight, γ (kN/m^3)	Plasticity Index, PI	Over-consolidation ratio, OCR
Fill	Sand	0	3	20	0	1
Organic Silt	Silt	3	3	17	15	1
Outwash Sand	Sand	6	9	19	0	1
Boston Blue Clay (overconsolidated)	Clay	15	3	18.5	25	2
Boston Blue Clay (normally consolidated)	Clay	18	33	18.5	15	1
Bedrock	Bedrock	51	—	27	—	—

Table 6.2. Full geotechnical and V_S profiles for Boston, Massachusetts

Layer No.	Material	Depth of layer top (m)	Thickness (m)	Unit weight, γ (kN/m^3)	Shear-wave velocity, Vs (m/s)	Plasticity Index, PI	Over-consolidation ratio, OCR	At-rest lateral earth pressure coef., K_o
1	Fill	0	1	20	151	0	1	0.5
2	Fill	1	1	20	162	0	1	0.5
3	Fill	2	1	20	166	0	1	0.5
4	Organic Silt	3	1	17	179	15	1	0.5
5	Organic Silt	4	1	17	182	15	1	0.5
6	Organic Silt	5	1	17	196	15	1	0.5
7	Outwash Sand	6	1	19	196	0	1	0.5
8	Outwash Sand	7	1	19	206	0	1	0.5
9	Outwash Sand	8	1	19	208	0	1	0.5
10	Outwash Sand	9	1	19	208	0	1	0.5
11	Outwash Sand	10	1	19	205	0	1	0.5
12	Outwash Sand	11	1	19	202	0	1	0.5
13	Outwash Sand	12	1	19	202	0	1	0.5
14	Outwash Sand	13	1	19	200	0	1	0.5
15	Outwash Sand	14	1	19	200	0	1	0.5
16	Boston Blue Clay	15	1	18.5	208	25	2	0.5
17	Boston Blue Clay	16	1	18.5	209	25	2	0.5
18	Boston Blue Clay	17	1	18.5	207	25	2	0.5
19	Boston Blue Clay	18	1	18.5	206	25	1	0.5
20	Boston Blue Clay	19	1	18.5	207	25	1	0.5
21	Boston Blue Clay	20	1	18.5	229	25	1	0.5
22	Boston Blue Clay	21	1	18.5	229	25	1	0.5
23	Boston Blue Clay	22	1	18.5	230	25	1	0.5
24	Boston Blue Clay	23	1	18.5	231	25	1	0.5
25	Boston Blue Clay	24	1	18.5	230	25	1	0.5
26	Boston Blue Clay	25	1	18.5	256	25	1	0.5
27	Boston Blue Clay	26	1	18.5	255	25	1	0.5
28	Boston Blue Clay	27	1	18.5	252	25	1	0.5
29	Boston Blue Clay	28	1	18.5	255	25	1	0.5
30	Boston Blue Clay	29	1	18.5	254	25	1	0.5
31	Boston Blue Clay	30	1	18.5	273	25	1	0.5
32	Boston Blue Clay	31	1	18.5	271	25	1	0.5
33	Boston Blue Clay	32	1	18.5	271	25	1	0.5
34	Boston Blue Clay	33	1	18.5	284	25	1	0.5
35	Boston Blue Clay	34	1	18.5	287	25	1	0.5
36	Boston Blue Clay	35	1	18.5	326	25	1	0.5
37	Boston Blue Clay	36	1	18.5	341	25	1	0.5
38	Boston Blue Clay	37	1	18.5	340	25	1	0.5
39	Boston Blue Clay	38	1	18.5	350	25	1	0.5
40	Boston Blue Clay	39	1	18.5	360	25	1	0.5
41	Boston Blue Clay	40	1	18.5	374	25	1	0.5
42	Boston Blue Clay	41	1	18.5	346	25	1	0.5
43	Boston Blue Clay	42	1	18.5	362	25	1	0.5
44	Boston Blue Clay	43	1	18.5	362	25	1	0.5
45	Boston Blue Clay	44	1	18.5	362	25	1	0.5

Layer No.	Material	Depth of layer top (m)	Thickness (m)	Unit weight, γ (kN/m^3)	Shear-wave velocity, Vs (m/s)	Plasticity Index, PI	Over-consolidation ratio, OCR	At-rest lateral earth pressure coef., K_o
46	Boston Blue Clay	45	1	18.5	378	25	1	0.5
47	Boston Blue Clay	46	1	18.5	378	25	1	0.5
48	Boston Blue Clay	47	1	18.5	378	25	1	0.5
49	Boston Blue Clay	48	1	18.5	378	25	1	0.5
50	Boston Blue Clay	49	1	18.5	378	25	1	0.5
51	Boston Blue Clay	50	1	18.5	395	25	1	0.5
52	Bedrock	51	—	27	2830	—	—	—

Seattle, Washington

The Seattle site consists of artificial fill over a thick layer of deltaic sand and estuarine silt, overlying a dense layer of reworked glacial deposits to a depth *H* of 56.5 m, which represents dense preglacial deposits that are modeled as soft rock (V_{Sb} = 760 m/s). The bottom of the soil profile is consistent with the lowest downhole seismometer at the Seattle Liquefaction Array (Shannon and Wilson, 2018); this report was also used as the basis for the assumed V_S profile (which was developed from suspension P-S logging). A layer of glacial till underlies the location of the downhole seismometer, and heavily overconsolidated pre-glacial layers exist beneath this location. Numerous studies in the Seattle area (e.g. Williams et al., 1999) evaluating ground-motion amplifications have concluded that most of the observed amplifications are due to the upper layers (which consist of younger alluvium, i.e. post-glacial Holocene deposits), specifically the impedance contrast between the younger and older alluvium. Therefore, site response will be neglected beneath a depth of 56.5 m. The source-to-receiver (S-R1) measurements at Boring S-3 were used as the basis for the V_S profile; the point measurements from the raw data of Shannon and Wilson (2018) were discretized into sublayers of 0.75 m to 1 m thick. The soil layer types and thicknesses were determined primarily from Boring S-3, although boring SD-122 was also considered (Shannon and Wilson, 2018). The groundwater table was assumed to be 3 m, consistent with many observations in the area and consistent with Boring S-3 (Shannon and Wilson, 2018). The unit weights of soils were derived from median values of Coduto et al. (2011) as a function of soil type. The plasticity indices of the clayey fill (CH) and estuarine silt (ML) were assumed from the results of Atterberg limit tests presented in Shannon and Wilson (2018); all other layers were assumed to be non-plastic. An overconsolidation ratio of 1 was assumed throughout the soil profile, and the at-rest lateral earth-pressure coefficient was assumed to be 0.5 in all layers.

The time-averaged shear-wave velocity over the top 30 m of the subsurface (V_{S30}) is 135.1 m/s, making this a NEHRP Class E site. The geologic materials beneath 56.5 m are assumed to represent Site Class B/C (760 m/s) and are modeled as an elastic halfspace with 2% damping (for time domain analyses, the damping of the elastic halfspace does not enter the calculation and has no impact on the results). The time-averaged shear-wave velocity over the entire 56.5-m-thick soil profile is 167.2 m/s, meaning that the fundamental site frequency (based on average shear-wave velocity) is $V_{S,avg}$ / (4H) = 0.74 Hz. The corresponding fundamental site period based on $V_{S,avg}$ is therefore 1 / (0.74 Hz) = 1.35 s. The one-dimensional (1D) linear theoretical surface/outcrop amplification spectrum for the Boston location is plotted in Figure 6.4. The fundamental peak of the 1D amplification spectrum occurs at 0.92 Hz, corresponding to a

fundamental site period of 1.09 s (slightly less than the fundamental site period based on $V_{S,avg}$). Analyses of earthquake data from Williams et al. (1999) near the Seattle downhole array indicate a resonant frequency of approximately 0.9 Hz, meaning the corresponding period is between 1.1 s and 1.2 s, consistent our estimates of the fundamental site periods.

A simplified geotechnical profile for Seattle is shown in Table 6.3. The minimum shear-wave velocity ($V_{S,min}$) is 90 m/s at the top of the profile. To ensure adequate sublayer thicknesses for the transmission of high-frequency seismic energy in nonlinear site response calculations, sublayer thicknesses of 0.75 m were used for the top 9 m of the profile, and sublayer thicknesses of 1 m were used for all depths greater than 9 m (with the exception of the bottom sublayer in the profile, which was 1.5 m). The maximum frequency of transmission at the top of the profile (the critical point) for nonlinear calculations is therefore $V_{S,min} / (4h)$ = 30 Hz. A table of the full geotechnical and shear-wave velocity profile (with entries for each sublayer) is provided in Table 6.4.

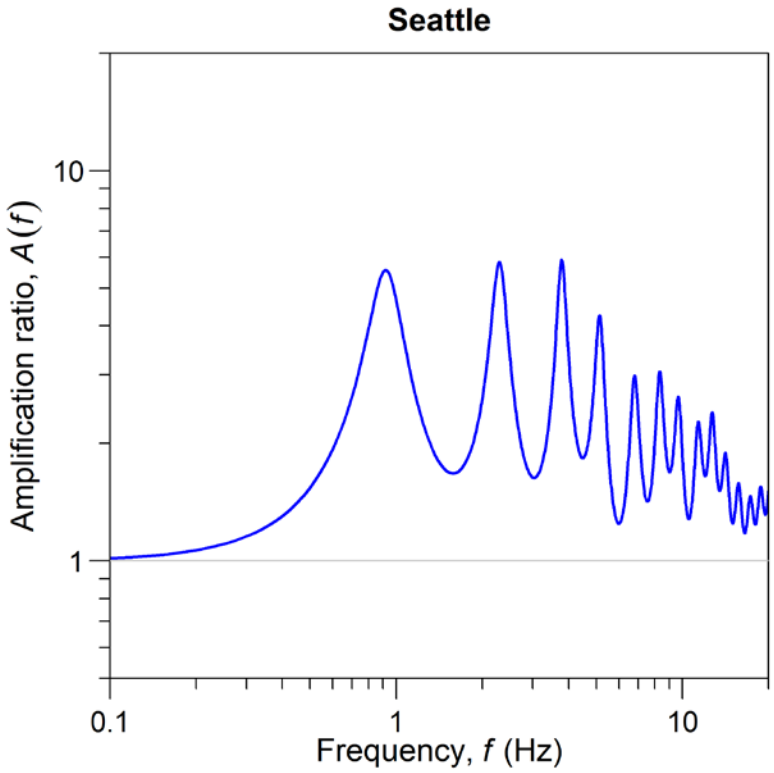

Figure 6.4. One-dimensional linear theoretical surface/outcrop amplification spectrum for Seattle.

Table 6.3. Simplified geotechnical profile for Seattle, Washington

Layer name	Geologic unit symbol	Predominant soil type and classification*	Depth of layer top (m)	Thick-ness (m)	Unit weight, γ (kN/m^3)	Plasticity Index, PI	Over-consolidation ratio, OCR
Gravelly fill	Hf	Gravel (GM)	0	1	18	0	1
Silty fill	Hf	Silt (ML)	1	2	15	0	1
Clayey fill	Hf/He	Clay (CH)	3	3	15	30	1
Deltaic sand	Ha	Sand (SP/SM)	6	35	19.5	0	1
Sandy silt / fine sand	Ha/He	Silt/sand (ML/SM)	41	4	18	0	1
Estuarine silt	He	Silt (ML)	45	8	16	15	1
Reworked glacial deposits / outwash sand	Hrw / Qpgo	Sand (SM)	53	3.5	21	0	1
Rock (B/C)		—	56.5	—	27	—	—

* From the Unified Soil Classification System

Table 6.4. Full geotechnical and V_S profiles for Seattle, Washington

Layer No.	Material	Depth of layer top (m)	Thickness (m)	Unit weight, γ (kN/m^3)	Shear-wave velocity, Vs (m/s)	Plasticity Index, PI	Over-consolidation ratio, OCR	At-rest lateral earth pressure coef., K_o
1	Gravelly fill	0	0.75	18	90	0	1	0.5
2	Silty fill	0.75	0.75	15	90	0	1	0.5
3	Silty fill	1.5	0.75	15	90	0	1	0.5
4	Silty fill	2.25	0.75	15	91	0	1	0.5
5	Clayey fill	3	0.75	15	99	30	1	0.5
6	Clayey fill	3.75	0.75	15	100	30	1	0.5
7	Clayey fill	4.5	0.75	15	103	30	1	0.5
8	Clayey fill	5.25	0.75	15	110	30	1	0.5
9	Deltaic sand	6	0.75	19.5	111	0	1	0.5
10	Deltaic sand	6.75	0.75	19.5	111	0	1	0.5
11	Deltaic sand	7.5	0.75	19.5	114	0	1	0.5
12	Deltaic sand	8.25	0.75	19.5	124	0	1	0.5
13	Deltaic sand	9	1	19.5	139	0	1	0.5
14	Deltaic sand	10	1	19.5	150	0	1	0.5
15	Deltaic sand	11	1	19.5	153	0	1	0.5
16	Deltaic sand	12	1	19.5	136	0	1	0.5
17	Deltaic sand	13	1	19.5	137	0	1	0.5
18	Deltaic sand	14	1	19.5	121	0	1	0.5

Layer No.	Material	Depth of layer top (m)	Thickness (m)	Unit weight, γ (kN/m^3)	Shear-wave velocity, Vs (m/s)	Plasticity Index, PI	Over-consolidation ratio, OCR	At-rest lateral earth pressure coef., K_o
19	Deltaic sand	15	1	19.5	129	0	1	0.5
20	Deltaic sand	16	1	19.5	148	0	1	0.5
21	Deltaic sand	17	1	19.5	142	0	1	0.5
22	Deltaic sand	18	1	19.5	155	0	1	0.5
23	Deltaic sand	19	1	19.5	160	0	1	0.5
24	Deltaic sand	20	1	19.5	154	0	1	0.5
25	Deltaic sand	21	1	19.5	160	0	1	0.5
26	Deltaic sand	22	1	19.5	175	0	1	0.5
27	Deltaic sand	23	1	19.5	179	0	1	0.5
28	Deltaic sand	24	1	19.5	181	0	1	0.5
29	Deltaic sand	25	1	19.5	181	0	1	0.5
30	Deltaic sand	26	1	19.5	189	0	1	0.5
31	Deltaic sand	27	1	19.5	195	0	1	0.5
32	Deltaic sand	28	1	19.5	192	0	1	0.5
33	Deltaic sand	29	1	19.5	193	0	1	0.5
34	Deltaic sand	30	1	19.5	200	0	1	0.5
35	Deltaic sand	31	1	19.5	205	0	1	0.5
36	Deltaic sand	32	1	19.5	208	0	1	0.5
37	Deltaic sand	33	1	19.5	213	0	1	0.5
38	Deltaic sand	34	1	19.5	216	0	1	0.5
39	Deltaic sand	35	1	19.5	216	0	1	0.5
40	Deltaic sand	36	1	19.5	210	0	1	0.5
41	Deltaic sand	37	1	19.5	216	0	1	0.5
42	Deltaic sand	38	1	19.5	217	0	1	0.5
43	Deltaic sand	39	1	19.5	212	0	1	0.5
44	Deltaic sand	40	1	19.5	213	0	1	0.5
45	Sandy silt / fine sand	41	1	18	210	0	1	0.5
46	Sandy silt / fine sand	42	1	18	213	0	1	0.5
47	Sandy silt / fine sand	43	1	18	213	0	1	0.5
48	Sandy silt / fine sand	44	1	18	216	0	1	0.5
49	Estuarine silt	45	1	16	215	15	1	0.5
50	Estuarine silt	46	1	16	218	15	1	0.5
51	Estuarine silt	47	1	16	220	15	1	0.5
52	Estuarine silt	48	1	16	216	15	1	0.5
53	Estuarine silt	49	1	16	219	15	1	0.5
54	Estuarine silt	50	1	16	219	15	1	0.5
55	Estuarine silt	51	1	16	224	15	1	0.5
56	Estuarine silt	52	1	16	260	15	1	0.5
57	Reworked glacial deposits	53	1	21	341	0	1	0.5
58	Reworked glacial deposits	54	1	21	377	0	1	0.5
59	Reworked glacial deposits	55	1.5	21	412	0	1	0.5
60	Rock (Site Class B/C)	56.5	—	27	760	—	—	—

6.3 Site Response Methods

The ground motions at the surface of the sites were predicted with site response analyses using the program DEEPSOIL (Hashash et al., 2018). A suite of ground motion predictions were obtained at the ground surface for the various input motions (applied at the base of the profile) and soil profiles. Within DEEPSOIL, a nonlinear (NL) total-stress site response analysis was performed in the time domain, and a complementary equivalent-linear (EQL) site response analysis was performed in the frequency domain. For all layers, the Darendeli (2001) modulus-reduction and damping curves were used in the equivalent-linear analyses and as the target relations for the nonlinear analyses. The assumed OCR, K_o, and PI are listed for each layer in Tables 6.2 and 6.4, and the default parameters recommended by Darendeli (2001) are used for number of cycles (N = 10) and frequency (f = 1). For the equivalent-linear (frequency domain) calculations, an effective shear strain ratio of 0.65, number of iterations of 15, and frequency-independent complex shear modulus were specified.

Nonlinear site response analyses were performed using the General Quadratic/Hyperbolic constitutive Model (GQ/H) (Groholski et al., 2016) coded into DEEPSOIL. This constitutive model incorporates shear strength corrections at large strains, is used instead of the Pressure-Dependent Modified Kondner Zelasko (MKZ) model (Matasovic and Vucetic, 1993) that does not account for shear strength. The large shear strains incurred throughout the soil profile in Seattle necessitated the use of a constitutive model that accounts for shear strength; the differences were less substantial in Boston, where the levels of induced shear strain were found to be smaller. At all sites, the shear strength *s* of fine-grained soils (silts and clays) was calculated after Ladd (1991) using an undrained total-stress analysis (where the shear strength is assumed to equal the undrained shear strength, s_u, without any contribution from the frictional resistance of the soil):

$$s = s_u = 0.22\ OCR^{0.8}\sigma'_{vo}\ , \tag{6.1}$$

where OCR = overconsolidation ratio and σ'_{vo} = initial effective vertical stress at the midpoint of the layer of interest. This calculation leads to $s = 0.22\sigma'_{vo}$ for OCR = 1, and $s = 0.383\sigma'_{vo}$ for OCR = 2. The shear-strength of coarse-grained soils was calculated using the Mohr-Coulomb strength criterion with generic values of effective friction angles (30° for sands and 35° for gravels):

$$s = \sigma'_{vo} \tan \phi'\ , \tag{6.2}$$

where ϕ' = effective friction angle of the soil. This calculation leads to $s = 0.577\sigma'_{vo}$ for sands, and $s = 0.700\sigma'_{vo}$ for gravels.

For the nonlinear (time domain) calculations, flexible step control with a maximum strain increment of 0.005%, implicit integration using the Newmark Beta method, and linear time-history interpolation were selected. The fitting for the non-Masing unload/reload parameters was performed using the MRDF pressure-dependent hyperbolic model procedure (Phillips and Hashash, 2009) in DEEPSOIL. The bedrock was represented as an elastic halfspace in all analyses.

6.4 Results of Site Response Analyses

Output of site response analyses

After the analyses are performed in DEEPSOIL, the following two types of information are extracted from the output:

1. Time series at the ground surface (acceleration, velocity, displacement, shear strain, shear stress ratio).
2. Profiles of maximum response versus depth, for each sublayer (peak ground acceleration, maximum shear strain, maximum shear stress ratio)

The post-processing and subsequent computational analyses of the site response results performed using the open-source statistical language and environment R (R Core Team, 2018). From the predicted acceleration time series at the ground surface, we calculated the 5%-damped pseudo-acceleration response spectra (PSA), amplification spectra (relative to the input motion at the base profile), and Husid plots of accumulated Arias Intensity as a function of time. The following ground-motion intensity measures were computed and tabulated for each record: peak ground acceleration (PGA); PSA at spectral periods (T) of 0.1, 0.2, 0.5, 1, and 3 s; cumulative absolute velocity (CAV); Arias Intensity (I_a); and significant duration measured from the portion of the time series corresponding to 5% to 95% seismic energy release ($D_{5\text{-}95}$), and 5% to 75% seismic energy release ($D_{5\text{-}75}$). The two horizontal components of ground motion were combined using the geometric mean.

Analysis of intra-suite ground-motion records

For each of the ground-motion suites assessed in this study, we created detailed plots of the input and predicted ground motions in order to gain a more physical understanding of the site response behavior. In Figures 6.5 and 6.6, we provide two example plots of the nonlinear site response results for Boston and Seattle, respectively. The results are provided for the conditional spectra for a hazard level of 2% in 50 years corresponding to a spectral period of T = 0.01 s. For Boston (Figure 6.5), the input motions were selected for the dominant scenario from the deaggregation representing a near-source earthquake of moment magnitude **M** = 5.5 and source-to-site distance R_{rup} = 30 km. For Seattle (Figure 6.6), the input motions were selected for the shallow-crustal earthquake dominant scenario with **M** = 7.0 and R_{rup} = 5 km. The figures display the following:

(a) Acceleration time series: input and predicted (for one horizontal component of the first record in the suite)
(b) Acceleration time series (zoomed at maximum acceleration), input and predicted (for one horizontal component of the first record in the suite)
(c) Husid plots, input and predicted (for one horizontal component of the first record in the suite)
(d) Response spectra, input and predicted (for each record in the suite, along with the median)
(e) Amplification spectra, predicted (for each record in the suite, along with the median)
(f) Profiles of PGA, predicted (for each record in the suite, along with the median)
(g) Shear-wave velocity, input
(h) Profiles of maximum shear strain, predicted (for each record in the suite, along with the median)

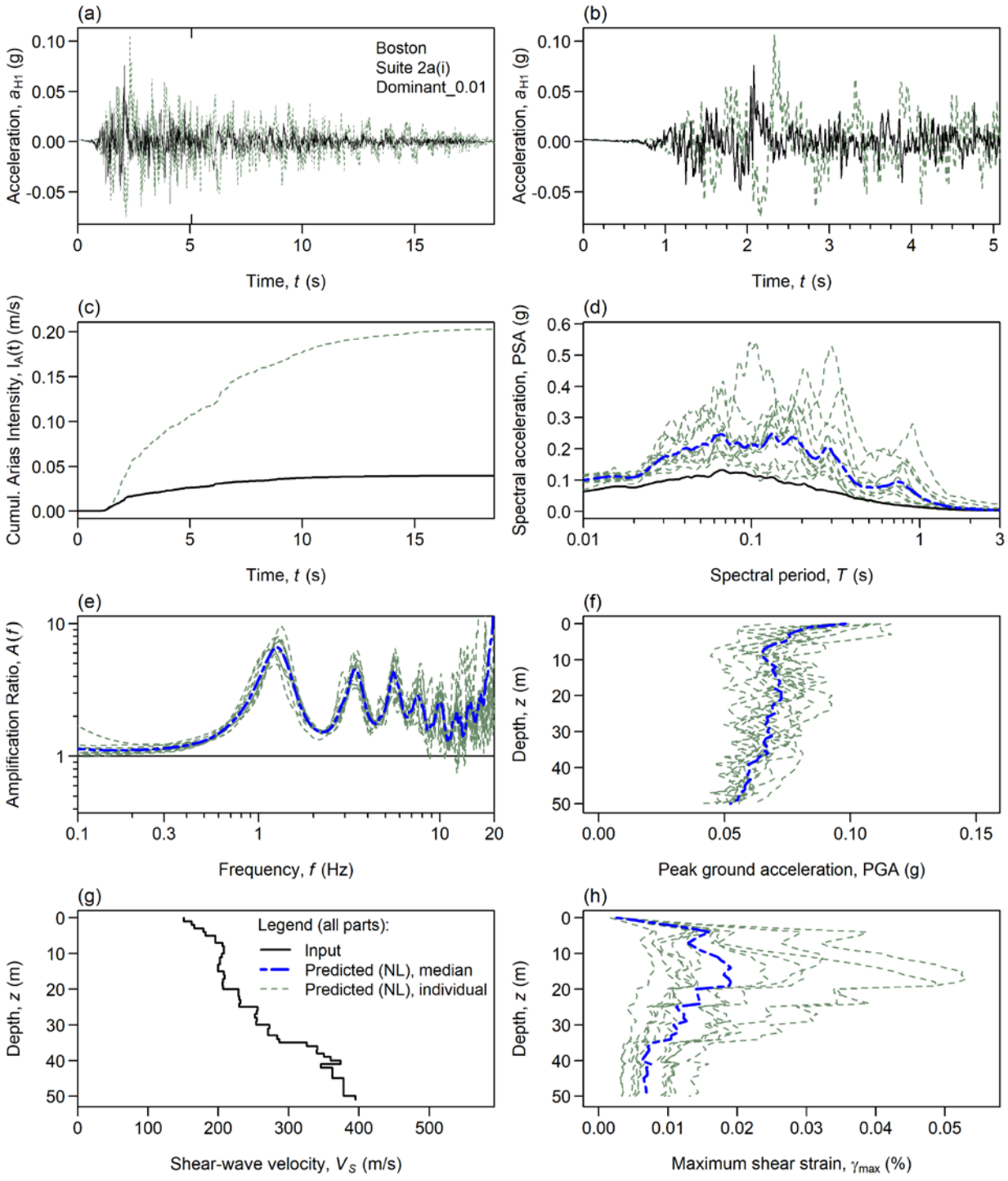

Figure 6.5. Detailed ground-motion plots for the NL analyses in Boston for the suite of ground motions obtained for the conditional spectra for a hazard level of 2% in 50 years corresponding to a spectral period of T = 0.01 s. In this figure, the input motions were selected for the dominant scenario from the deaggregation representing a near-source earthquake of moment magnitude **M** = 5.5 and source-to-site distance R_{rup} = 30 km [Suite 2a(i)]. The figure displays (a) acceleration time series throughout the whole record, (b) acceleration time series zoomed at maximum acceleration, (c) Husid plots, (d) response spectra, (e) amplification spectra, (f) profiles of PGA versus depth, (g) V_S profile, and (h) profiles of maximum shear strain versus depth.

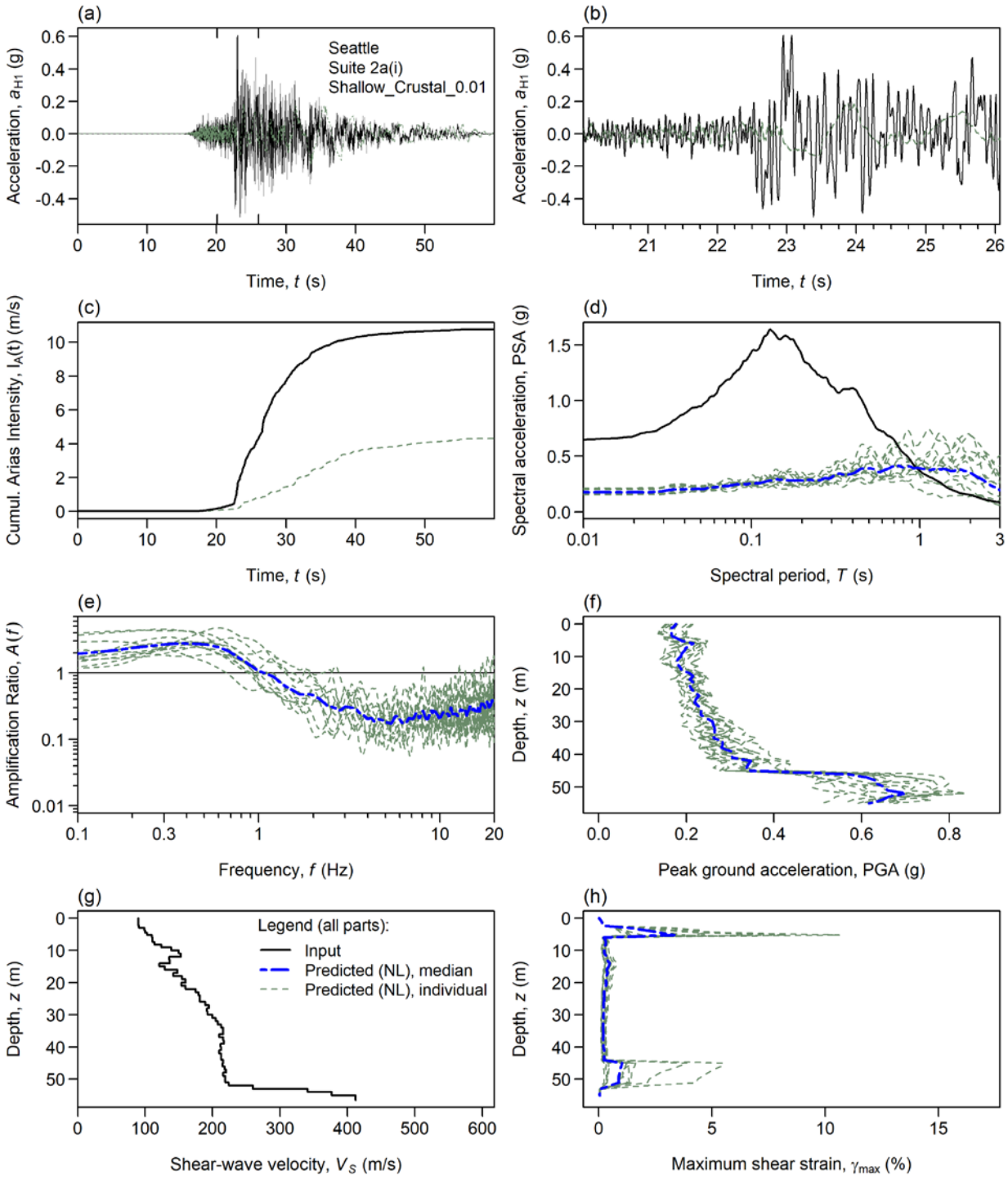

Figure 6.6. Detailed ground-motion plots for the NL analyses in Seattle for the suite of ground motions obtained for the conditional spectra for a hazard level of 2% in 50 years corresponding to a spectral period of T = 0.01 s. In this figure, the input motions were selected for the shallow crustal earthquake dominant scenario from the deaggregation representing a near-source earthquake of moment magnitude **M** = 7.0 and source-to-site distance R_{rup} = 5 km [Suite 2a(i)]. The figure displays (a) acceleration time series throughout the whole record, (b) acceleration time series zoomed at maximum acceleration, (c) Husid plots, (d) response spectra, (e) amplification spectra, (f) profiles of PGA versus depth, (g) V_S profile, and (h) profiles of maximum shear strain versus depth.

For Boston (Figure 6.5), the site response analyses resulted in significant ground-motion amplifications across all frequencies. In Figure 6.5(d), every individual predicted response spectrum at the ground surface plots above the response spectrum from the input motion. There is considerable variation in the individual predicted response spectra, reflecting the differences in the individual input motions. In Figure 6.5(e), all the amplification spectra are greater than unity at nearly every frequency. The PGA profile in Figure 6.5(f) continually increases throughout the profile from the base to the ground surface. The greatest maximum shear strain occurs between depths of 12 and 20 m, in the bottom of the glacial outwash layer and the top of the Boston Blue Clay; the median maximum shear strain is approximately 0.02%, which does not represent a high level of nonlinearity (Kaklamanos et al., 2015; Kaklamanos and Bradley, 2018a).

The results for Seattle are markedly different than those of Boston. The results show an excessive amount of nonlinearity is observed for design-level ground motions in Seattle, leading to significant deamplifications and excessive dissipations of seismic energy within the profile. At frequencies less than 1 Hz (periods greater than 1 s), ground-motion amplifications are observed for nearly all the records, as seen in both the response spectra in Figure 6.6(d) and the amplification spectra in Figure 6.6(e). Nonlinear soil behavior is not expected at such low frequencies, so this result is not surprising. However, at frequencies greater than 1 Hz (periods less than 1 s), all the ground-motion records experience deamplification, and often a significant amount of deamplification. The PGA profile exhibits a continual decrease from the base of the profile to the ground surface, with a substantial decrease occurring near the bottom of the profile during the transition from estuarine silt to deltaic sand. An extreme localization of shear strain occurs at approximately 5 m depth (with a median maximum shear strain of approximately 3%); there are occasional strain localizations deeper in the profile as well. One interesting thing to note about the results for Seattle is that the variability of the predicted response spectra within the suite decreases significantly at short periods.

Additional figures depicting the predicted ground motions from other suites are available in the appendix to this report. In the aggregate, the observed trends for Boston and Seattle are similar to those presented in Figures 6.5 and Figure 6.6. In the next subsection, we will compare the site response results for the different suites of input motions.

Inter-suite comparisons of predicted median response spectra

Figures 6.7 to 6.16 display the predicted surface response spectra (EQL and NL) for the median of each suite of 11 ground motions for Boston and Seattle. The surface response spectra at short periods in Boston display greater variability than those of Seattle, particularly for the CS spectra conditioned at a period of 1 s. The surface response spectra based on the mean values is significantly lower than the surface response spectra based on the dominant scenario. For all CS suites in Boston, the amplifications are similar in the vicinity of the fundamental period of the site (approximately 0.7 s) and at longer periods. For the two UHS suites (representing hazard levels of 2% and 10% probability of exceedance in 50 years), the predicted response spectra for the higher hazard level (lower annual probability of exceedance) is greatest at all periods. For the levels of ground motion associated with these input motions, amplification is being observed (consistent with the results in Figure 6.5). There are minimal differences between the EQL and NL

predictions; for these levels of ground motion, large EQL-NL deviations would not be expected (e.g., Kaklamanos and Bradley, 2018a).

On the other hand, for Seattle, the surface response spectra are much more similar at short periods than at long periods. Despite significant variations in the spectra of the input motions, it is notable that all the surface response spectra appear to converge at short periods. The median spectra from NL site response models converge between 0.15–0.20*g* at short periods, and the median spectra from EQL site response models converge between 0.20–0.30*g* at short periods. However, due to the high level of nonlinear soil behavior expected for these ground motions, the EQL results are less reliable than the NL results. The conditional spectra conditioned at longer periods (e.g., at T = 1 s and 3 s) show remarkable similarity among the three seismic sources (shallow crustal, intraslab, and interface). The conditional spectra conditioned at shorter periods (up to 0.5 s), however, show much greater deviations at longer periods: the median spectra from intraslab events are substantially lower than the interface and shallow crustal spectra for T > 0.5 s. The intraslab spectra are slightly higher than the other two spectra at moderate periods (T = 0.1 to 0.5 s). All spectra, however, converge at shorter periods.

A high degree of nonlinearity is predicted at Seattle; relative to the input spectra, there is significant deamplification in the surface ground motions at short periods. It is striking that the predicted peak ground accelerations appear similar for many suites between Boston and Seattle, two cities with extremely different seismic hazards. Nonlinear effects are less significant at longer periods, and therefore the predicted long-period motion is significantly greater for Seattle than Boston, as expected. For Seattle, the difference in the surface response spectra for three different scenarios – particularly at long periods – considered shows the importance of considering all dominant scenarios.

The influence of input motion selection protocol seems to have a greater influence in Boston (where the level of nonlinear soil behavior is smaller) compared to Seattle. In Seattle, the effects of the site response modeling assumptions and parameters will likely trump those of the input motion selection protocols, particularly at short periods. In terms of structural demands in Seattle, a more severe loading may ultimately occur for a smaller input motion (i.e. corresponding to a lower hazard level), where less deamplification in the soil profile will occur. For example, the two UHS suites (representing hazard levels of 2% and 10% probability of exceedance in 50 years) offer similar predictions at spectral periods less than 1 s. Future sensitivity analyses may determine the hazard level that results in the greatest predicted surface ground motions. Given the relationship between amplification and nonlinearity in Seattle, the most severe surface ground motions may not necessarily correspond to the largest input motions; that is, a lower hazard level (with less deamplification) may govern.

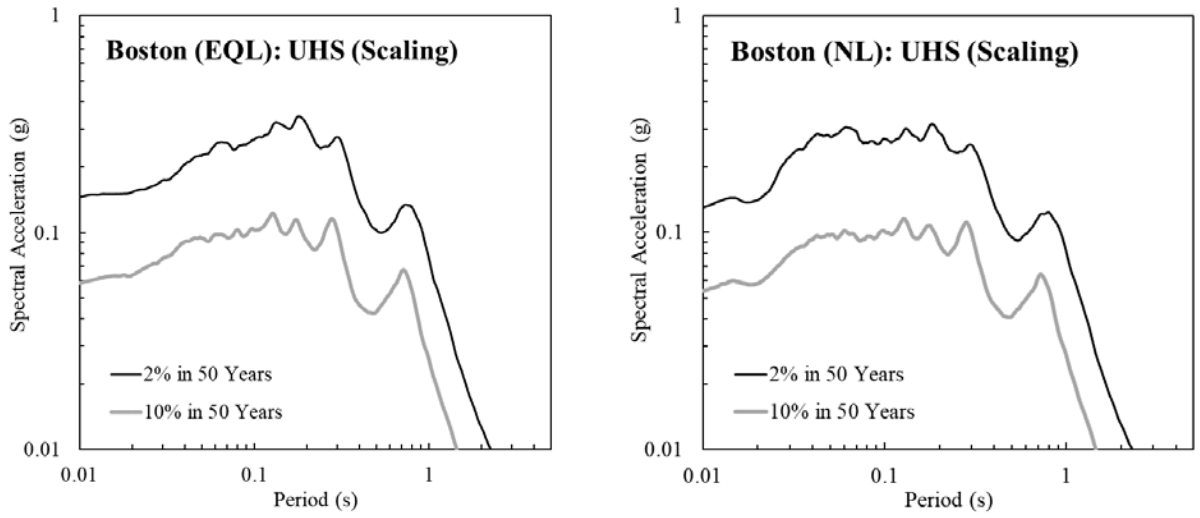

Figure 6.7. Predicted surface response spectra from EQL and NL site response analyses for the medians of two suites obtained by scaling to the Uniform Hazard Spectra (UHS) in Boston.

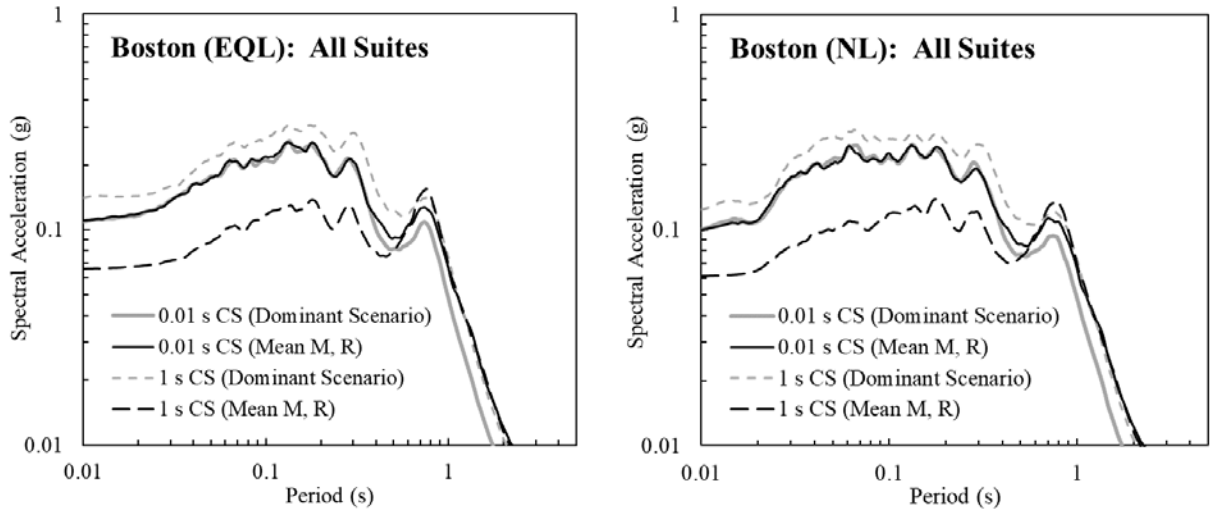

Figure 6.8. Predicted surface response spectra from EQL and NL site response analyses for the medians of the four suites obtained by scaling to the Conditional Spectra (CS) in Boston.

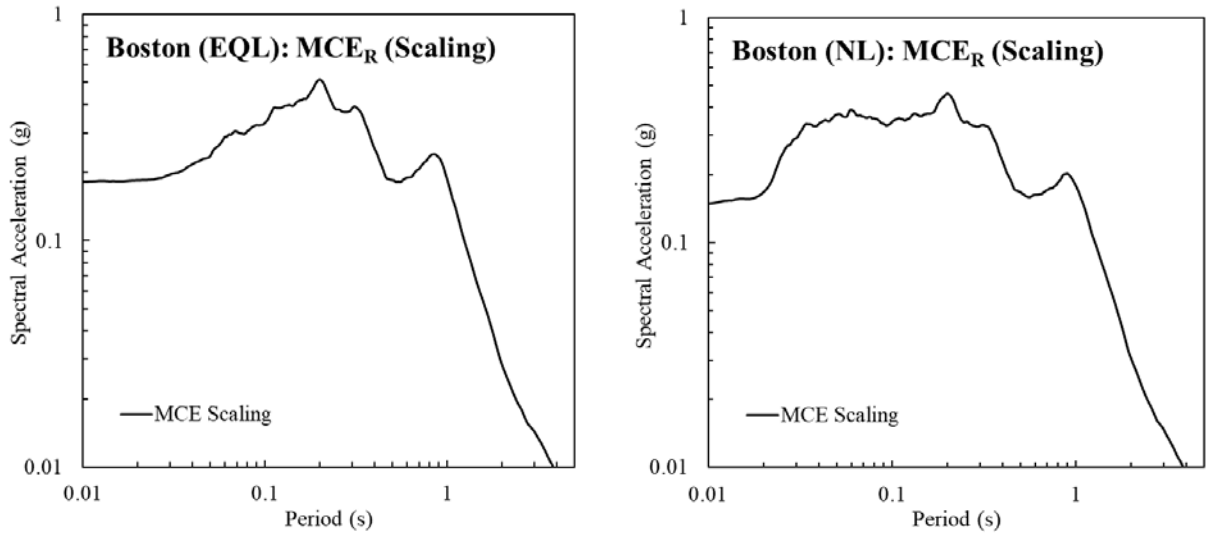

Figure 6.9. Predicted surface response spectra from EQL and NL site response analyses for the medians of the four suites obtained by scaling to the MCE_R spectrum in Boston.

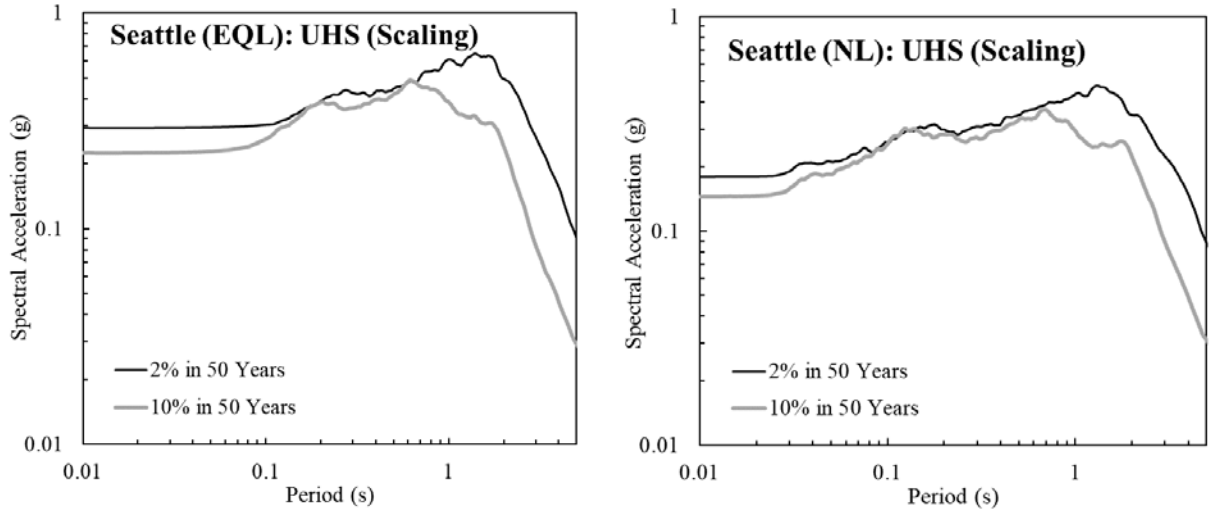

Figure 6.10. Predicted surface response spectra from EQL and NL site response analyses for the medians of the two suites obtained by scaling to the Uniform Hazard Spectra (UHS) in Seattle.

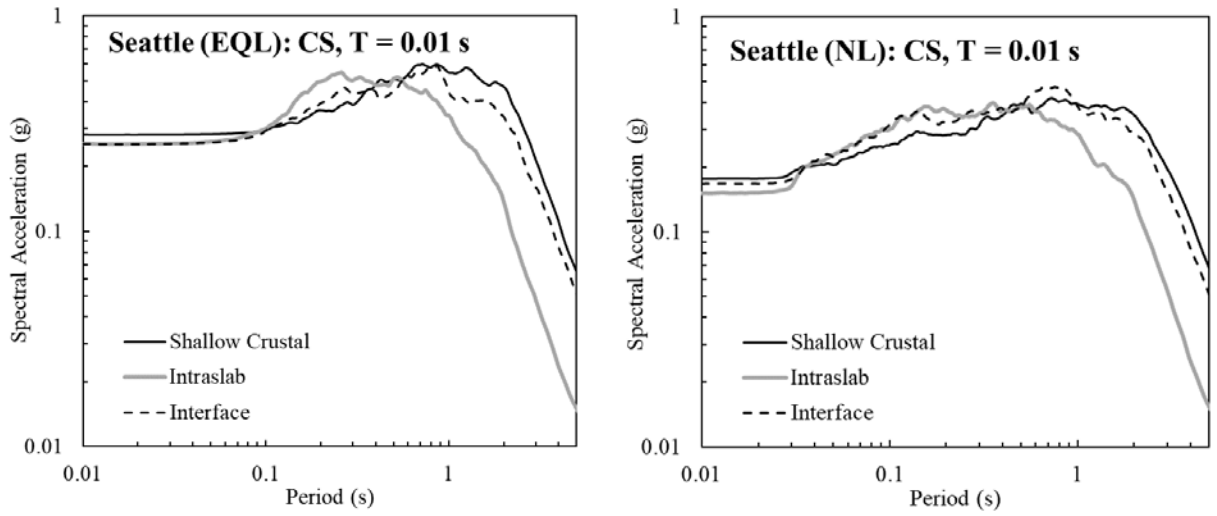

Figure 6.11. Predicted surface response spectra from EQL and NL site response analyses for the medians of the three suites (representing three distinct seismic sources) matching the Conditional Spectrum (CS) at T = 0.01 s in Seattle.

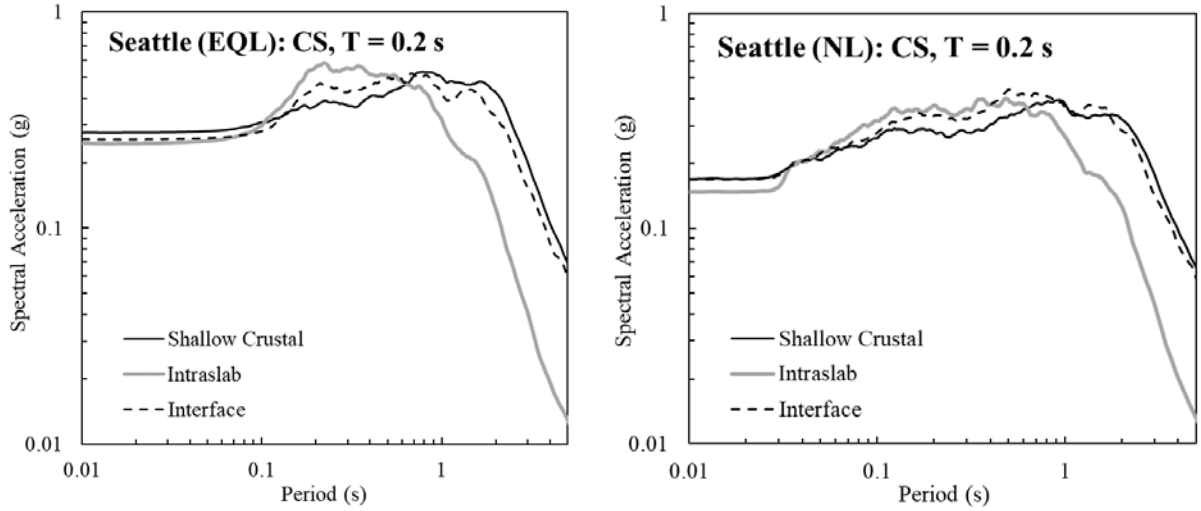

Figure 6.12. Predicted surface response spectra from EQL and NL site response analyses for the medians of the three suites matching the Conditional Spectrum (CS) at T = 0.2 s in Seattle.

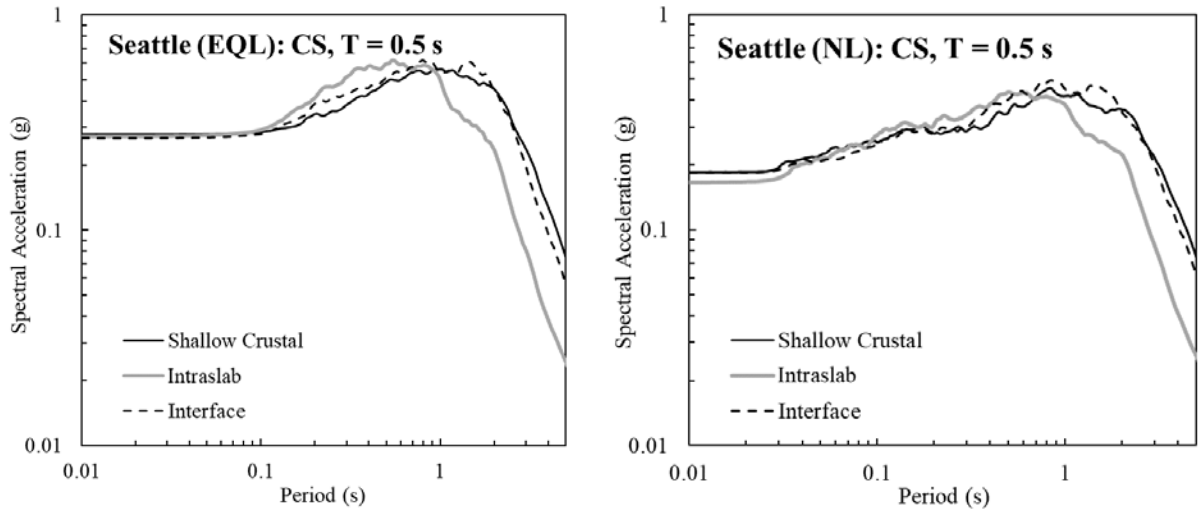

Figure 6.13. Predicted surface response spectra from EQL and NL site response analyses for the medians of the three suites matching the Conditional Spectrum (CS) at T = 0.5 s in Seattle.

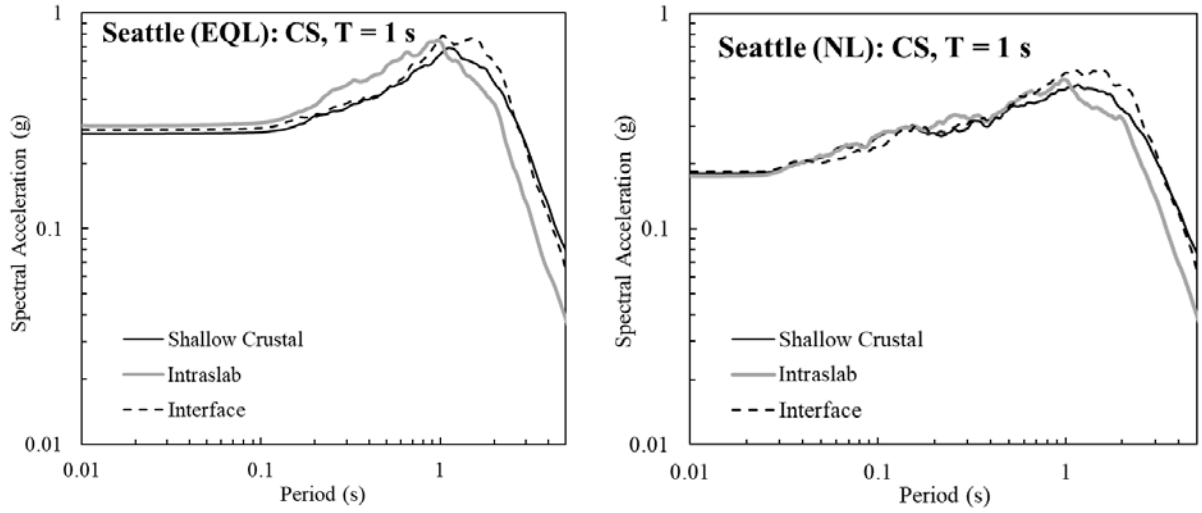

Figure 6.14. Predicted surface response spectra from EQL and NL site response analyses for the medians of the three suites matching the Conditional Spectrum (CS) at T = 1 s in Seattle.

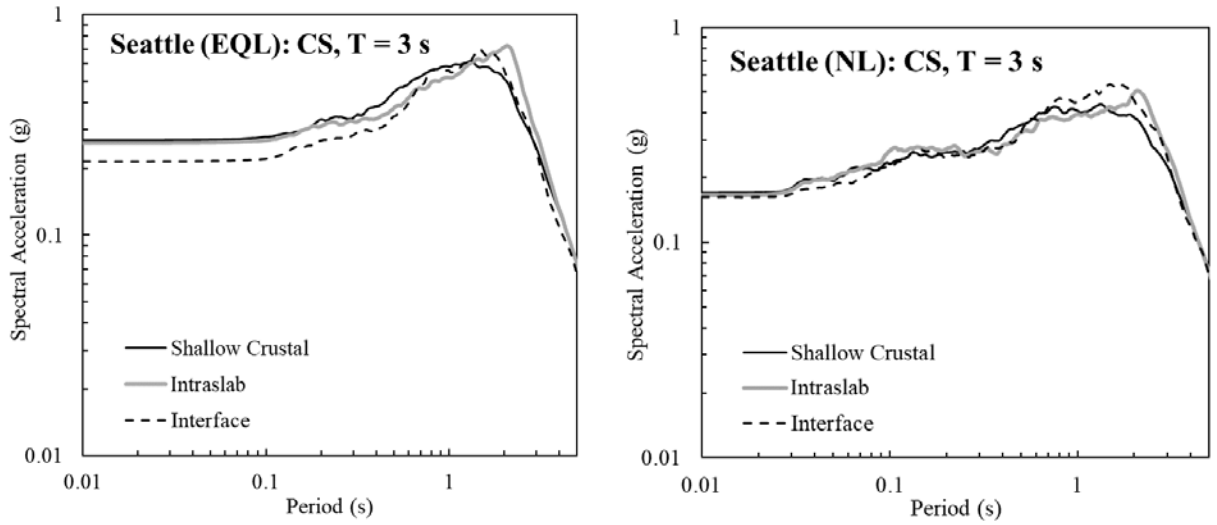

Figure 6.15. Predicted surface response spectra from EQL and NL site response analyses for the medians of the three suites matching the Conditional Spectrum (CS) at T = 3 s in Seattle.

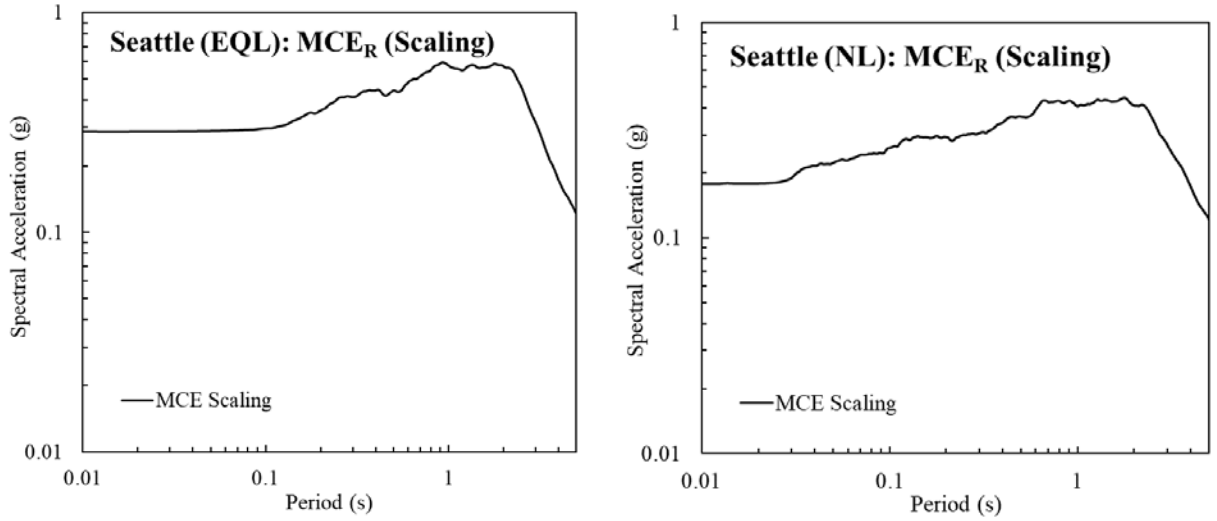

Figure 6.16. Predicted surface response spectra from EQL and NL site response analyses for the median of the suite obtained by scaling to the Maximum Considered Earthquake (MCE_R) from ASCE 7-16 in Seattle.

Intra-suite comparisons of variability in median response spectra

The results in this chapter have illustrated that there is surprisingly low variability in the short-period predicted surface response spectra for Seattle, across all suites and the ground motions within these suites. In Figures 6.17 to 6.19, to further investigate this observation, we display plots of the intra-suite standard deviation $\sigma_{\ln SA}$ of the predicted NL response spectra within each suite, as a function of spectral period. Figure 6.17 displays $\sigma_{\ln SA}$ for the UHS and CS suites in Boston, and Figures 6.18 and 6.19 display the corresponding spectra for Seattle.

Across the board, there is significantly less variability in the predicted surface ground motions in Seattle than Boston. For all sites and suites (with the exception of the CS suites conditioned at T = 1 s in Boston), the variability is greatest at longer periods, and there is a decrease in the variability as the spectral period decreases. However, the extremely low values of $\sigma_{\ln SA}$ at short periods for the Seattle suites are noteworthy; we find that $\sigma_{\ln PGA} < 0.2$ for all suites in Seattle; for some suites, the intra-suite standard deviations for PGA are closer to 0.1 natural logarithmic unit. For Boston, the CS suites conditioned at T = 0.01 s have $\sigma_{\ln PGA} \approx 0.2$ (corresponding to the conditioning period), but the values are greater for all other suites, and exceed 0.4 natural logarithmic units for three of the four other suites considered. These results underscore our finding that input motion selection protocols have a more significant influence on site-response model predictions at short spectral periods in cases where less nonlinear soil behavior occurs.

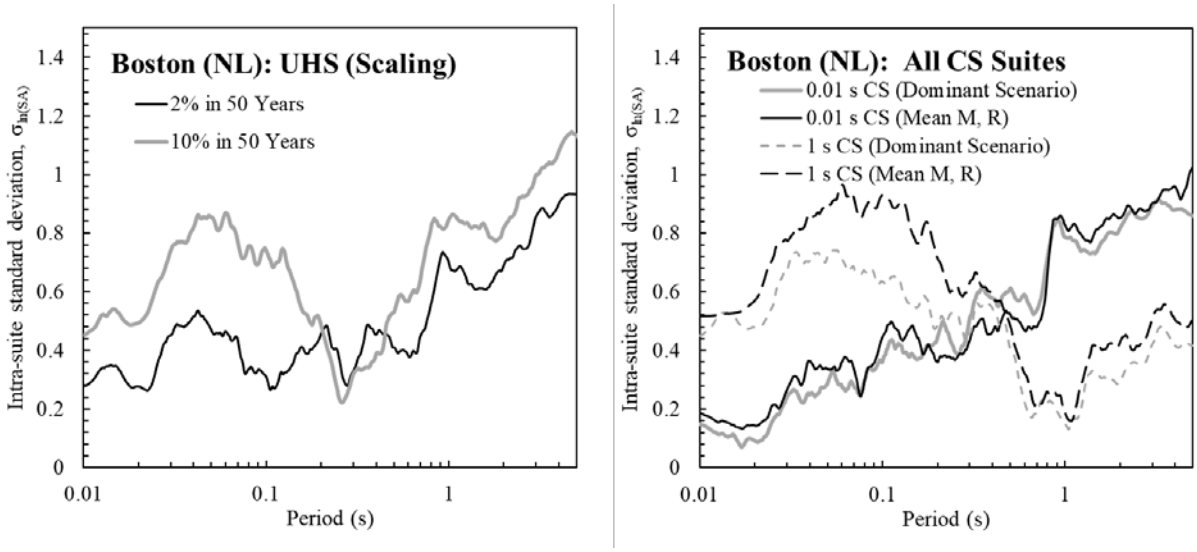

Figure 6.17. Plots of the intra-suite standard deviation for the predicted UHS and CS response spectra as a function of spectral period for Boston.

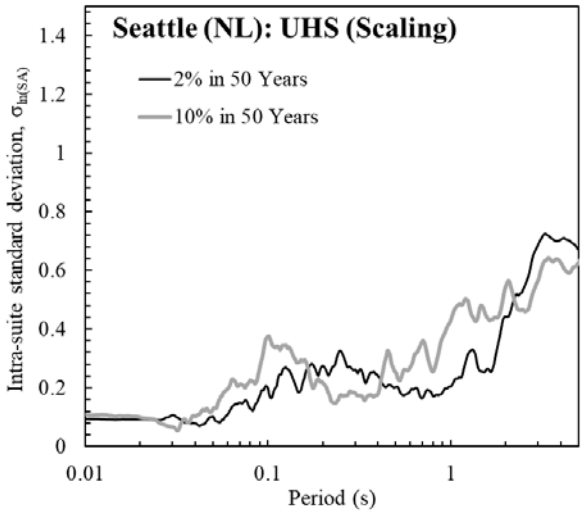

Figure 6.18. Plots of the intra-suite standard deviation for the predicted UHS response spectra as a function of spectral period for Seattle.

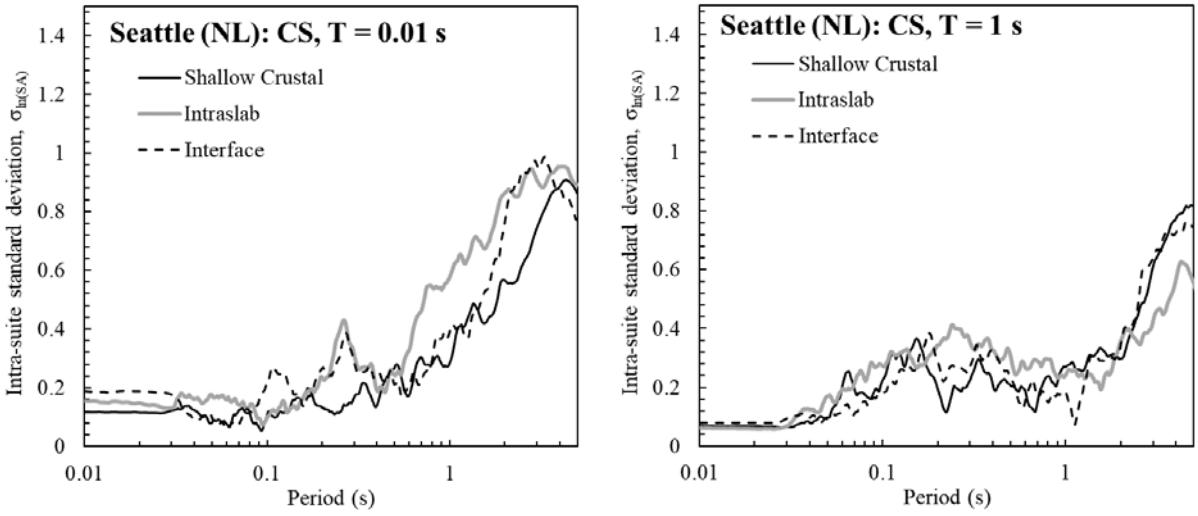

Figure 6.19. Plots of the intra-suite standard deviation for the predicted CS response spectra (at conditioning periods of 0.01 s and 1 s) as a function of spectral period for Seattle.

7 Discussion

7.1 Comparison of CMS for Different M-R Scenarios

For CMS calculations, most studies have focused on selecting the mean magnitude-distance (M-R) values from deaggregations at the conditioning period (Baker 2011, Stewart et al. 2014). In several cases, the dominant earthquake scenario, which has the highest contribution to the hazard, was used (Baker 2015, Haselton et al. 2017). Harmsen et al. (1999) had studied the deaggregation plots of 49 cities in the CEUS and investigated the effects using of mean and modal M-R values in deterministic engineering design. They found that the mean values may correspond to the earthquakes having little contribution to the hazard and that the modal values can be dependent on the binning details of the PSHA. Moreover, the mean tends to average out the M and R values, as it considers small-magnitude earthquakes. Lin et al. (2013) calculated the CMS incorporating multiple causal earthquakes and GMPEs, and compared those to the CMS calculated from the mean M-R combination and single GMPEs. They presented three approximate methods and one exact method for the CMS calculation. The exact method, the most complex one, uses all the M-R bins and deaggregation weights for each GMPE from the PSHA. However, due to the complexity of this method and often the extensive deaggregation results not being available, researchers are still widely using a single M-R combination to calculate the CMS instead (e.g. Hashash et al. 2015, Petermann and Rathje 2017). Moreover, the exact CMS can have the tendency to average out the CMS due to consideration of M-R bins with low contribution to the hazard. Using a single M-R combination may not always be representative of the hazard at the site, especially in cases where the site has multiple contributors to the seismic hazard (i.e., multiple seismic sources). Such conditions may arise due to the complex tectonic setting of the site and may result in multiple dominant scenarios (M-R combinations having highest contribution to the hazard). This is exactly the case of our study site in Seattle.

Seattle has dominant M-R scenarios resulting from shallow crustal, subduction-intraslab, and subduction-interface events (Figure 5.1). For the purposes of input motion selection for the CMS, solely focusing on the mean magnitude-distance combination (M = 7.13, R = 47.88 km) will not provide us with the complete picture of the seismic hazard at this site. Moreover, the diverse tectonic setting in Seattle requires multiple types of GMPEs to be used for the PSHA. Choosing a single type of GMPE to calculate the CMS using the mean M-R values from the deaggregation in such environments poses a challenge. We computed the CMS for the mean M-R combination using crustal GMPEs and subduction intraslab GMPEs separately for comparison purposes. We also computed the conditional mean spectra for shallow crustal, subduction-interface, and subduction-intraslab dominant scenarios separately using their corresponding GMPEs. Figure 7.1 shows the comparison of CMS computed with different M-R scenarios and GMPEs for Seattle.

It can be observed from Figure 7.1 that the target spectra for the mean M-R scenarios often have lower values than the other dominant scenarios. Hence, the usage of a mean M-R combination from the deaggregation is not always representative of the seismic hazard at the site. The shallow crustal and intraslab dominant scenarios (not the mean) have higher spectral accelerations at shorter periods (Figure 7.1b). In contrast, the interface events have higher spectral accelerations at longer periods, which are expected for distant large magnitude earthquakes (e.g. M = 9.0, R = 100 km).

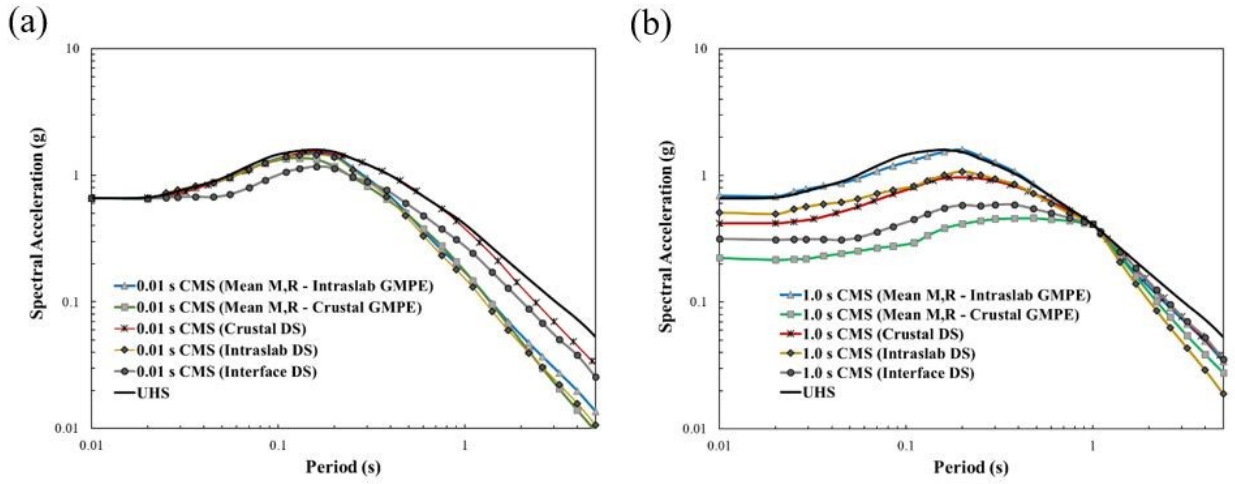

Figure 7.1. UHS and CMS at Seattle for selected scenarios (M-R combinations) for conditioning periods of (a) 0.01 s and (b) 1 s.

Boston, on the other hand, has diffuse seismicity and no particular dominant source (Figure 5.3). The deaggregation plot for Boston corresponding to the 1 s period (Figure 5.3b) does not show any predominant contribution to the hazard associated with a particular seismic source. The mean M-R combination for this case is M = 6.22, R = 149.21 km, which represents a distant earthquake. For comparison purposes, we choose a near-source earthquake with similar contribution to hazard as the dominant scenario (M = 6, R = 30 km). For the 0.01 s conditioning period, we observe higher contributions to the hazard coming from nearby areal sources at distances of 10-50 km (Figure 5.3a). Therefore, we select causal parameters corresponding to this dominant scenario (M = 5.5, R = 30 km) and compare it to results based on mean values from the deaggregation (M = 5.77, R = 58.1 km). Figure 7.2 shows the comparison of CMS computed with different M-R scenarios for Boston.

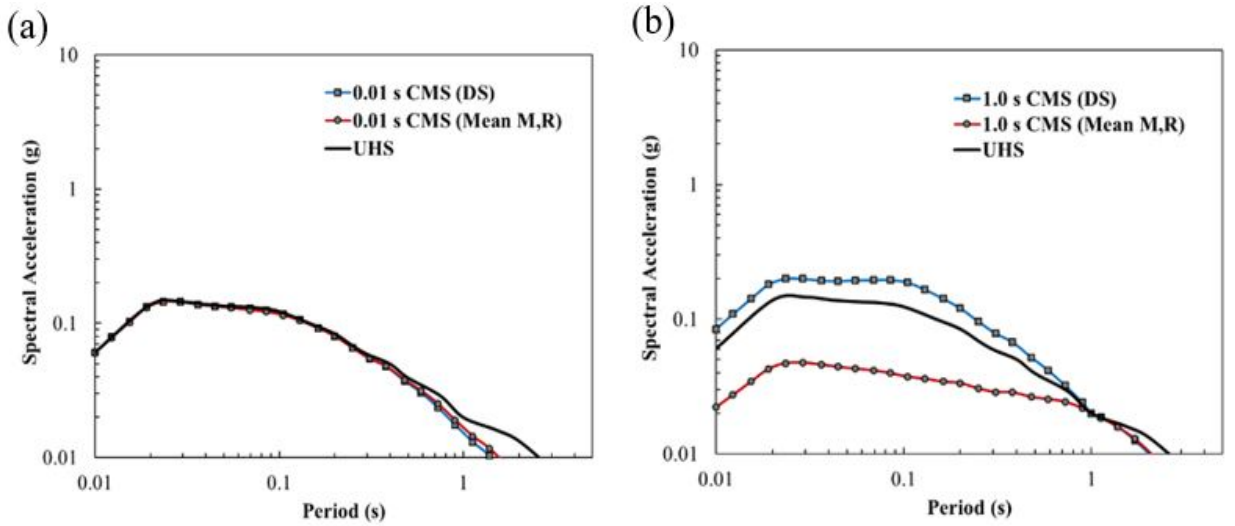

Figure 7.2. UHS and CMS at Boston for selected scenarios (M-R combinations) for conditioning periods of (a) 0.01 s and (b) 1 s.

In the case of Boston, the differences in spectral shapes between the CMS for dominant and mean scenarios at a conditioning period of 0.01 s are not significant (Figure 7.2a). This is expected because the selected dominant scenario (M = 5.5, R = 30 km) is very similar to the mean values (M = 5.77, R = 58.1 km). Nevertheless, the 1.0 s CMS (Figure 7.2b) presents a notable disagreement between the spectral shape corresponding to the mean values and dominant scenarios. Interestingly, we observe that the dominant scenario based on CMS exceeds the UHS. This can be due to the fact that CMS comes from a combination of deterministic and probabilistic method, and it is not unusual for a deterministic spectrum to exceed the UHS.

Figure 7.3 displays the predicted surface response spectra for the medians of the CMS suites conditioned at T = 0.01 s and T = 1 s for Boston and Seattle. The surface response spectra at short periods in Boston display greater variability than those for Seattle, particularly for the spectra conditioned at a period of 1 s. For Boston, the surface response spectra based on the mean values is significantly lower than the surface response spectra based on the dominant scenario (for the CMS conditioned at T = 1 s). For all suites in Boston, the amplifications are similar in the vicinity of the fundamental period of the site (approximately 0.7 s) and at longer periods. For Seattle, the surface response spectra are much similar at short periods than at long periods. Despite significant variations in the CMS of the input motions conditioned at a period of 1 s (Figure 7.1b), it is notable that all the surface response spectra appear to converge between 0.15-0.20*g* for short periods (Figure 7.3). A high degree of nonlinearity is predicted at this site; relative to the input spectra, there is significant deamplification in the surface ground motions at short periods. It is striking that the predicted surface response spectra at short periods (< 0.2 s) are similar between Boston and Seattle, two cities with extremely different seismic hazards. Nonlinear effects are less significant at longer periods, and therefore the predicted long-period motion is greater for Seattle than Boston. For Seattle (Figure 7.3b), the difference in the surface response spectra associated with three different scenarios considered for input motion selection shows the importance of considering all dominant scenarios.

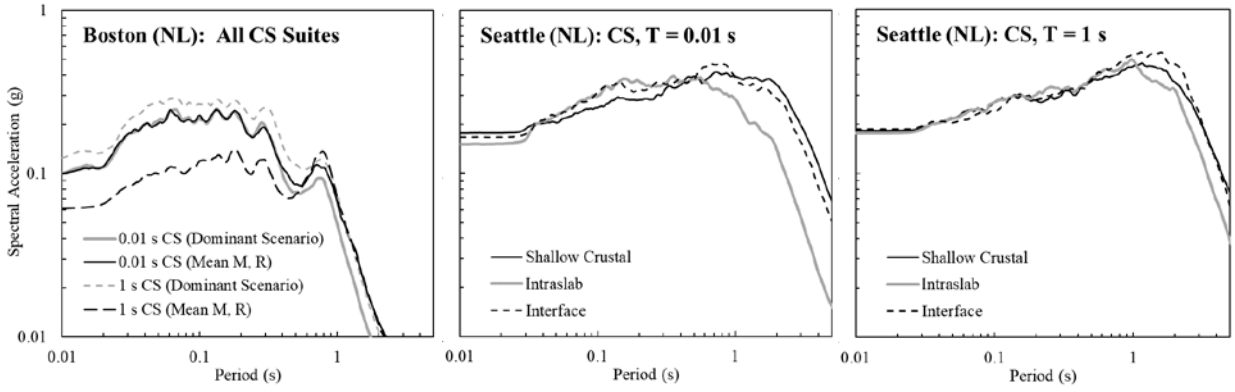

Figure 7.3. Predicted surface response spectra from nonlinear site response analyses for the medians of various suites of ground motions in Boston (left) and Seattle (center and right).

7.2 Comparison of CMS at Different Conditioning Periods

The CMS provides us with an opportunity to observe the differences between target spectra computed for different conditioning periods. Each CMS is computed for a specific conditioning period, and this conditioning period is often the fundamental period of the structure or any other period of interest (e.g., site period). For Seattle, multiple conditional mean spectra were calculated for three different tectonic scenarios: shallow crustal, subduction-intraslab and subduction-interface. In this study, we have computed CMS at different periods ranging from short periods (0.01s, 0.2s, and 0.5s) to longer periods (1s, and 3s) for these three tectonic scenarios. Figure 7.4 shows the comparison of CMS (left) and corresponding predicted response spectra at the surface (equivalent linear in the middle, and nonlinear on the right) after site response analyses are conducted for the different CMS suites (conditioned at different periods) for Seattle. Figures 7.4(a-c) correspond to the shallow crustal scenario (M = 7, R = 5 km), Figure 7.4(d-f) refer to the subduction intraslab scenario (M = 7, R = 50 km) and Figures 7.4(g-i) correspond to the subduction interface scenario (M = 9, R = 100 km).

From Figures 7.4(b-c), we can observe that the response spectra for the shallow crustal earthquake scenario for different conditioning periods are quite similar, with negligible variations in the 0.1-2.0 s period range. The spectra seem compatible with each other before and after this range. However, higher variation is observed for intraslab and interface scenarios [Figures 7.4(e-f) and Figures 7.4(h-i)]. The intraslab scenario has significant variation at both short and long periods. Moreover, the predicted response spectra at the ground surface do not converge for the different input definitions at longer periods, in contrast to the shallow crustal and interface scenarios. The higher variations in the interface response spectra [Figures 7.4(h-i)] is expected because of the variation observed in corresponding target spectra [Figure 7.4(g)]. Hence, the choice of conditioning period seems more crucial for subduction events.

7.3 Comparison of Different Target Spectra

In this study, three types of target spectra are calculated and the corresponding site response results have been compared: uniform hazard spectra (UHS), conditional spectra (CS), and risk-targeted maximum considered earthquake (MCE_R) design spectra. Details of these spectra were presented in Chapter 5. To provide a clear comparison between these spectra, only two CS spectra are chosen, one for a short period of 0.2 s and the other for a long period of 1.0 s. Figure 7.5 shows the comparison of different target spectra (left) and corresponding predicted response spectra at the ground surface (equivalent linear in middle and nonlinear on the right) after site response analyses are conducted for different dominant scenarios (considered for the CMS calculations) for Seattle. The UHS and MCE_R spectra do not vary from scenario to scenario, but they are plotted three times to facilitate the comparison of different tectonic conditions considered for the CMS. The median response spectra corresponding to the UHS and MCE_R spectra for Seattle are quite similar. The response spectra related to shallow crustal scenario CMS (both 0.2 s and 1.0 s) also conforms well to the UHS and MCE_R spectra. However, we observe higher differences for both of the subduction scenarios [Figures 7.5 e, f, h and i). The response spectra has crossed the UHS and MCE_R response spectra at some period ranges even though the target spectra are below those limits. It can be a concern for Seattle where intraslab earthquakes are quite likely (such as the 2001 **M** 6.8 Nisqually earthquake). Further investigations are required to assess if these phenomena are attributed to the use of a different database (such as KiK-net) for ground motion selection.

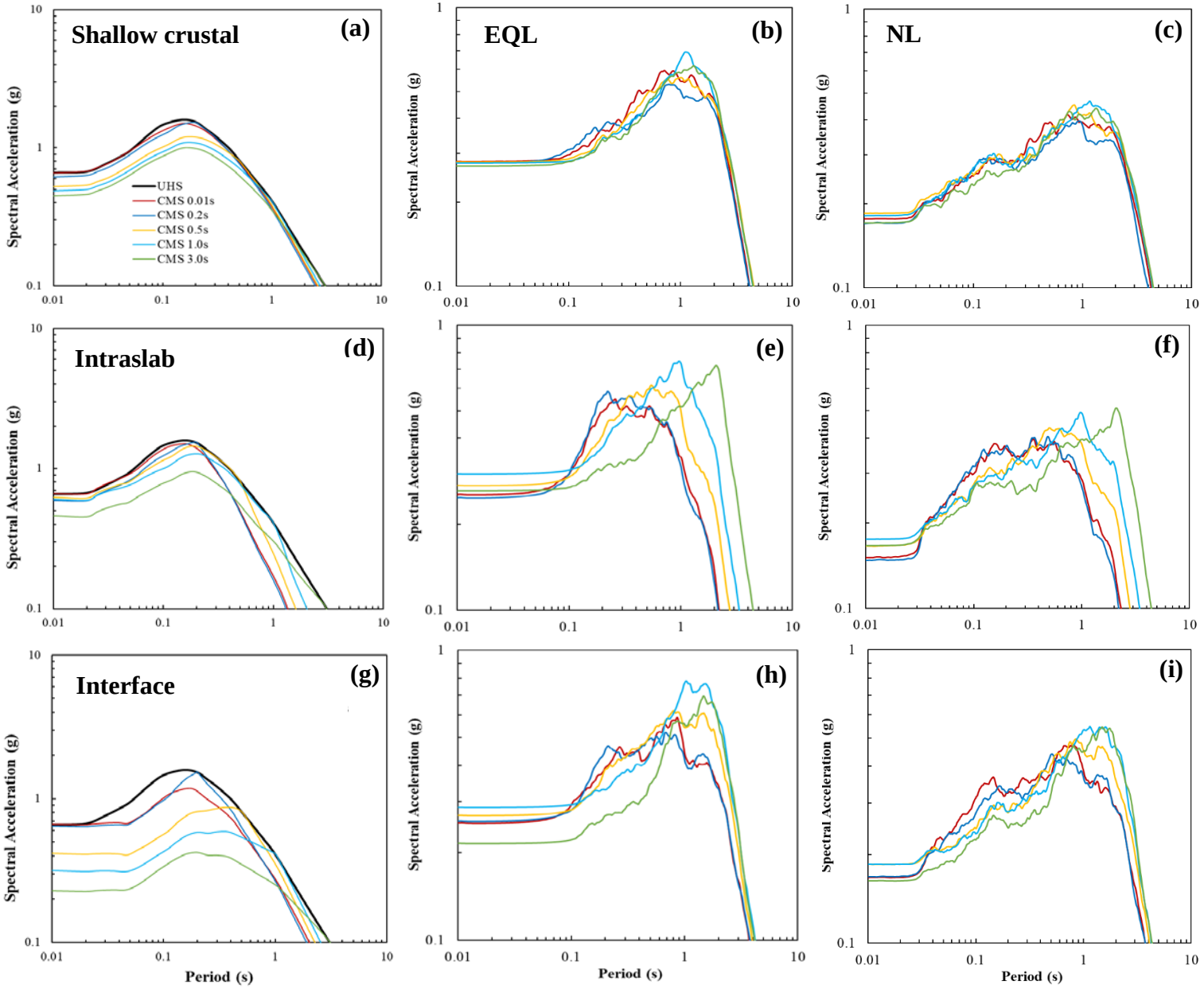

Figure 7.4. Comparison of the CMS (left) and corresponding median predicted surface response spectra (equivalent linear in middle and nonlinear at right) from site response analyses at different conditioning periods for Seattle: (a-c) shallow crustal, (d-f) intraslab, and (g-i) interface events.

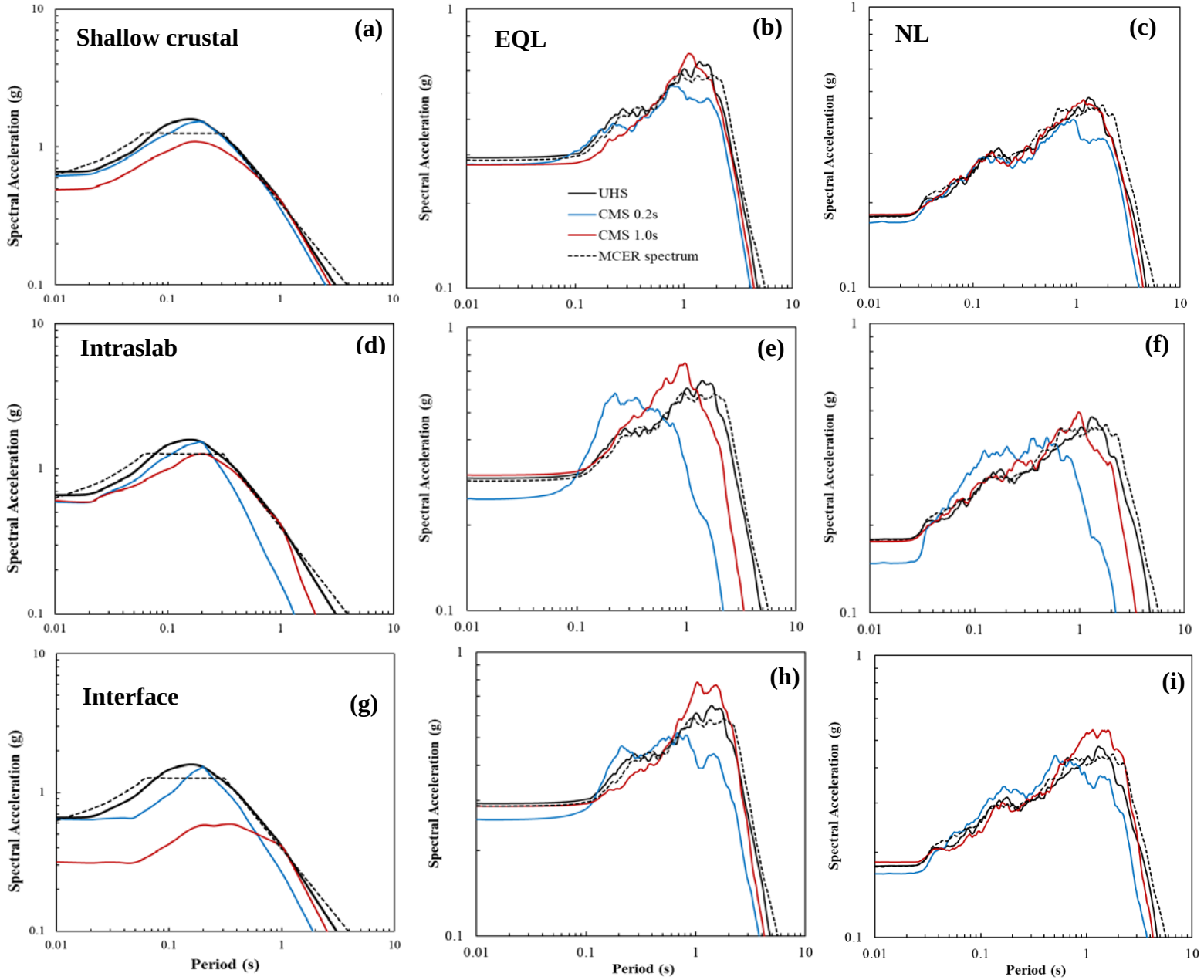

Figure 7.5. Comparison of different target spectra (left) and corresponding median predicted surface response spectra (equivalent linear in middle and nonlinear at right) from site response analyses at different dominant scenarios (considered for the CMS calculation) for Seattle: (a-c) shallow crustal, (d-f) intraslab, and (g-i) interface events.

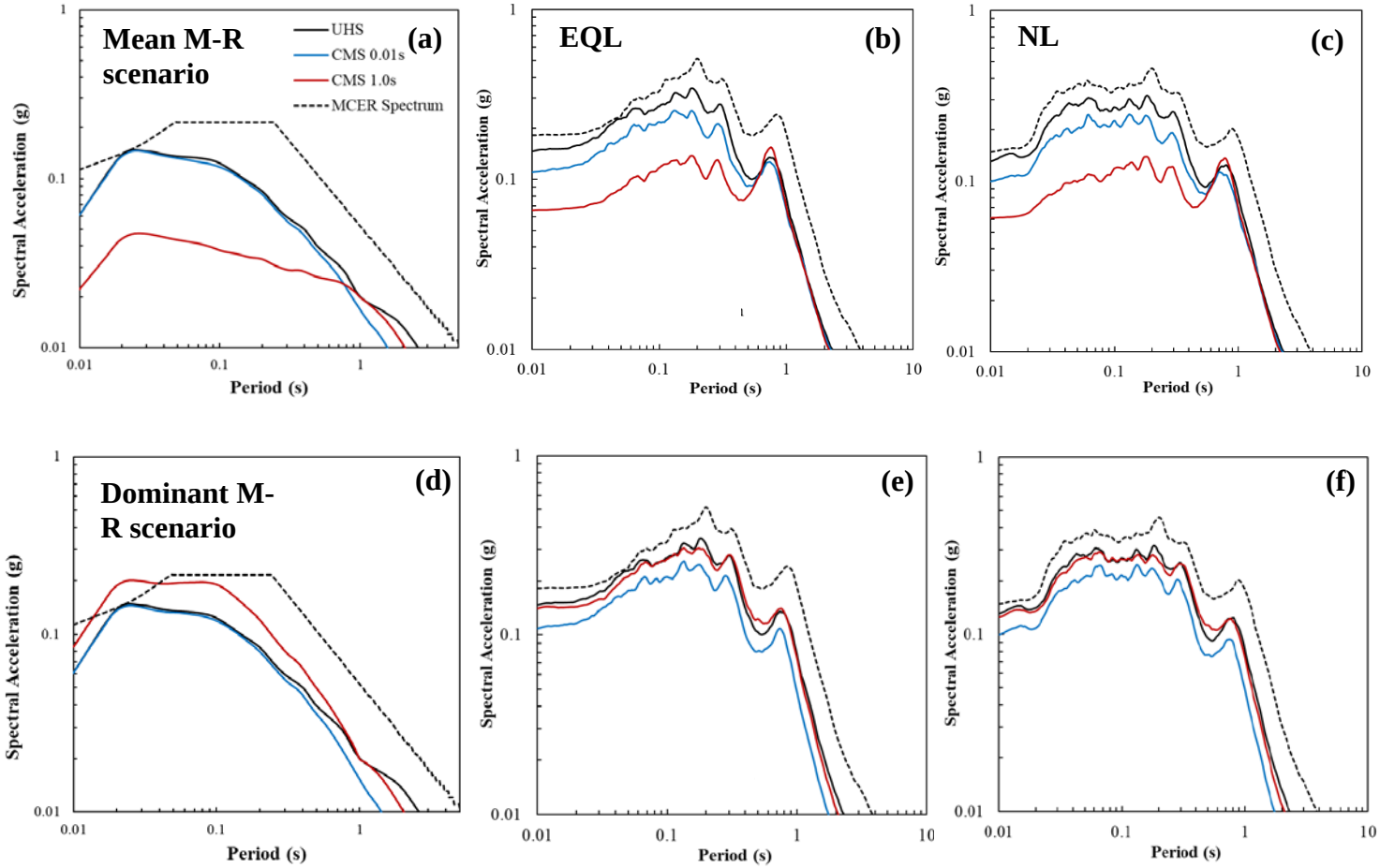

Figure 7.6. Comparison of different target spectra (left) and corresponding median predicted surface response spectra (equivalent linear in middle and nonlinear at right) from site response analyses for different M-R scenarios (considered for the CMS calculation) for Boston: (a-c) mean M-R values, and (d-f) dominant M-R scenario.

Figure 7.6 shows the comparison of different target spectra (left) and corresponding response spectra (equivalent linear in middle and nonlinear on the right) from site response analyses at the Boston site. Two different M-R scenarios (mean and dominant) are considered for the CMS calculation, as discussed in section 7.1. The UHS and MCE_R spectra for Boston have significant differences that result in discrepancies in the corresponding predicted response spectra at the ground surface. The target response spectra for mean M-R scenario CMS at conditioning periods of 0.01 s and 1.0 s have significant differences at short periods (Fig. 7.6a), which clearly propagate to the estimated response spectra at the surface (Figs. 7.6b-c). For the dominant M-R scenario CMS, the target response spectra are more similar (Fig. 7.6d), resulting in similar estimated response spectra at the ground surface (Figs. 7.6e-f). It is interesting to note that the response spectra at the ground surface for the 1.0-sec CMS is similar to that of UHS in spite of the fact that the corresponding target spectra crosses the UHS.

7.4 Comparison of Ground Motions from Different Databases

Three different databases were used in this study, as mentioned in section 5.3: NGA-West2 and KiK-net (intraslab and interface separately) for the Seattle study site, and NGA-East for the Boston study site. The NGA-West2 ground motions are scaled to match the UHS, MCE_R, and CS corresponding to the shallow crustal event scenario. Figure 7.7 shows the magnitude-distance distribution of the selected ground motion suites from the NGA-West2 database matching the different target spectra. The magnitude range is similar but the distance range is higher for the UHS and MCE_R spectrum compared to that of the CS.

Figure 7.8 shows the magnitude-distance distribution of the selected ground motion suites matching the CS from the NGA-West2, KiK-net intraslab, and KiK-net interface databases. The differences between these databases are significantly visible for both the 0.2-sec CS and the 1.0-sec CS. The subduction databases have longer distances and the interface database has larger magnitude earthquakes.

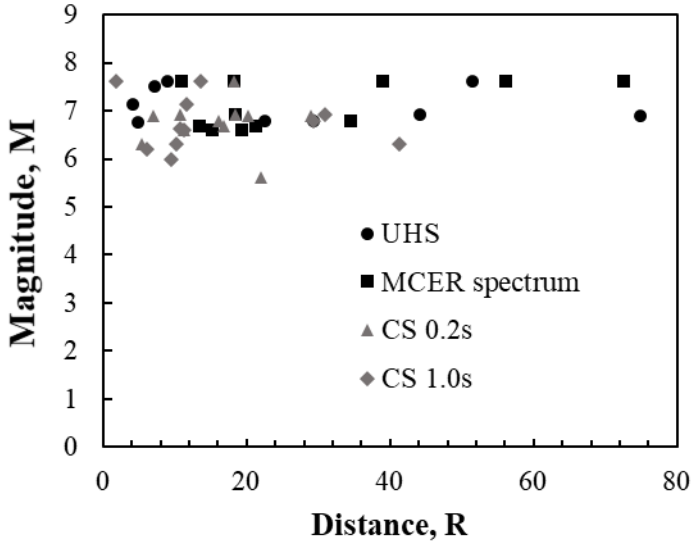

Figure 7.7. Magnitude-distance distribution of selected ground motion suites for Seattle. Note that the CS in this figure is from shallow crustal scenario.

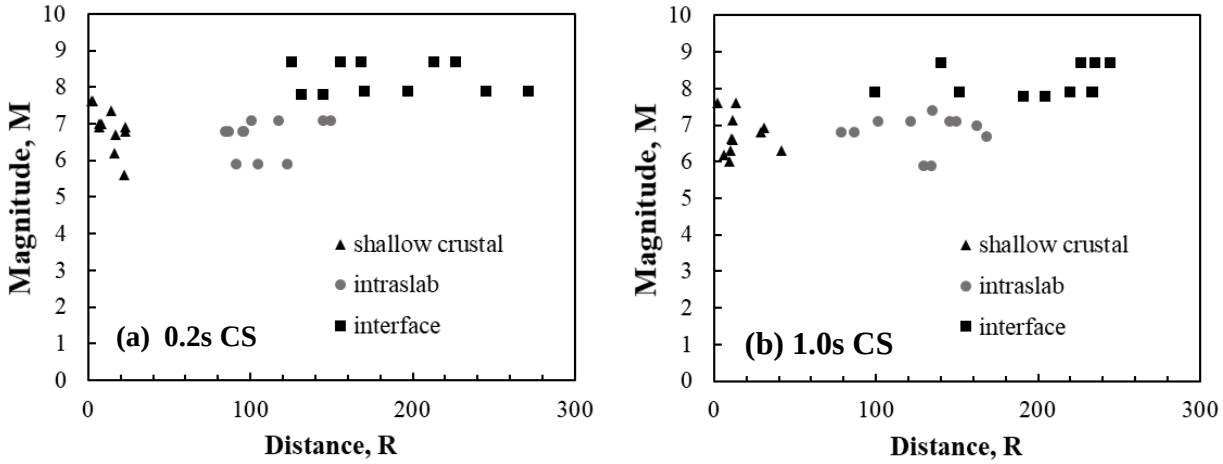

Figure 7.8. Magnitude-distance distribution of selected ground motion suites for Seattle: (a) CS at a conditioning period of 0.2 s, and (b) CS at a conditioning period of 1.0 s.

Figure 7.9 shows the magnitude-distance distribution of the selected ground motion suites matching different target spectra from NGA-East database. The distribution does not have any significant difference between the target spectra considered herein.

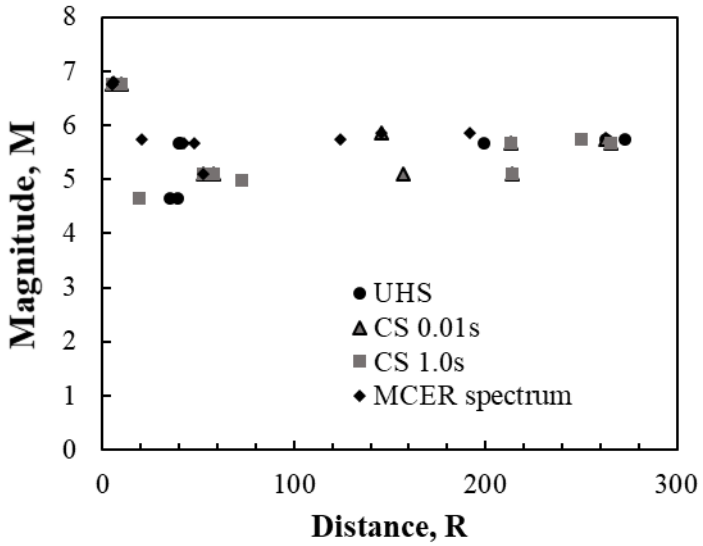

Figure 7.9. Magnitude-distance distribution of selected ground motion suites for Boston. Note that the CS in this figure is from dominant M-R scenario.

7.5 Discrepancies for Target Spectra in Boston

Figures 5.9-5.11 displayed the match between the target spectra and selected ground motion suites for Boston. It is evident that compared to Seattle, the mean of selected motions has a poor match to the target spectra, even though we had relaxed the causal parameter (M, R, V_{S30}) ranges to obtain an acceptable match. One potential cause of this discrepancy is the paucity of strong ground motion records in the NGA-East database (as a result of infrequent earthquakes in CEUS). Moreover, the CMS for Boston exceeded the UHS at a few instances (Figure 7.6d), which is not a common scenario for other sites like Seattle. Further research is deemed necessary to ensure that the GMPEs represent realistic target spectra for input ground motion selection in CEUS.

7.6 Variability in Ground-Motion Intensity Measures

The selected input motions in this study were scaled to match the target spectra, which certainly has the ability to change their original characteristics as evidenced in ground motion intensity measures such as peak ground acceleration (PGA), Arias intensity (Ia), cumulative absolute velocity (CAV), significant duration (for 5-75% and 5-95% energy release), 5%-damped pseudo-acceleration response spectra, etc. After site response analyses are conducted, the output motions will also show different characteristics as a result of the influence of soil nonlinear behavior under cyclic loading. To evaluate these changes, we have calculated multiple ground motion intensity measures (IMs) for each original input ground motion, corresponding scaled input motion, and surface output motion after site response analyses. Tables 7.1 and 7.2 display the median of these ground-motion intensity measures for each ground motion suite selected in this study. To provide a more concise summary of the medians and standard deviations, Tables 7.3 and 7.4 display the overall median and overall standard deviation (in natural logarithmic space) across all ground-motion records at each site.

When comparing the original (unscaled) input motions for Boston and Seattle (by considering the medians in Tables 7.3 and 7.4), all IMs are substantially larger for Seattle, with the exception of significant duration, which is comparable between the two cities. The variability in the original (unscaled) input motions is greater for Boston than Seattle, again with the exception of significant duration. The significant durations of subduction-zone events are known to be preferentially larger than those of shallow crustal events, so therefore this difference for duration is not surprising. In the aggregate, when the input motions are scaled, the median IMs increase and the variability decreases. Significant duration, however, is unaffected by scaling because it is a normalized measure; the medians and standard deviations are therefore unchanged. The decrease in variability is most pronounced for the ground motions in Boston, where scaling causes the standard deviations for most IMs (PGA, Ia, PSA(T)) to decrease by a factor of two in terms of ln units. For Seattle, the decrease is less significant. In both Boston and Seattle, the effect of scaling is less significant for CAV compared to PGA, Ia, and PSA(T).

The output motions at the ground surface, however, display different trends for Boston and Seattle. In the aggregate, all the median ground-motion IMs for Boston increase when propagated from bedrock to the ground surface during the site response analysis. In Boston, for example, the

median PGA for the scaled input rock motions is 0.062*g*, and the median PGA for the ground motions at the surface is 0.095*g*. These results are consistent with the overall trend of amplification at this site. For Seattle, however, nearly all the median ground-motion IMs decrease (due to significant deamplification from nonlinear soil behavior) when propagated through the soil profile. In Seattle, the median PGA for the scaled input rock motions is 0.529*g*, and the median PGA for the ground motions at the surface is only 0.169*g* (not far above the median value in Boston). The only IMs that do not decrease due to nonlinear soil behavior are those that are characterized by long periods (at which the effects of nonlinear soil behavior will be minimal), as well as significant duration. For Seattle, the PSA values for $T \geq 1$ s increase from the scaled input to the output, and there is a minimal change in CAV (which tends to be characterized by longer-period motion than Arias Intensity).

The variability in the ground-motion IMs at the ground surface, tabulated in Table 7.4, is generally greater for Boston than Seattle, with the exception of CAV and significant duration. The larger variability for the output motions in Boston reflects the larger variability of the corresponding input motions. When comparing the variability of the scaled input motions to the output motions, there is a decrease in the standard deviations of most IMs for the output motions. However, the decrease is most substantial (by far) for short-period motions (PGA and PSA(T) for $T < 1$ s) in Seattle. For example, the standard deviation of PGA decreased from 0.582 ln units for the scaled input motions to 0.149 ln units for the output motions in Seattle. These results illustrate that nonlinear soil behavior tends to override the effect of input motion selection for short periods when the input motion motions are large enough to induce significant deamplification.

Table 7.1. Median ground motion parameters PGA, CAV, I_a, $D_{5\text{-}75}$, and $D_{5\text{-}95}$ for all ground motions in each suite for original (unscaled) input motions, scaled input motions, and output motions.

				Peak ground acceleration, PGA (g)			Cumulative absolute velocity, CAV (g-s)			Arias intensity, I_a (m/s)			Significant duration, $D_{5\text{-}75}$ (s)			Significant duration, $D_{5\text{-}95}$ (s)		
Suite No.	Site	Suite ID	Set descriptor	Original (unscaled) input motion	Scaled input motion	Output motion	Original (unscaled) input motion	Scaled input motion	Output motion	Original (unscaled) input motion	Scaled input motion	Output motion	Original (unscaled) input motion	Scaled input motion	Output motion	Original (unscaled) input motion	Scaled input motion	Output motion
1	Boston	1a(i)	UHS_2% in 50 yrs	0.025	0.097	0.128	0.158	0.611	1.322	0.014	0.214	0.758	9.11	9.11	12.65	23.77	23.77	31.30
2	Boston	1b(i)	UHS_10% in 50 yrs	0.011	0.025	0.053	0.103	0.236	0.637	0.004	0.022	0.144	14.03	14.03	15.34	32.50	32.50	36.24
3	Boston	2a(i)	CS_Dominant_0.01s	0.036	0.060	0.098	0.248	0.411	0.971	0.036	0.098	0.451	11.48	11.48	13.91	24.67	24.67	29.53
4	Boston	2a(ii)	CS_Mean_0.01s	0.036	0.061	0.099	0.251	0.427	1.014	0.037	0.107	0.496	11.62	11.62	14.34	26.59	26.59	31.33
5	Boston	2d(i)	CS_Dominant_1s	0.034	0.096	0.121	0.219	0.621	1.275	0.029	0.233	0.743	11.35	11.35	15.45	25.00	25.00	32.50
6	Boston	2d(ii)	CS_Mean_1s	0.017	0.028	0.060	0.170	0.276	0.833	0.011	0.029	0.230	15.48	15.48	18.02	35.20	35.20	40.05
7	Boston	3a(i)	MCE_R	0.088	0.141	0.147	0.419	0.668	1.349	0.155	0.394	1.102	7.16	7.16	11.45	17.09	17.09	24.39
8	Seattle	1a(i)	UHS_2% in 50 yrs	0.262	0.657	0.179	1.296	3.247	2.222	1.776	11.149	2.912	7.15	7.15	13.43	12.73	12.73	24.19
9	Seattle	1b(i)	UHS_10% in 50 yrs	0.196	0.378	0.144	0.874	1.683	1.725	0.769	2.855	1.614	7.08	7.08	12.86	12.82	12.82	27.59
10	Seattle	2a(i)	CS_Shallow_Crustal_0.01s	0.398	0.640	0.176	1.782	2.867	2.136	3.693	9.561	2.465	4.84	4.84	10.99	9.83	9.83	25.40
11	Seattle	2a(ii)	CS_Intraslab_0.01s	0.144	0.661	0.151	1.123	5.144	3.773	0.661	13.876	2.876	15.24	15.24	31.93	27.09	27.09	66.23
12	Seattle	2a(iii)	CS_Interface_0.01s	0.137	0.661	0.167	2.790	13.471	9.788	1.441	33.577	8.940	42.50	42.50	81.03	76.42	76.42	145.37
13	Seattle	2b(i)	CS_Shallow_Crustal_0.2s	0.437	0.670	0.169	1.698	2.600	1.890	3.561	8.347	2.033	5.04	5.04	11.43	10.81	10.81	24.48
14	Seattle	2b(ii)	CS_Intraslab_0.2s	0.157	0.627	0.148	1.150	4.602	3.336	0.806	12.904	2.528	8.84	8.84	23.68	17.91	17.91	52.19
15	Seattle	2b(iii)	CS_Interface_0.2s	0.111	0.587	0.168	2.225	11.778	9.195	0.976	27.375	8.353	48.74	48.74	79.20	76.04	76.04	133.50
16	Seattle	2c(i)	CS_Shallow_Crustal_0.5s	0.434	0.564	0.185	2.325	3.017	2.848	4.517	7.608	2.902	5.97	5.97	14.66	13.34	13.34	41.30
17	Seattle	2c(ii)	CS_Intraslab_0.5s	0.159	0.646	0.166	1.162	4.732	3.978	0.738	12.256	3.232	9.19	9.19	24.99	19.73	19.73	63.13
18	Seattle	2c(iii)	CS_Interface_0.5s	0.080	0.426	0.185	1.798	9.583	10.113	0.598	16.999	9.958	41.50	41.50	79.44	83.95	83.95	142.77
19	Seattle	2d(i)	CS_Shallow_Crustal_1s	0.340	0.529	0.181	1.689	2.634	2.534	2.679	6.513	2.873	6.25	6.25	13.58	13.10	13.10	33.61
20	Seattle	2d(ii)	CS_Intraslab_1s	0.131	0.667	0.175	1.024	5.210	4.507	0.503	13.024	3.813	12.65	12.65	31.50	26.10	26.10	70.20
21	Seattle	2d(iii)	CS_Interface_1s	0.074	0.329	0.185	1.646	7.315	8.818	0.506	9.997	8.931	38.36	38.36	64.26	67.15	67.15	113.97
22	Seattle	2e(i)	CS_Shallow_Crustal_3s	0.362	0.471	0.170	1.667	2.173	1.995	2.835	4.820	2.255	5.52	5.52	11.60	13.07	13.07	23.97
23	Seattle	2e(ii)	CS_Intraslab_3s	0.114	0.459	0.166	1.079	4.345	5.275	0.439	7.125	4.563	14.41	14.41	37.83	31.58	31.58	83.74
24	Seattle	2e(iii)	CS_Interface_3s	0.025	0.238	0.162	0.691	6.663	9.601	0.070	6.464	8.561	39.16	39.16	74.50	111.15	111.15	158.12
25	Seattle	3a(i)	MCE_R	0.221	0.671	0.178	1.283	3.896	2.923	1.303	12.008	3.563	7.17	7.17	15.62	15.72	15.72	35.63

Table 7.2. Median 5%-damped pseudo-acceleration response spectra (PSA) for all ground motions in each suite for original (unscaled) input motions, scaled input motions, and output motions.

				PSA(T = 0.1s) (g)			PSA(T = 0.2s) (g)			PSA(T = 0.5s) (g)			PSA(T = 1s) (g)			PSA(T = 3s) (g)		
Suite No.	Site	Suite ID	Set descriptor	Original (unscaled) input motion	Scaled input motion	Output motion	Original (unscaled) input motion	Scaled input motion	Output motion	Original (unscaled) input motion	Scaled input motion	Output motion	Original (unscaled) input motion	Scaled input motion	Output motion	Original (unscaled) input motion	Scaled input motion	Output motion
1	Boston	1a(i)	UHS_2% in 50 yrs	0.044	0.170	0.271	0.032	0.123	0.289	0.012	0.045	0.095	0.005	0.021	0.081	0.001	0.004	0.007
2	Boston	1b(i)	UHS_10% in 50 yrs	0.018	0.042	0.102	0.015	0.035	0.089	0.007	0.017	0.041	0.003	0.008	0.027	0.001	0.002	0.003
3	Boston	2a(i)	CS_Dominant_0.01s	0.069	0.115	0.216	0.052	0.087	0.209	0.021	0.035	0.077	0.008	0.013	0.048	0.001	0.002	0.004
4	Boston	2a(ii)	CS_Mean_0.01s	0.072	0.123	0.226	0.051	0.087	0.214	0.024	0.041	0.086	0.011	0.019	0.066	0.003	0.005	0.007
5	Boston	2d(i)	CS_Dominant_1s	0.063	0.179	0.265	0.041	0.117	0.257	0.018	0.052	0.113	0.007	0.019	0.073	0.001	0.003	0.005
6	Boston	2d(ii)	CS_Mean_1s	0.032	0.053	0.119	0.029	0.047	0.122	0.019	0.031	0.075	0.012	0.020	0.070	0.003	0.005	0.006
7	Boston	3a(i)	MCE_R	0.189	0.301	0.343	0.152	0.242	0.458	0.053	0.085	0.167	0.029	0.045	0.178	0.006	0.009	0.015
8	Seattle	1a(i)	UHS_2% in 50 yrs	0.486	1.217	0.257	0.598	1.497	0.297	0.333	0.835	0.348	0.177	0.445	0.435	0.040	0.101	0.222
9	Seattle	1b(i)	UHS_10% in 50 yrs	0.403	0.777	0.255	0.463	0.892	0.282	0.191	0.367	0.331	0.088	0.170	0.293	0.022	0.042	0.088
10	Seattle	2a(i)	CS_Shallow_Crustal_0.01s	0.893	1.437	0.253	0.869	1.398	0.281	0.539	0.867	0.393	0.231	0.371	0.392	0.052	0.084	0.197
11	Seattle	2a(ii)	CS_Intraslab_0.01s	0.327	1.499	0.299	0.310	1.423	0.368	0.114	0.523	0.379	0.037	0.170	0.285	0.005	0.024	0.054
12	Seattle	2a(iii)	CS_Interface_0.01s	0.285	1.376	0.313	0.271	1.310	0.325	0.126	0.610	0.375	0.057	0.275	0.384	0.015	0.075	0.156
13	Seattle	2b(i)	CS_Shallow_Crustal_0.2s	0.864	1.323	0.263	0.948	1.452	0.282	0.485	0.742	0.332	0.231	0.353	0.381	0.053	0.081	0.179
14	Seattle	2b(ii)	CS_Intraslab_0.2s	0.460	1.842	0.317	0.385	1.541	0.375	0.130	0.521	0.397	0.038	0.153	0.269	0.005	0.021	0.044
15	Seattle	2b(iii)	CS_Interface_0.2s	0.245	1.296	0.278	0.291	1.539	0.332	0.132	0.698	0.440	0.051	0.268	0.365	0.013	0.068	0.142
16	Seattle	2c(i)	CS_Shallow_Crustal_0.5s	0.865	1.123	0.254	1.082	1.404	0.280	0.597	0.775	0.351	0.278	0.361	0.416	0.072	0.094	0.216
17	Seattle	2c(ii)	CS_Intraslab_0.5s	0.354	1.443	0.275	0.329	1.339	0.305	0.201	0.817	0.434	0.068	0.277	0.381	0.009	0.036	0.085
18	Seattle	2c(iii)	CS_Interface_0.5s	0.140	0.747	0.246	0.197	1.048	0.279	0.153	0.816	0.406	0.065	0.347	0.452	0.015	0.081	0.201
19	Seattle	2d(i)	CS_Shallow_Crustal_1s	0.659	1.028	0.270	0.771	1.202	0.278	0.511	0.797	0.362	0.259	0.403	0.447	0.061	0.095	0.213
20	Seattle	2d(ii)	CS_Intraslab_1s	0.268	1.362	0.272	0.276	1.406	0.300	0.175	0.890	0.379	0.081	0.414	0.490	0.011	0.054	0.141
21	Seattle	2d(iii)	CS_Interface_1s	0.107	0.475	0.236	0.171	0.761	0.280	0.143	0.636	0.372	0.093	0.414	0.532	0.020	0.090	0.232
22	Seattle	2e(i)	CS_Shallow_Crustal_3s	0.691	0.901	0.233	0.861	1.123	0.263	0.546	0.713	0.353	0.279	0.364	0.410	0.075	0.098	0.227
23	Seattle	2e(ii)	CS_Intraslab_3s	0.254	1.025	0.267	0.253	1.021	0.272	0.135	0.544	0.326	0.082	0.329	0.396	0.026	0.104	0.270
24	Seattle	2e(iii)	CS_Interface_3s	0.047	0.450	0.225	0.056	0.543	0.247	0.041	0.393	0.325	0.030	0.288	0.451	0.011	0.104	0.249
25	Seattle	3a(i)	MCE_R	0.372	1.129	0.262	0.423	1.283	0.293	0.295	0.895	0.365	0.137	0.416	0.408	0.040	0.122	0.271

Table 7.3. Median and standard deviation (natural logarithmic space) of PGA, CAV, I_a, $D_{5\text{-}75}$, and $D_{5\text{-}95}$ across all ground-motion records and suites at each site for original (unscaled) input motions, scaled input motions, and output motions.

		Peak ground acceleration, PGA (g)			Cumulative absolute velocity, CAV (g-s)			Arias intensity, I_a (m/s)			Significant duration, $D_{5\text{-}75}$ (s)			Significant duration, $D_{5\text{-}95}$ (s)		
Statistics of intensity measures (IMs) across all records	Site	Original (unscaled) input motion	Scaled input motion	Output motion	Original (unscaled) input motion	Scaled input motion	Output motion	Original (unscaled) input motion	Scaled input motion	Output motion	Original (unscaled) input motion	Scaled input motion	Output motion	Original (unscaled) input motion	Scaled input motion	Output motion
Median	Boston	0.029	0.062	0.095	0.206	0.434	1.025	0.024	0.104	0.464	11.15	11.15	14.32	25.81	25.81	31.86
	Seattle	0.169	0.529	0.169	1.427	4.474	3.969	1.041	10.227	3.863	12.47	12.47	26.55	25.29	25.29	56.22
Standard deviation (natural logarithmic space)	Boston	1.641	0.819	0.485	1.115	0.800	0.670	2.782	1.454	0.968	0.783	0.783	0.697	0.722	0.722	0.711
	Seattle	1.052	0.582	0.149	0.781	0.764	0.733	1.731	1.092	0.747	1.054	1.054	0.908	0.981	0.981	0.850

Table 7.4. Median and standard deviation (natural logarithmic space) of 5%-damped pseudo-acceleration response spectra (PSA) across all ground-motion records and suites at each site for original (unscaled) input motions, scaled input motions, and output motions.

		PSA(T = 0.1s) (g)			PSA(T = 0.2s) (g)			PSA(T = 0.5s) (g)			PSA(T = 1s) (g)			PSA(T = 3s) (g)		
Statistics of intensity measures (IMs) across all records	Site	Original (unscaled) input motion	Scaled input motion	Output motion	Original (unscaled) input motion	Scaled input motion	Output motion	Original (unscaled) input motion	Scaled input motion	Output motion	Original (unscaled) input motion	Scaled input motion	Output motion	Original (unscaled) input motion	Scaled input motion	Output motion
Median	Boston	0.055	0.116	0.204	0.042	0.089	0.207	0.019	0.039	0.087	0.009	0.018	0.068	0.002	0.004	0.006
	Seattle	0.341	1.069	0.264	0.381	1.194	0.295	0.214	0.669	0.369	0.099	0.309	0.393	0.022	0.069	0.158
Standard deviation (natural logarithmic space)	Boston	1.672	0.948	0.692	1.566	0.795	0.688	1.647	0.720	0.608	1.699	0.735	0.794	2.003	1.070	0.891
	Seattle	1.182	0.783	0.227	1.102	0.663	0.260	1.080	0.601	0.250	1.074	0.651	0.389	1.189	0.818	0.859

8 Conclusions

A holistic assessment of the contribution of input ground motion selection procedures to uncertainty in ground motion intensity measures relevant to geotechnical engineering analysis has been conducted. Multiple definitions of the target spectrum were explored for two study sites, including the uniform hazard spectrum, the risk-targeted maximum considered earthquake spectrum, and the conditional spectrum. Seattle, WA and Boston, MA served as case studies to investigate the effects of 25 different sets of input ground motions on ground motion intensity measures estimated at the ground surface via equivalent-linear and fully nonlinear site response analysis. The 25 different sets of input motions represented variations in the target spectrum definition, hazard levels, spectral period of interest, selected dominant scenario (e.g., from considering multiple types of earthquakes, to considering mean values from the deaggregation of hazard). Key findings from this work are outlined as follows:

- In diverse tectonic settings, identifying multiple earthquake scenarios which are representative of the different seismic sources contributing to the hazard is recommended. Moreover, using such scenarios to define different target spectra and select appropriate records for each type of seismicity can facilitate the definition of the most critical seismic demand at the site of interest.
- In low-to-moderate seismicity regions, where the sources of hazard are much more diffuse, comparisons between scenarios based on mean values from the deaggregation and apparent dominant scenarios (i.e., critical scenarios such as larger magnitudes with a relatively larger contribution to the hazard) can help envelope the uncertainty in the development of appropriate target spectra for input motion selection.
- It is well known that single ground motion recordings cannot provide a good fit to spectral shapes corresponding to the uniform hazard spectrum (UHS), and the risk-targeted maximum considered earthquake spectrum (MCE_R). We found that the conditional spectrum (CS) is a suitable alternative for input motion selection in the context of geotechnical earthquake engineering analyses, such as site response analyses. The CS has been more commonly used in structural engineering applications, with only a few case studies integrating it to geotechnical analyses.
- The selection of compatible records to hard-rock conditions representative of the bedrock in most sites in the CEUS continues to be challenge. Similarly, ground motion recordings from subduction events are also limited. Efforts toward expanding and improving ground motion databases for low-to-moderate seismicity regions and subduction zones remain a priority for our scientific community.
- Future research is necessary to elucidate the effects of spectral matching on input ground motions and the variability of the resulting ground motion intensity measures. Only linear scaling was used in this project, and a large variability of scaling factors was observed as a function of the availability of records (i.e., larger scale factors were often required for records from the NGA-East database).
- A reasonable match to the UHS was often achieved for the Seattle site, but one of the strengths of utilizing the CS spectra (i.e., accounting for variability in the target spectrum explicitly) results in an even better match between the target spectrum and the mean spectral values from selected and scaled motions. Fitting the spectral shape of the design spectrum provides the

poorest match among all target spectra considered in Seattle, which is expected given the difficulty of real ground motions to be compatible with that spectral shape.

- In Boston, achieving a reasonable agreement with defined target spectra proved more difficult. A good match was often only achieved for a given range of periods. This is likely the result of the limited number of ground motion recordings available in the CEUS region.
- Seattle has dominant earthquake scenarios resulting from shallow crustal, subduction-intraslab and subduction-interface events. Reducing the selection of meaningful scenarios to the mean Magnitude-Distance combination from the deaggregation of hazard for the CMS computation, cannot provide the complete picture of the seismic hazard at this site.
- The choice of conditioning period in the calculation of the CS seems more crucial for subduction events.
- The predicted surface response spectra at short periods in Boston display greater variability than those for Seattle, particularly for the spectra conditioned at a period of 1 s. The surface response spectra based on the mean values (for Boston) is significantly lower than the surface response spectra based on the assumed dominant scenario (for the CMS conditioned at T = 1 s).
- For Seattle, the surface response spectra are much similar at short periods than at long periods. Despite significant variations in the CMS of the input motions, it is notable that all the surface response spectra appear to converge for short periods. This observation might be due to a high degree of nonlinearity predicted at this site (i.e., there is significant deamplification in the surface ground motions at short periods). However, the noticeable differences in the surface response spectra associated with three different scenarios considered for input motion selection in Seattle (particularly at moderate to long periods) shows the importance of considering all dominant scenarios.

This study has illustrated how input motion selection protocols offer varying contributions to uncertainty for different ground-motion intensity measures in different tectonic environments. Based on the two sites considered in this study, the input motion selection protocol seems to have a greater influence in stable continental regions (where input ground motions are often smaller) compared to more active tectonic regions, particularly at shorter periods. When nonlinear soil behavior is excessive, the effects of the site response modeling assumptions and parameters may outweigh the effects of the input motion selection protocols at short spectral periods. At longer spectral periods, nonlinear soil behavior is less prevalent, and predicted surface ground motions are more greatly affected by the input motion selection protocol. Intensity measures relevant to liquefaction analyses, such as PGA, will be more greatly affected by the input motion selection protocol when nonlinear soil behavior does not result in significant deamplifications. On the other hand, landslides are often associated with longer period motion, and therefore intensity measures relevant to slope stability analyses will be affected by the input motion selection protocol over a wider range of ground motions. The results of this study will work towards improving the selection of input ground motions for geotechnical engineering applications, and on improving our understanding of how input motion selection protocols influence ground-motion intensity measures.

9 Data and Resources

The earthquake ground-motion records for shallow crustal earthquakes and stable continental earthquakes were obtained from the PEER NGA-West2 and NGA-East database, respectively (https://ngawest2.berkeley.edu/) (last accessed March 2019). The ground-motion records for the subduction-zone environments were obtained from the Kiban-Kyoshin network (KiK-net) database at http://www.kyoshin.bosai.go.jp/ (last accessed March 2019). The probabilistic seismic hazard analysis calculations were performed using the HAZ46 Seismic Hazard Analysis Software (Abrahamson and Gregor, 2018), available at https://github.com/abrahamson/HAZ (last accessed March 2019). The risk-targeted maximum considered earthquake (MCE_R) spectra were computed using the ASCE 7 Hazard Tool, available at https://asce7hazardtool.online/ (last accessed March 2019).

A MATLAB code for the selection algorithm proposed by Baker and Lee (2017) was used for this study. The NGA-West2 database already incorporated in the code was used. The authors of this study added three new databases (NGA-East, KiK-net subduction-intraslab and KiK-net subduction-interface) to that code.

Information about the Northeastern University Seismic Recording Station (the location of the assumed profile in Boston) is available at http://www.coe.neu.edu/Research/srs/ (last accessed March 2019). Data contained in Yegian (2004), Thompson et al. (2014), Baise et al. (2016), and Woodhouse and Barosh (2011/2012) were used to develop the 1D geotechnical profile for the Boston site, as detailed in Chapter 6 of this report. Information about the Seattle Liquefaction Array (the location of the assumed profile in Seattle) is available at http://www.nees.ucsb.edu/facilities/seattle-liquefaction-array (last accessed March 2019). Data contained in Shannon and Wilson (2018) were used to develop the 1D geotechnical profile for the Seattle site, as detailed in Chapter 6 of this report.

All site response calculations were performed using DEEPSOIL (Hashash et al., 2018), and the post-processing and subsequent analysis of the results were performed using the open-source statistical language and environment R (R Core Team, 2018), available at http://www.r-project.org (last accessed March 2019). To compute the 5%-damped PSA from the acceleration time series, we used the Boore (2008) FORTRAN programs.

The project involved a large amount of electronic data and modeling results, although no new seismic or geotechnical data were collected as part of this project. The site and ground-motion data are available at the locations indicated in the prior paragraphs. The key aspects of the investigations will be published at least one journal article, and additional data supporting our results will appear as an electronic supplement to the published journal article(s). These data will be available (through either linking or direct posting) on the PIs' research websites for public access (https://cabas.wordpress.ncsu.edu/ and http://www.kaklamanos.com/).

10 Acknowledgments

This material is based upon work supported by the U.S. Geological Survey under Grant Nos. G18AP00015 and G18AP00016; this financial support is gratefully acknowledged. The views and conclusions contained in this document are those of the authors and should not be interpreted as representing the opinions or policies of the U.S. Geological Survey. Mention of trade names or commercial products does not constitute their endorsement by the U.S. Geological Survey. Professor Kaklamanos was also supported by a Zampell Family Faculty Fellowship internally through Merrimack College.

In addition to the principal investigators on these proposals, several individuals contributed to the success of this project. Ms. Ishika Chowdhury, Ph.D. Student at North Carolina State University, performed the calculations for the input motions and performed much of the writing associated with the project. Dr. Albert Kottke served as a seismic consultant for this project, providing useful perspectives on the uncertainty modeling and hazard analyses, and in interpreting the results. Dr. Nick Gregor performed the probabilistic seismic hazard analysis calculations and contributed to Chapter 4 of this report. Ms. Kayla Lang, an undergraduate student at Merrimack College, helped develop the geotechnical profiles for Boston and Seattle. Professor Joseph Wartman of the University of Washington provided useful feedback on the geological and geotechnical conditions in Seattle.

11 Bibliography

The following publications resulted from this project. At least one manuscript is currently being prepared for submission to a peer-reviewed journal, and results from this project are presented at two conferences (resulting in one peer-reviewed conference paper and two peer-reviewed conference abstracts):

Cabas, A., Chowdhury, I. N., J. Kaklamanos, A. Kottke, and N. Gregor. (2019). Bridging the gap between input motion selection protocols and geotechnical engineering analyses, *2019 Annual Meeting of the Seismological Society of America*, Seattle, Washington, 23–26 April 2019 (abstract printed in *Seismological Research Letters*, Vol. 90, No. 2B, p. 955).

Chowdhury, I. N., A. Cabas, J. Kaklamanos, A. Kottke, and N. Gregor (2019). Challenges and consequences of input motion selection for subduction zone environments: Seattle, Washington, *2019 Annual Meeting of the Seismological Society of America*, Seattle, Washington, 23–26 April 2019 (abstract printed in *Seismological Research Letters*, Vol. 90, No. 2B, p. 917).

Chowdhury, I. N., A. Cabas, J. Kaklamanos, A. Kottke, N. Gregor, and K. M. Lang (2019). Hazard-consistent ground motions: Insights on selection and scaling for different tectonic, geological, and geotechnical environments, *Seventh International Conference on Earthquake Geotechnical Engineering*, Paper No. 11067, Rome, Italy, 17–20 June 2019, 9 pp.

12 References

Abrahamson, N. A. and N. Gregor. (2018). Haz46, Seismic Hazard Analysis Software.

Abrahamson, N. A., Silva, W. J., and R. Kamai. (2014). Summary of the ASK14 ground motion relation for active crustal regions. Earthquake Spectra, Vol. 30, No. 3, pp. 1025-1055.

Abrahamson, N., Gregor, N., and Addo, K. (2016). BC Hydro Ground Motion Prediction Equations for Subduction Earthquakes. *Earthquake Spectra*, Vol. 32, No. 1, pp. 23-44.

Al Atik, L. and R. R. Youngs. (2014). Epistemic uncertainty for NGA-West2 Models. Earthquake Spectra, Vol. 30, No. 3, pp. 1301-1318.

Al Atik, L and Abrahamson, N (2010). An Improved Method for Nonstationary Spectral Matching. Earthquake Spectra, Volume 26, No. 3, pages 601–617.

American Society of Civil Engineers [ASCE] (2016). *Minimum Design Loads for Buildings and Other Structures (Standards ASCE/SEI 7-16).* American Society of Civil Engineers, Reston, Virginia.

Ancheta, T. D., Darragh, R. B. , Stewart, J. P., Seyhan, E., Silva, W. J., Chiou, B. S., Wooddell, K. E., Graves, R. W., Kottke, A. R., Boore, D. M., et al. 2013. PEER NGA-West2 Database. Pacific Earthquake Engineering Research Center, University of California, Berkeley, California, p. 172.

Baise, L. G., Kaklamanos, J., Berry, B. M., and Thompson, E. M. (2016). Soil amplification with a strong impedance contrast: Boston, Massachusetts, *Engineering Geology*, 202, 1–13.

Baker, J. W. (2007). Measuring bias in structural response caused by ground motion scaling, *Proceedings of the 8th Pacific Conference on Earthquake Engineering*, Singapore.

Baker, J. W. (2011). Conditional mean spectrum: Tool for ground motion selection, *ASCE Journal of Structural Engineering*, 137(3), 322–331.

Baker, J. W., and Cornell, C. A. (2006). Spectral shape, epsilon, and record selection, *Earthquake Engineering and Structural Dynamics*, 35, 1077–1095.

Baker, J. W., and Jayaram, N. (2008). Correlation of spectral acceleration values from NGA ground motion models, *Earthquake Spectra*, 24, 299–317.

Baker, J.W., and Lee, C. (2017). An Improved Algorithm for Selecting Ground Motions to Match a Conditional Spectrum. *Journal of Earthquake Engineering*, 22(4), 708–723.

Bazzurro, P., and C. A. Cornell (2004). Ground-motion amplification in nonlinear soil sites with uncertain properties, *Bulletin of the Seismological Society of America*, 94, 2090–2109.

BC Hydro (2012). Probabilistic Seismic Hazard Analysis (PSHA) Model, Vols. 1 – 4, BC Hydro Engineering Report E658, Vancouver.

Boore, D. M. (2008). TSPP—A collection of FORTRAN programs for processing and manipulating time series, *U.S. Geol. Surv. Open-File Rept. 2008-1111*, 57 pp.

Bommer, J., and Acevedo, A. (2004). The use of real earthquake accelerograms as input to dynamic analysis, *Journal of Earthquake Engineering*, 8, 43–91.

Bozorgnia, Y., Abrahamson, N., Al Atik, L., Ancheta, T.D., Atkinson, G.M., Baker, J.W., Baltay, A., Boore, D.M., Campbell, K.W., Chiou, B.S.J., et al. (2014). NGA-West2 Research Project. *Earthquake Spectra*, Vol. 30, No. 3, pp. 973-987.

Bradley, B. A. (2010). A generalized conditional intensity measure approach and holistic ground-motion selection, *Earthquake Engineering and Structural Dynamics*, 39, 1321–1342.

Bradley, B. A. (2012). A ground motion selection algorithm based on the generalized conditional intensity measure approach, *Soil Dynamics and Earthquake Engineering*, 40, 48–61.

Brankman, C. M., and L. G. Baise (2008). Liquefaction susceptibility mapping in Boston, Massachusetts, *Eng. Environ. Geosci.* XIV(1), 1–16.

Cabas, A. (2015). V_S-κ correction factors for input ground motions used in seismic site response analysis. *Earthquake Engineering Research Institute (EERI) 67th Annual Meeting 2015*, Boston, MA, USA, March 31 - April 3, 2015.

Cabas, A., and Rodriguez-Marek, A. (2017). V_S-κ_0 correction factors for input ground motions used in seismic site response analysis, *Earthquake Spectra*, Vol. 33, No. 3, pp. 917-941.

Carlton, B., and Abrahamson, N. (2014). Issues and Approaches for Implementing Conditional Mean Spectra in Practice. *Bulletin of the Seismological Society of America*, Vol. 104, No. 1, pp. 503–512.

Chandra, J., Guéguen, P., and Bonilla, L.F. (2016). PGA-PGV/Vs considered as a stress–strain proxy for predicting nonlinear soil response, *Soil Dynamics and Earthquake Engineering*, 85, 146–160.

Chiou, B., and Youngs, R. R. (2008). An NGA model for the average horizontal component of peak ground motion and response spectra, *Earthq. Spectra* 24, 173–215.

Coduto, D. P., Yeung, M. R., and Kitch, W. A. (2011). *Geotechnical Engineering: Principles and Practices, Second Edition*, Prentice Hall: Upper Saddle River, New Jersey, 794 p.

Darendeli, M.B. (2001). Development of a new family of normalized modulus reduction and material damping curves, *Ph.D. Thesis*, University of Texas at Austin, Austin, Texas, 396 pp.

Dawood, H., Rodriguez-Marek, A., Bayless, J., Goulet, C., and Thompson, E. (2016). A Flatfile for the KiK-net Database Processed Using an Automated Protocol. *Earthquake Spectra*, Vol. 32, No. 2, pp. 1281-1302.

EPRI (2004). CEUS Ground Motion Project Final Report, EPRI Report No. 1009684.

EPRI (2012). Central and Eastern United States Seismic Source Characterization for Nuclear Facilities. EPRI Report #1021097.

Galster, R. W., and W. T . Laprade (1991). Geology of Seattle, Washington, United States of America, *Bull Eng Geol Environ* 28(3), 235-302.

Goulet, C.A., Kishida, T., Ancheta, T.D., Cramer, C.H., Darragh, R.B., Silva, W.J., Hashash, Y.M.A., Harmon, J., Stewart, J.P., Wooddell, K.E., Youngs, R.R. (2014). NGA-East Database. Pacific Earthquake Engineering Research Center, University of California, Berkeley, California.

Groholski, D. R., Y. M. A. Hashash, B. Kim, M. Musgrove, J. Harmon, and J. P. Stewart (2016). Simplified model for small-strain nonlinearity and strength in 1D seismic site response

analysis, *J. Geotech. Geoenviron. Eng.* 142(9), DOI: 10.1061/(ASCE)GT.1943-5606.0001496.

Harmsen, S., Perkins, D., and Frankel, A. (1999). Deaggregation of Probabilistic Ground Motions in the Central and Eastern United States. *Bulletin of the Seismological Society of America*, Vol. 89, No. 1, pp. 1-13.

Haselton, C. B., Baker, J. W., Stewart, J. P., Whittaker, A. S., Luco, N., Fry, A., Hamburger, R. O., Zimmerman, R. B., Hooper, J. D., Charney, F. A., and Pekelnicky, R. G. (2017). Response history analysis for the design of new buildings in the NEHRP provisions and ASCE/SEI 7 Standard: Part I - overview and specification of ground motions, *Earthq. Spectra*, doi: 10.1193/032114EQS039M.

Hashash, Y.M.A., Abrahamson, N.A., Olson, S.M., Hague, S., and Kim, B. (2015). Conditional Mean Spectra in Site-Specific Seismic Hazard Evaluation for a Major River Crossing in the Central United States. *Earthquake Spectra*, Vol. 31, No. 1, pp. 47-69.

Hashash, Y. M. A., Musgrove, M. I., Harmon, J. A., Groholski, D. R., Phillips, C. A., and Park, D. (2016). DEEPSOIL 6.1, *User Manual*, Univ. of Illinois at Urbana-Champaign, Champaign, Illinois, 135 pp.

Heo, Y.A., Kunnath, S.K. and Abrahamson, N. (2011). Amplitude-scaled versus spectrum-matched ground motions for seismic performance assessment. J Struct Eng, 137 (3), pp. 278-288.

Hough, S. E. (2012). Initial assessment of the intensity distribution of the 2011 M_w 5.8 Mineral, Virginia earthquake, *Seismological Research Letters*, 83(4), 649–657.

Jayaram, N., Lin, T., and Baker J. W. (2011). A computationally efficient ground-motion selection algorithm for matching a target response spectrum mean and variance, *Earthq. Spectra*, 27, 797–815.

Kaklamanos, J., and Bradley, B. A. (2018a). Challenges in predicting seismic site response with 1D analyses: Conclusions from 114 KiK-net vertical seismometer arrays, *Bulletin of the Seismological Society of America*, 108(5A), 2816–2838.

Kaklamanos, J., and Bradley, B. A. (2018b). Insights from KiK-net data: What input parameters should be addressed to improve site response predictions? *Geotechnical Earthquake Engineering and Soil Dynamics V: Seismic Hazard Analysis, Earthquake Ground Motions, and Regional-Scale Assessment*, 10–13 June 2018, Austin, Texas, American Society of Civil Engineers (ASCE) Geotechnical Special Publication No. 291, S. J. Brandenberg and M. T. Manzari (eds.), 454–464.

Kaklamanos, J., Bradley, B. A., Thompson, E. M., and Baise, L. G. (2013). Critical parameters affecting bias and variability in site response analyses using KiK-net downhole array data. *Bulletin of the Seismological Society of America*, *103*(3), 1733–1749.

Kaklamanos, J., Baise, L. G., Thompson, E. M., and Dorfmann, L. (2015). Comparison of 1D linear, equivalent-linear, and nonlinear site response models at six KiK-net validation sites, *Soil Dynamics and Earthquake Engineering*, 69, 207–219.

Kim, B., Hashash, Y. M., Stewart, J. P., Rathje, E. M., Harmon, J. A., Musgrove, M. I., and Silva, W. J. (2016). Relative differences between nonlinear and equivalent-linear 1-D site response analyses. *Earthquake Spectra*, 32(3), 1845–1865.

Kwok, A. O., Stewart, J. P., and Hashash, Y. M. A. (2008). Nonlinear ground response analysis of Turkey Flat shallow stiff soil site to strong ground motion, *Bull. Seismol. Soc. Am.*, 98(1), 331–343.

Kwong, N. S., and Chopra, A. K. (2015). Selection and scaling of ground motions for nonlinear response history analysis of buildings in performance-based earthquake engineering, *PEER Report 2015/11*, Pacific Earthquake Engineering Research Center, University of California, Berkeley, Calif., 223 pp.

Ladd, C. C. (1991). Stability evaluation during staged construction, *J. Geotech. Eng.* 117, 540–615.

Li, W., and Assimaki, D. (2010). Site and ground motion dependent parametric uncertainty of nonlinear site response analyses in earthquake simulations, *Bull Seismol. Soc. Am.*, 100(3), 954–968.

Lin, T., Harmsen, S,C,, Baker, J.W., Luco, N. (2013). Conditional spectrum computation incorporating multiple causal earthquakes and ground motion prediction models. *Bulletin of the Seismological Society of America,* 103(2A), pp. 1103–1116.

Matasović, N., and Vucetic, M. (1993). Cyclic characterization of liquefiable sands, *J. Geotech. Eng.* 119, 1805–1822.

McGuire, R. K., Silva, W. J., and Constantino, C. J. (2001). Technical Basis for Revision of Regulatory Guidance on Design Ground Motions: Hazard- and Risk-consistent Ground Motion Spectra Guidelines, *NUREG/CR-6728*, Prepared for U.S. Nuclear Regulatory Commission, Washington, DC.

NEHRP Consultants Joint Venture (2011). Selecting and scaling earthquake ground motions for performing response-history analyses, NIST GCR 11-917-15. *Technical Report,* National Institute of Standards and Technology, Washington, D.C.

Okada, Y., K. Kasahara, S. Hori, K. Obara, S. Sekiguchi, H. Fujiwara, and A. Yamamoto (2004). Recent progress of seismic observations networks in Japan – Hi-net, F-net, K-net and KiK-net, Earth Planets Space 56, xv–xxviii.

PEER (2015). NGA-East: Median Ground-Motion Models for the Central and Eastern North American Region, PEER Report No. 2015/04.

Peterman, B.R., and Rathje, E.M. (2017). Evaluation of Ground Motion Selection Techniques for Seismic Rigid Sliding Block Analyses. *J. Geotech. Geoenviron. Eng*., 143(4).

Phillips, C., and Hashash, Y. M. A. (2009). Damping formulation for nonlinear 1D site response analyses, *Soil Dynam. Earthq. Eng.* 29, 1143–1158.

R Core Team (2018). R: A language and environment for statistical computing. R Foundation for Statistical Computing, Vienna, Austria, ISBN 3-900051-07-0.

Rathje, E. M., Kottke, A. R., and Trent, W. L. (2010). Influence of input motion and site property variabilities on seismic site response analysis. *J. Geotech. Geoenviron. Engin.*, 136(4), 607–619.

Régnier, J., Cadet, H., Bonilla, L.F., Bertrand, E., and Semblat, J.-F. (2013). Assessing nonlinear behavior of soils in seismic site response: statistical analysis on KiK-net strong-motion data, *Bulletin of the Seismological Society of America,* 103(3), 1750–1770.

Shannon and Wilson (2018). Geotechnical data report, Stanford center liquefaction monitoring array, Seattle, Washington, *Report No. 21-1-21441-001*, Seattle, Washington, 333 pp.

Silva, W., Gregor, N., and Darragh, R. (2002). Development of regional hard rock attenuation relations for central and eastern North America, Pacific Engineering and Analysis Technical Report, El Cerrito, Calif., 57 pp.

Stewart, J. P., Afshari, K., and Hashash, Y. M. A. (2014). Guidelines for performing hazard-consistent one-dimensional ground response analysis for ground motion prediction, *PEER Report 2014/16*, Pacific Earthquake Engineering Research Center, University of California, Berkeley, California, 152 pp.

Toro, G. R. (1995). Probabilistic models of site velocity profiles for generic and site-specific ground-motion amplification studies, *Technical Report No. 779574*, Brookhaven National Laboratory, Upton, N.Y.

Thompson, E. M., Carkin, B., Baise, L. G., and Kayen, R. E. (2014). Surface wave site characterization at 27 locations near Boston, Massachusetts, including 2 strong-motion stations. *U.S. Geological Survey Open-File Report 2014–1232*, 27 pp.

University of Washington (2018). Washington earthquakes, http://www.washington.edu/uwem/preparedness/know-your-hazards/earthquake/the-triple-threat-of-washington-faults/. Last accessed 1 December 2018.

USGS (2014). Documentation for the 2014 Update of the United States National Seismic Hazard Maps. Open-file Report 2014-1091, 243 pp.

Williams, R. A., Stephenson, W. J., Frankel, A. D., and Odum, J. K. (1999). Surface seismic measurements of near-surface P- and S-wave seismic velocities at earthquake recording stations, Seattle, Washington. *Earthquake Spectra* 15, 565–584.

Woodhouse, D., and Barosh, P. J. (2011/2012). Geotechnical factors in Boston. *Civil Engineering Practice*, 26/27, 237–263.

Yegian, M. K. (2004). Seismic recording station at Northeastern University, Boston, Massachusetts. *Proceedings of the COSMOS International Workshop on Strong Motion Instrumentation*, 26-27 May 2004, Richmond, California, Consortium of Organizations for Strong Motion Observation Systems (COSMOS), 15 pp.

Yilar, E., Baise, L. G., and Ebel, J. E. (2017). Using H/V measurements to determine depth to bedrock and V_{S30} in Boston, Massachusetts. *Engineering Geology* 217, 12–22.

Zimmerman, R., Baker, J. W., Hooper, J. D., Bono, S., Haselton, C. B., Engel, A., Hamburger, R. O., Celikbas, A., and Jalalian, A., (2017). Response history analysis for the design of new buildings in the NEHRP provisions and ASCE/SEI 7 standard: Part III - Example applications to illustrate the recommended methodology, *Earthquake Spectra* 33, 419–447.

APPENDIX

This appendix contains one table and 16 figures that provide additional documentation for the results of this study. Visualizations and numerical data regarding the observations and model predictions are provided in multiple formats.

First, Table S1 displays details of our library of ground motions and suites considered in this study. Details of each ground-motion record are provided, including its data source, record sequence number, scale factor, time step, earthquake magnitude, epicentral distance, and average shear-wave velocity.

Figures S1 to S16 are detailed plots of the input and predicted ground motions for a sampling of suites assessed in this study. These figures are identical in format to Figures 6.5 and 6.6, and they display the following:

(a) Acceleration time series: input and predicted (for one horizontal component of the first record in the suite)
(b) Acceleration time series (zoomed at maximum acceleration), input and predicted (for one horizontal component of the first record in the suite)
(c) Husid plots, input and predicted (for one horizontal component of the first record in the suite)
(d) Response spectra, input and predicted (for each record in the suite, along with the median)
(e) Amplification spectra, predicted (for each record in the suite, along with the median)
(f) Profiles of PGA, predicted (for each record in the suite, along with the median)
(g) Shear-wave velocity, input
(h) Profiles of maximum shear strain, predicted (for each record in the suite, along with the median)

Ground-motion plots are provided for the uniform hazard spectra (corresponding to 2% and 10% probability of exceedance in 50 years), the conditional spectra for conditioning periods of T = 0.01 s and T = 1 s, and the risk-targeted maximum considered earthquake (MCE_R) spectra at each site. A total of 7 figures are provided for Boston and 9 figures are provided for Seattle.

Table S1. Library of suites and ground motions used in this study

Suite no.	Site	Suite ID	Set descriptor	Data source	Our library no.	Source record seq. no.	Scale factor	Time step, dt (s)	Moment magnitude, **M**	Source-to-site distance, R_{rup} (km)	Avg. S-wave vel., V_{S30} (m/s)
1	Boston	1a	Uniform Hazard Spectrum, 2% probability of exceedance in 50 years	NGA-East	1	1688	5.1	0.01	4.65	19.05	2000
					2	1681	7.5	0.01	4.65	39.01	2000
					3	10056	2	0.005	5.68	40.62	591
					4	10055	2	0.005	5.68	39.73	725
					5	3982	6.5	0.01	5.1	57.99	2000
					6	5711	0.5	0.005	6.76	5.32	1700
					7	8775	7.7	0.025	5.74	262.87	1404.6
					8	4027	3.9	0.01	5.1	52.94	1700
					9	10518	7	0.025	5.68	199.42	358.7
					10	2749	4	0.025	4.64	35.25	475
					11	8407	6.7	0.01	5.74	273.08	494.4
2	Boston	1b	Uniform Hazard Spectrum, 10% probability of exceedance in 50 years	NGA-East	12	1681	2.4	0.01	4.65	39.01	2000
					13	10056	0.6	0.005	5.68	40.62	591
					14	5711	0.2	0.005	6.76	5.32	1700
					15	1688	1.6	0.01	4.65	19.05	2000
					16	1684	3.5	0.01	4.65	61.57	2000
					17	3982	1.9	0.01	5.1	57.99	2000
					18	8762	5.6	0.025	5.74	377.14	578.9
					19	8425	6.6	0.025	5.74	485.48	1064.6
					20	10531	4.9	0.025	5.68	299.22	506.6
					21	8384	4.5	0.05	5.74	298.64	940
					22	10042	3.6	0.01	5.68	265.24	1015
3	Boston	2a(i)	Conditional Spectra, 2% in 50 years, T = 0.01 s; Dominant scenario (near-source moderate-magnitude earthquake)	NGA-East	23	5710	0.14	0.005	6.76	4.93	1700
					24	5709	0.05	0.005	6.76	9.6	1700
					25	5711	0.3	0.005	6.76	5.32	1700
					26	4027	1.46	0.01	5.1	52.94	1700
					27	4043	6.52	0.01	5.1	156.78	2000
					28	52	1.22	0.005	5.85	145.85	2000
					29	10488	7.51	0.025	5.68	213.27	1133.9
					30	3982	3.32	0.01	5.1	57.99	2000
					31	8775	9.1	0.025	5.74	262.87	1404.6
					32	3984	6.56	0.01	5.1	213.67	2000
					33	10042	7.14	0.01	5.68	265.24	1015

Table S1. Library of suites and ground motions used in this study (continued)

Suite no.	Site	Suite ID	Set descriptor	Data source	Our library no.	Source record seq. no.	Scale factor	Time step, dt (s)	Moment magnitude, **M**	Source-to-site distance, R_{rup} (km)	Avg. S-wave vel., V_{S30} (m/s)
4	Boston	2a(ii)	Conditional Spectra, 2% in 50 years, T = 0.01 s; Mean from deaggregation	NGA-East	34	8567	0.54	0.1	5.74	138.42	523.9
					35	3982	3.32	0.01	5.1	57.99	2000
					36	10055	2.14	0.005	5.68	39.73	725
					37	4043	6.52	0.01	5.1	156.78	2000
					38	10054	2.39	0.005	5.68	48.04	615
					39	8571	0.31	0.005	5.74	20.44	553.5
					40	9948	9.74	0.025	4.73	124.02	655.2
					41	5710	0.14	0.005	6.76	4.93	1700
					42	5711	0.3	0.005	6.76	5.32	1700
					43	9936	18.7	0.025	4.73	72.18	563.6
					44	10056	2.44	0.005	5.68	40.62	591
5	Boston	2b(i)	Conditional Spectra, 2% in 50 years, T = 1 s; Dominant scenario (near-source moderate-magnitude earthquake)	NGA-East	45	4027	6.51	0.01	5.1	52.94	1700
					46	3982	8.22	0.01	5.1	57.99	2000
					47	5711	0.78	0.005	6.76	5.32	1700
					48	1688	6.47	0.01	4.65	19.05	2000
					49	646	11.53	0.025	4.99	73.01	1503
					50	8946	5.63	0.025	5.74	250.17	1290.4
					51	10042	11.03	0.01	5.68	265.24	1015
					52	3984	10.44	0.01	5.1	213.67	2000
					53	5709	0.04	0.005	6.76	9.6	1700
					54	5710	0.09	0.005	6.76	4.93	1700
					55	10488	13.05	0.025	5.68	213.27	1133.9
6	Boston	2b(ii)	Conditional Spectra, 2% in 50 years, T = 1 s; Mean from deaggregation	NGA-East	56	10055	0.87	0.005	5.68	39.73	725
					57	8379	6.51	0.05	5.74	741.87	692.4
					58	10058	1.37	0.005	5.68	42.78	606
					59	5711	0.78	0.005	6.76	5.32	1700
					60	8932	10.37	0.025	5.74	943.66	651.2
					61	10054	1.19	0.005	5.68	48.04	615
					62	66	4.17	0.005	5.85	320.51	866.7
					63	10506	5.52	0.025	5.68	161.6	1050.8
					64	5710	0.09	0.005	6.76	4.93	1700
					65	8566	0.25	0.1	5.74	47.81	777.3
					66	1794	5.35	0.02	4.65	176.32	665.9

Table S1. Library of suites and ground motions used in this study (continued)

Suite no.	Site	Suite ID	Set descriptor	Data source	Our library no.	Source record seq. no.	Scale factor	Time step, dt (s)	Moment magnitude, **M**	Source-to-site distance, R_{rup} (km)	Avg. S-wave vel., V_{S30} (m/s)
7	Boston	3a	Risk-targeted Maximum Considered Earthquake (MCE_R), scaling [ASCE 7-16 design response spectrum multiplied by 1.5]	NGA-East	67	64	2.5	0.005	5.85	192.07	822.1
					68	8529	2.3	0.005	5.74	124.11	429.6
					69	4027	7.6	0.01	5.1	52.94	1700
					70	10058	3.2	0.005	5.68	42.78	606
					71	10056	4	0.005	5.68	40.62	591
					72	5710	0.3	0.005	6.76	4.93	1700
					73	4721	0.1	0.0066	6.8	5.46	300.9
					74	5711	0.9	0.005	6.76	5.32	1700
					75	8571	0.7	0.005	5.74	20.44	553.5
					76	52	3.6	0.005	5.85	145.85	2000
					77	10054	4.4	0.005	5.68	48.04	615
8	Seattle	1a	Uniform Hazard Spectrum, 2% probability of exceedance in 50 years	NGA-W2	78	1020	3.8	0.01	6.69	21.36	602.1
					79	4845	1.7	0.01	6.8	22.48	610.05
					80	8165	1	0.004	7.14	4.21	760
					81	1521	1.6	0.005	7.62	9	671.52
					82	810	2	0.005	6.93	18.41	713.59
					83	1280	4.5	0.005	7.62	51.46	602.29
					84	5791	3.8	0.01	6.9	74.82	640.14
					85	496	2.1	0.0025	6.76	4.93	605.04
					86	748	4.4	0.005	6.93	44.11	627.59
					87	1165	2.2	0.005	7.51	7.21	811
					88	4869	3.4	0.01	6.8	29.25	640.14
9	Seattle	1b	Uniform Hazard Spectrum, 10% probability of exceedance in 50 years	NGA-W2	89	3926	2.2	0.005	6.61	24.84	694.21
					90	5659	3.3	0.01	6.9	43.59	670.31
					91	1020	1.8	0.01	6.69	21.36	602.1
					92	495	0.5	0.0025	6.76	9.6	605.04
					93	1041	3.8	0.02	6.69	35.88	680.37
					94	1338	3.4	0.005	7.62	66.88	621.06
					95	1284	2.9	0.005	7.62	48.35	677.49
					96	1485	0.6	0.005	7.62	26	704.64
					97	2635	2.9	0.005	6.2	9.81	671.52
					98	1126	2.9	0.005	6.4	19.54	649.67
					99	1165	1.1	0.005	7.51	7.21	811

Table S1. Library of suites and ground motions used in this study (continued)

Suite no.	Site	Suite ID	Set descriptor	Data source	Our library no.	Source record seq. no.	Scale factor	Time step, dt (s)	Moment magnitude, **M**	Source-to-site distance, R_{rup} (km)	Avg. S-wave vel., V_{S30} (m/s)
10	Seattle	2a(i)	Conditional Spectra, 2% in 50 years, T = 0.01 s; Shallow crustal earthquakes	NGA-W2	100	5775	2.48	0.01	6.9	28.91	561.59
					101	4483	1.9	0.005	6.3	5.38	717
					102	1520	1.26	0.005	7.62	18.16	665.2
					103	4864	1.93	0.01	6.8	16.1	655.45
					104	1078	2.55	0.005	6.69	16.74	715.12
					105	809	1.76	0.005	6.93	18.51	713.59
					106	1642	2.38	0.02	5.61	22	680.37
					107	1111	1.38	0.01	6.9	7.08	609
					108	5663	0.9	0.01	6.9	20.18	479.37
					109	741	1.4	0.005	6.93	10.72	476.54
					110	3964	0.88	0.01	6.61	11.29	469.79
11	Seattle	2a(ii)	Conditional Spectra, 2% in 50 years, T = 0.01 s; Intraslab earthquakes	KiK-net	111	15016	2.09	0.005	6.8	53.59	461.46
					112	48995	6.87	0.005	6.8	94.69	604.72
					113	98430	3.22	0.01	7.4	134.85	438.04
					114	129296	7.05	0.01	6.3	82.67	521.09
					115	21530	4.47	0.005	7.1	144.45	455.93
					116	56823	6.24	0.005	6.8	78.26	629.48
					117	98718	5.8	0.01	7.4	148.97	431.65
					118	36618	2.64	0.005	7.1	100.7	748.29
					119	127476	7.29	0.01	6.3	119.03	448.55
					120	33875	3.34	0.005	7.1	110.82	933.96
					121	98631	5.52	0.01	5.9	91.13	455.93
12	Seattle	2a(iii)	Conditional Spectra, 2% in 50 years, T = 0.01 s; Interface earthquakes	KiK-net	122	157976	3.16	0.005	7.9	170.13	310.81
					123	105963	7.86	0.01	8.7	233.01	310.88
					124	97825	1.69	0.01	8.7	168.34	829.12
					125	94248	11.81	0.01	8.7	265.84	535.72
					126	99282	4.55	0.01	8.7	155.57	1269.78
					127	103485	11.77	0.01	7.8	155.26	371.62
					128	96235	12.31	0.01	7.8	108.92	448.55
					129	99735	14.28	0.01	7.8	281.26	670.31
					130	99548	1.57	0.01	8.7	120.97	922.89
					131	54216	1.42	0.005	7.9	102.5	353.21
					132	156640	3.19	0.005	7.9	151.28	412.21

Table S1. Library of suites and ground motions used in this study (continued)

Suite no.	Site	Suite ID	Set descriptor	Data source	Our library no.	Source record seq. no.	Scale factor	Time step, dt (s)	Moment magnitude, **M**	Source-to-site distance, R_{rup} (km)	Avg. S-wave vel., V_{S30} (m/s)
13	Seattle	2b(i)	Conditional Spectra, 2% in 50 years, T = 0.2 s; Shallow crustal earthquakes	NGA-W2	133	825	0.76	0.02	7.01	6.96	567.78
					134	2622	1.98	0.005	6.2	16.46	624.85
					135	1549	0.92	0.005	7.62	1.83	511.18
					136	139	1.53	0.02	7.35	13.94	471.53
					137	1078	1.67	0.005	6.69	16.74	715.12
					138	4842	1.25	0.01	6.8	22.74	655.45
					139	1511	1.74	0.005	7.62	2.74	614.98
					140	1642	2.88	0.02	5.61	22	680.37
					141	5819	2.57	0.01	6.9	23.02	640.14
					142	828	1.56	0.02	7.01	8.18	422.17
					143	1111	1.22	0.01	6.9	7.08	609
14	Seattle	2b(ii)	Conditional Spectra, 2% in 50 years, T = 0.2 s; Intraslab earthquakes	KiK-net	144	36618	4.29	0.005	7.1	100.7	748.29
					145	98631	4.18	0.01	5.9	91.13	455.93
					146	5972	2.46	0.005	6.8	86.39	363.85
					147	85515	4.42	0.01	5.9	104.91	347.54
					148	99709	4.74	0.01	5.9	122.8	371.06
					149	19375	3.92	0.01	6.8	96	558.56
					150	26426	3.59	0.005	7.1	149.72	371.06
					151	14901	4.18	0.005	6.8	95.31	370.59
					152	21530	4.79	0.005	7.1	144.45	455.93
					153	15182	4.98	0.005	6.8	84.49	495.15
					154	34230	3.24	0.005	7.1	117.11	849.83
15	Seattle	2b(iii)	Conditional Spectra, 2% in 50 years, T = 0.2 s; Interface earthquakes	KiK-net	155	101096	1.61	0.01	8.7	125.61	748.29
					156	157976	2.31	0.005	7.9	170.13	310.81
					157	99282	6.98	0.01	8.7	155.57	1269.78
					158	104171	12.74	0.01	7.8	144.66	468.4
					159	157579	12.81	0.005	7.9	245.08	367.94
					160	95775	5	0.01	8.7	226.29	349.74
					161	97825	1.73	0.01	8.7	168.34	829.12
					162	95891	2.23	0.01	8.7	213.35	596.03
					163	96505	11.36	0.01	7.8	131.19	307.18
					164	157261	7.2	0.005	7.9	271.28	389.57
					165	156914	13.72	0.005	7.9	197.08	541.81

Table S1. Library of suites and ground motions used in this study (continued)

Suite no.	Site	Suite ID	Set descriptor	Data source	Our library no.	Source record seq. no.	Scale factor	Time step, dt (s)	Moment magnitude, **M**	Source-to-site distance, R_{rup} (km)	Avg. S-wave vel., V_{S30} (m/s)
16	Seattle	2c(i)	Conditional Spectra, 2% in 50 years, T = 0.5 s; Shallow crustal earthquakes	NGA-W2	166	5663	1.62	0.01	6.9	20.18	479.37
					167	1227	1.5	0.005	7.62	10.8	553.43
					168	3966	1.25	0.01	6.61	8.83	420.2
					169	1487	1.06	0.005	7.62	35	520.37
					170	4482	1.01	0.005	6.3	6.55	552
					171	5267	2.64	0.01	6.8	29.8	418.5
					172	3964	0.62	0.01	6.61	11.29	469.79
					173	5657	0.47	0.01	6.9	4.8	506.44
					174	1208	2.82	0.005	7.62	24.1	442.15
					175	8158	1.26	0.005	6.2	6.12	649.67
					176	4149	1.98	0.005	6	9.47	466.12
17	Seattle	2c(ii)	Conditional Spectra, 2% in 50 years, T = 0.5 s; Intraslab earthquakes	KiK-net	177	56823	5.7	0.005	6.8	78.26	629.48
					178	36244	2.78	0.005	7.1	100.91	859.19
					179	85508	7.54	0.01	5.9	129.1	358.25
					180	165578	6.58	0.005	7	162.17	372.41
					181	5972	0.87	0.005	6.8	86.39	363.85
					182	35664	2.45	0.005	7.1	153.68	358.25
					183	98435	7.14	0.01	6.6	165.71	438.04
					184	21530	6.34	0.005	7.1	144.45	455.93
					185	36618	5.16	0.005	7.1	100.7	748.29
					186	127700	6.04	0.01	6.3	97.66	338.06
					187	26426	2.17	0.005	7.1	149.72	371.06
18	Seattle	2c(iii)	Conditional Spectra, 2% in 50 years, T = 0.5 s; Interface earthquakes	KiK-net	188	97271	7.38	0.01	7.8	206.52	323.08
					189	157976	2.41	0.005	7.9	170.13	310.81
					190	104285	2.55	0.01	8.7	231.97	328.98
					191	93724	5.86	0.01	8.7	244.65	475.09
					192	100947	9.9	0.01	7.8	179.91	358.25
					193	94940	13.44	0.01	8.7	282.15	329.03
					194	94513	6.41	0.01	8.7	241.14	431
					195	93840	8.12	0.01	8.7	256.66	320.23
					196	104171	10.58	0.01	7.8	144.66	468.4
					197	98099	3.23	0.01	8.7	228.93	692.31
					198	54216	1.57	0.005	7.9	102.5	353.21

Table S1. Library of suites and ground motions used in this study (continued)

Suite no.	Site	Suite ID	Set descriptor	Data source	Our library no.	Source record seq. no.	Scale factor	Time step, dt (s)	Moment magnitude, **M**	Source-to-site distance, R_{rup} (km)	Avg. S-wave vel., V_{S30} (m/s)
19	Seattle	2d(i)	Conditional Spectra, 2% in 50 years, T = 1 s; Shallow crustal earthquakes	NGA-W2	199	787	0.78	0.005	6.93	30.86	425.3
					200	4148	2.39	0.005	6	9.47	466.12
					201	1549	0.72	0.005	7.62	1.83	511.18
					202	4869	2.63	0.01	6.8	29.25	640.14
					203	3964	2.27	0.01	6.61	11.29	469.79
					204	8158	1.27	0.005	6.2	6.12	649.67
					205	3475	1.15	0.005	6.3	10.2	489.32
					206	3269	2.87	0.005	6.3	41.36	544.74
					207	4229	1.8	0.005	6.63	10.72	564.25
					208	1488	1.92	0.005	7.62	13.53	551.21
					209	1787	1.14	0.01	7.13	11.66	726
20	Seattle	2d(ii)	Conditional Spectra, 2% in 50 years, T = 1 s; Intraslab earthquakes	KiK-net	210	36244	7.45	0.005	7.1	100.91	859.19
					211	21893	5.44	0.005	7.1	121.07	429.2
					212	5972	3.58	0.005	6.8	86.39	363.85
					213	26426	2.45	0.005	7.1	149.72	371.06
					214	165584	6.51	0.005	6.7	168.37	372.41
					215	135443	7.57	0.01	5.9	134.15	358.25
					216	85508	7.32	0.01	5.9	129.1	358.25
					217	34668	4.54	0.005	7.1	145.44	305.33
					218	56823	5	0.005	6.8	78.26	629.48
					219	165578	2.86	0.005	7	162.17	372.41
					220	98430	7.08	0.01	7.4	134.85	438.04
21	Seattle	2d(iii)	Conditional Spectra, 2% in 50 years, T = 1 s; Interface earthquakes	KiK-net	221	93724	4.39	0.01	8.7	244.65	475.09
					222	93951	8.79	0.01	8.7	234.94	829.46
					223	14470	0.91	0.005	7.9	99.19	459.06
					224	156640	0.65	0.005	7.9	151.28	412.21
					225	95775	2.74	0.01	8.7	226.29	349.74
					226	155910	9.37	0.005	7.9	233.26	378.36
					227	159542	7.85	0.005	7.9	233.9	315.92
					228	158045	11.38	0.005	7.9	219.8	355.5
					229	105094	14.77	0.01	7.8	204.54	459.49
					230	97226	11.73	0.01	7.8	190.85	406.76
					231	96569	1.47	0.01	8.7	139.95	338.06

Table S1. Library of suites and ground motions used in this study (continued)

Suite no.	Site	Suite ID	Set descriptor	Data source	Our library no.	Source record seq. no.	Scale factor	Time step, dt (s)	Moment magnitude, **M**	Source-to-site distance, R_{rup} (km)	Avg. S-wave vel., V_{S30} (m/s)
22	Seattle	2e(i)	Conditional Spectra, 2% in 50 years, T = 3 s; Shallow crustal earthquakes	NGA-W2	232	8157	1.13	0.005	6.2	3.36	422
					233	1504	0.58	0.005	7.62	0.62	433.63
					234	1549	0.96	0.005	7.62	1.83	511.18
					235	4854	2.56	0.01	6.8	35.93	570.62
					236	4350	1.19	0.005	6	35.91	492
					237	763	2.35	0.005	6.93	9.96	729.65
					238	1231	0.6	0.005	7.62	2.69	496.21
					239	8158	0.96	0.005	6.2	6.12	649.67
					240	6928	1.78	0.005	7	25.67	649.67
					241	4016	2.46	0.005	6.52	31.39	493.5
					242	5773	1.63	0.01	6.9	41.13	531.25
23	Seattle	2e(ii)	Conditional Spectra, 2% in 50 years, T = 3 s; Intraslab earthquakes	KiK-net	243	31056	3.31	0.005	7	104.07	388.89
					244	99225	3.66	0.01	7.4	162.11	534.71
					245	35907	1.88	0.005	7.1	130.98	347.54
					246	98	5.89	0.005	7	125.76	394.29
					247	53262	6.61	0.005	7	150.04	444.94
					248	26426	6.19	0.005	7.1	149.72	371.06
					249	53725	7.34	0.005	7	144.95	337.28
					250	14613	1.86	0.01	6.8	112.92	459.06
					251	34668	3.7	0.005	7.1	145.44	305.33
					252	35664	4.02	0.005	7.1	153.68	358.25
					253	165578	4.07	0.005	7	162.17	372.41
24	Seattle	2e(iii)	Conditional Spectra, 2% in 50 years, T = 3 s; Interface earthquakes	KiK-net	254	95737	14.92	0.01	7.8	189.88	507.56
					255	100947	13.05	0.01	7.8	179.91	358.25
					256	97126	15.4	0.01	7.8	207.71	623.87
					257	105968	16.65	0.01	7.8	240.83	310.88
					258	104285	3.29	0.01	8.7	231.97	328.98
					259	94215	4.61	0.01	8.7	277.86	389.24
					260	104479	6.95	0.01	7.8	127.96	423
					261	157383	8.83	0.005	7.9	255.63	431.65
					262	105094	13.45	0.01	7.8	204.54	459.49
					263	105713	6.68	0.01	7.8	193.95	371.57
					264	101736	16.01	0.01	7.8	275.67	526.87

Table S1. Library of suites and ground motions used in this study (continued)

Suite no.	Site	Suite ID	Set descriptor	Data source	Our library no.	Source record seq. no.	Scale factor	Time step, dt (s)	Moment magnitude, **M**	Source-to-site distance, R_{rup} (km)	Avg. S-wave vel., V_{S30} (m/s)
25	Seattle	3a	Risk-targeted Maximum Considered Earthquake (MCE_R) [ASCE 7-16 design response spectrum multiplied by 1.5]	NGA-W2	265	1464	4.3	0.005	7.62	72.61	607.4
					266	3925	4.7	0.005	6.61	15.23	940.2
					267	71	3.6	0.01	6.61	19.3	602.1
					268	1020	4.1	0.01	6.69	21.36	602.1
					269	4870	4.3	0.01	6.8	34.51	561.59
					270	1080	1.4	0.01	6.69	13.42	557.42
					271	1475	3.5	0.005	7.62	56.12	569.98
					272	1211	4.5	0.004	7.62	39.02	573.04
					273	1520	1.8	0.005	7.62	18.16	665.2
					274	810	2.2	0.005	6.93	18.41	713.59
					275	1198	1.8	0.005	7.62	10.96	544.74

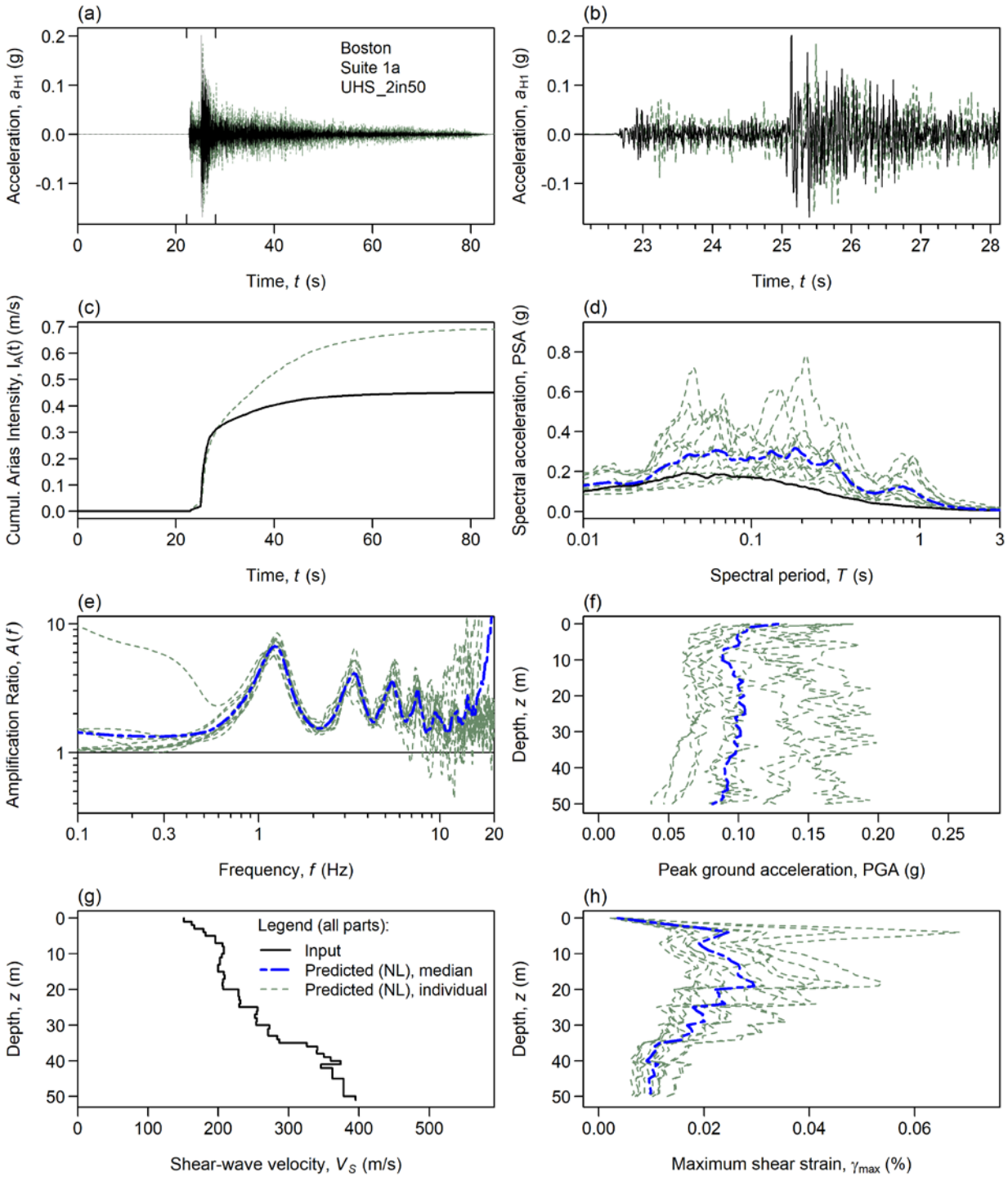

Figure S1. Detailed ground-motion plots for the NL analyses in Boston for the suite of ground motions obtained for the uniform hazard spectrum for a 2% probability of exceedance in 50 years [Suite 1a]. The figure displays (a) acceleration time series throughout the whole record, (b) acceleration time series zoomed at maximum acceleration, (c) Husid plots, (d) response spectra, (e) amplification spectra, (f) profiles of PGA versus depth, (g) V_S profile, and (h) profiles of maximum shear strain versus depth.

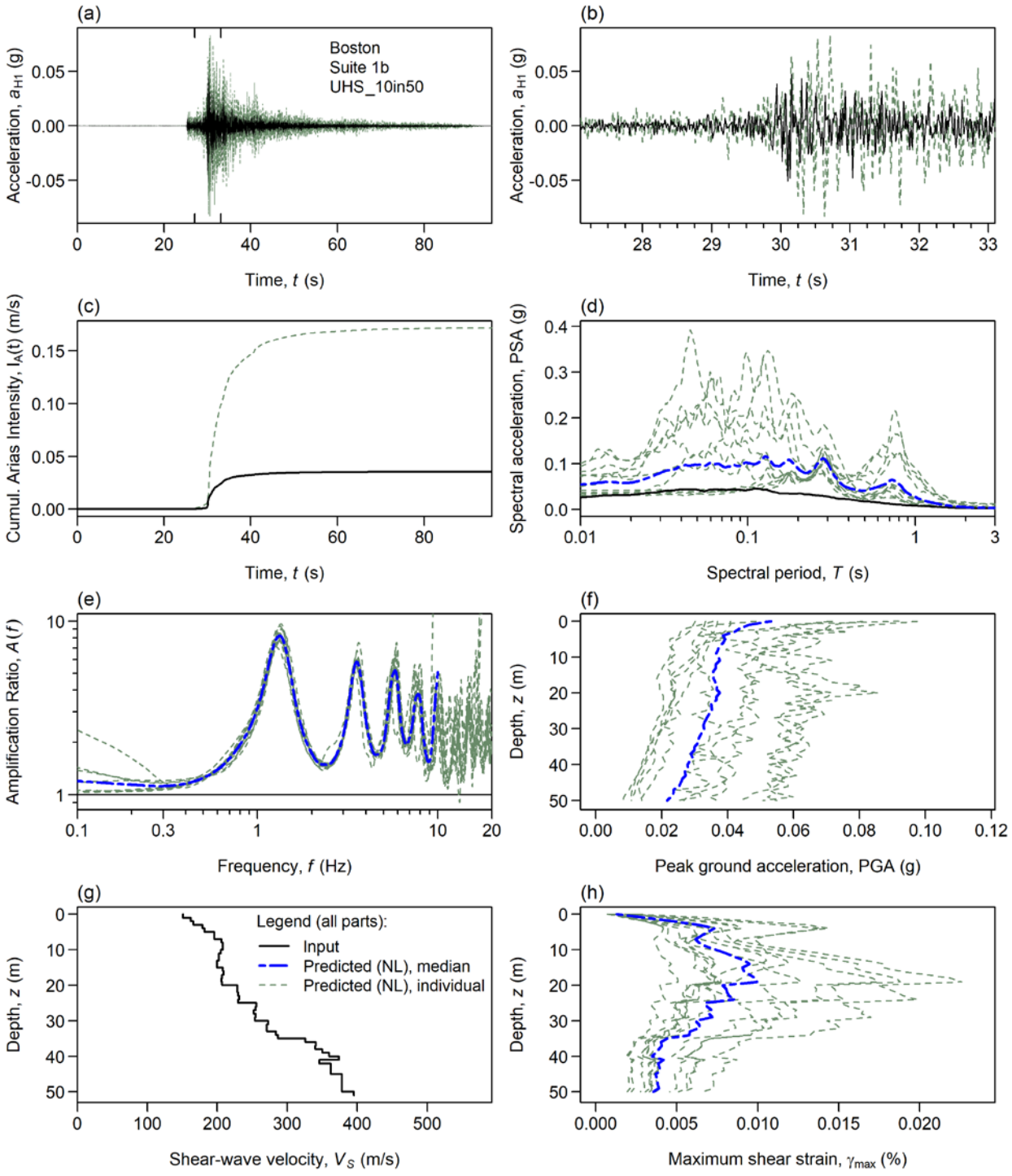

Figure S2. Detailed ground-motion plots for the NL analyses in Boston for the suite of ground motions obtained for the uniform hazard spectrum for a 10% probability of exceedance in 50 years [Suite 1b]. The figure (and all the figures to follow) has the same format as Figure S1.

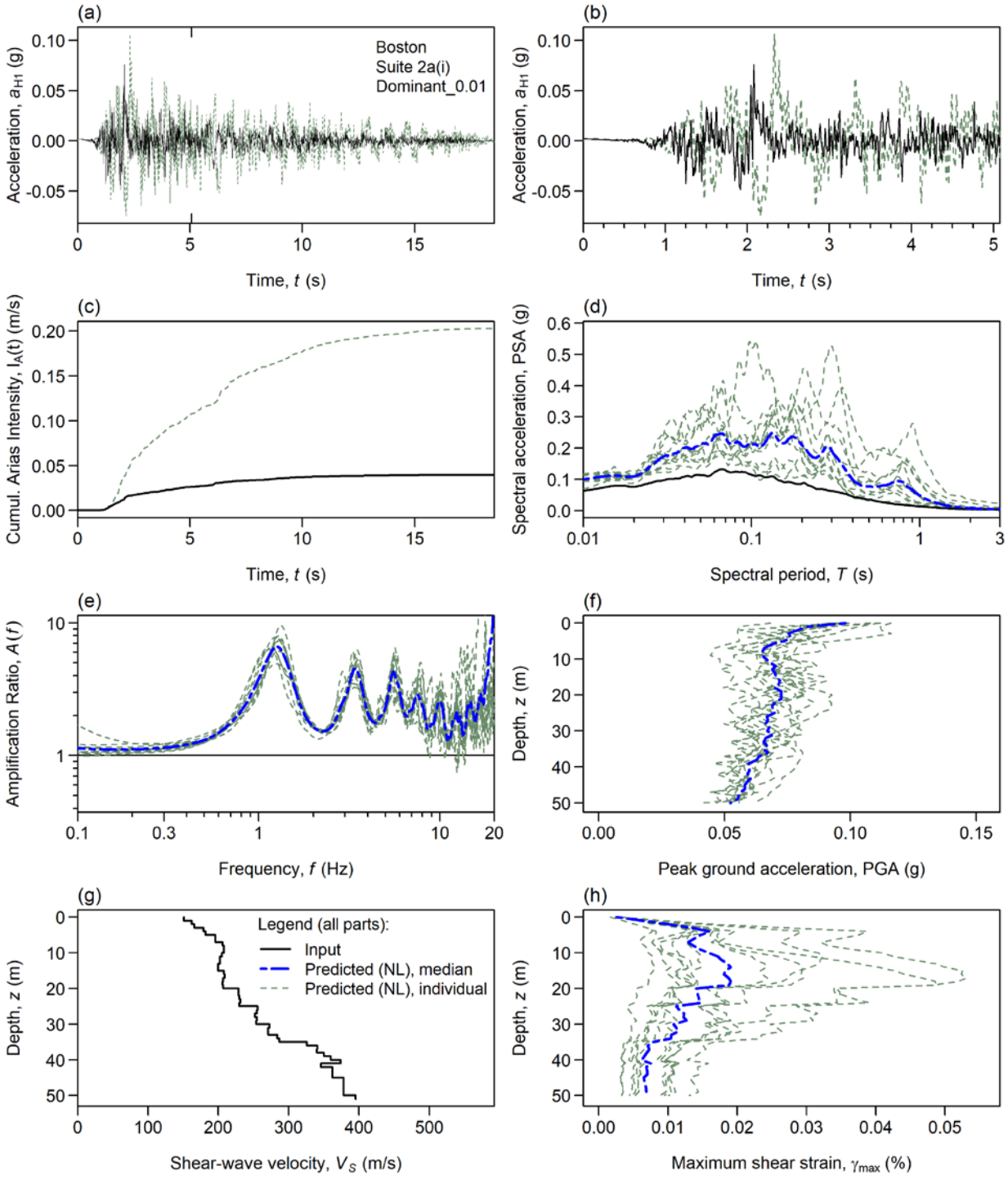

Figure S3. Detailed ground-motion plots for the NL analyses in Boston for the suite of ground motions obtained from the conditional spectra for a hazard level of 2% in 50 years corresponding to a spectral period of T = 0.01 s. For this suite (also shown in Figure 6.5), the input motions were selected for the dominant scenario from the deaggregation representing a near-source earthquake of moment magnitude **M** = 5.5 and source-to-site distance R_{rup} = 30 km [Suite 2a(i)].

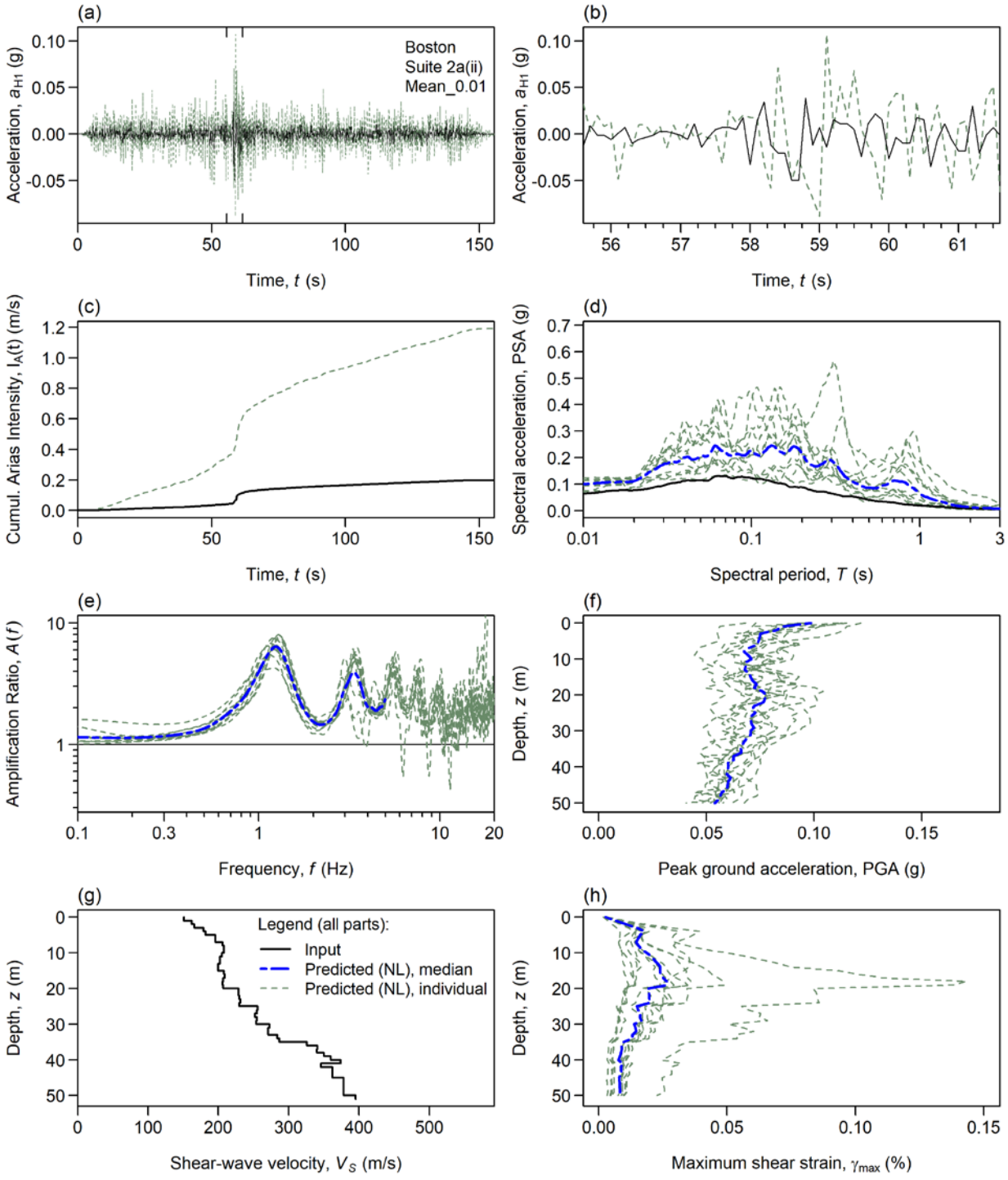

Figure S4. Detailed ground-motion plots for the NL analyses in Boston for the suite of ground motions obtained from the conditional spectra for a hazard level of 2% in 50 years corresponding to a spectral period of T = 0.01 s. For this suite, the input motions were selected for the mean M, R combination from the deaggregation: **M** = 5.77 and source-to-site distance R_{rup} = 58.1 km [Suite 2a(ii)].

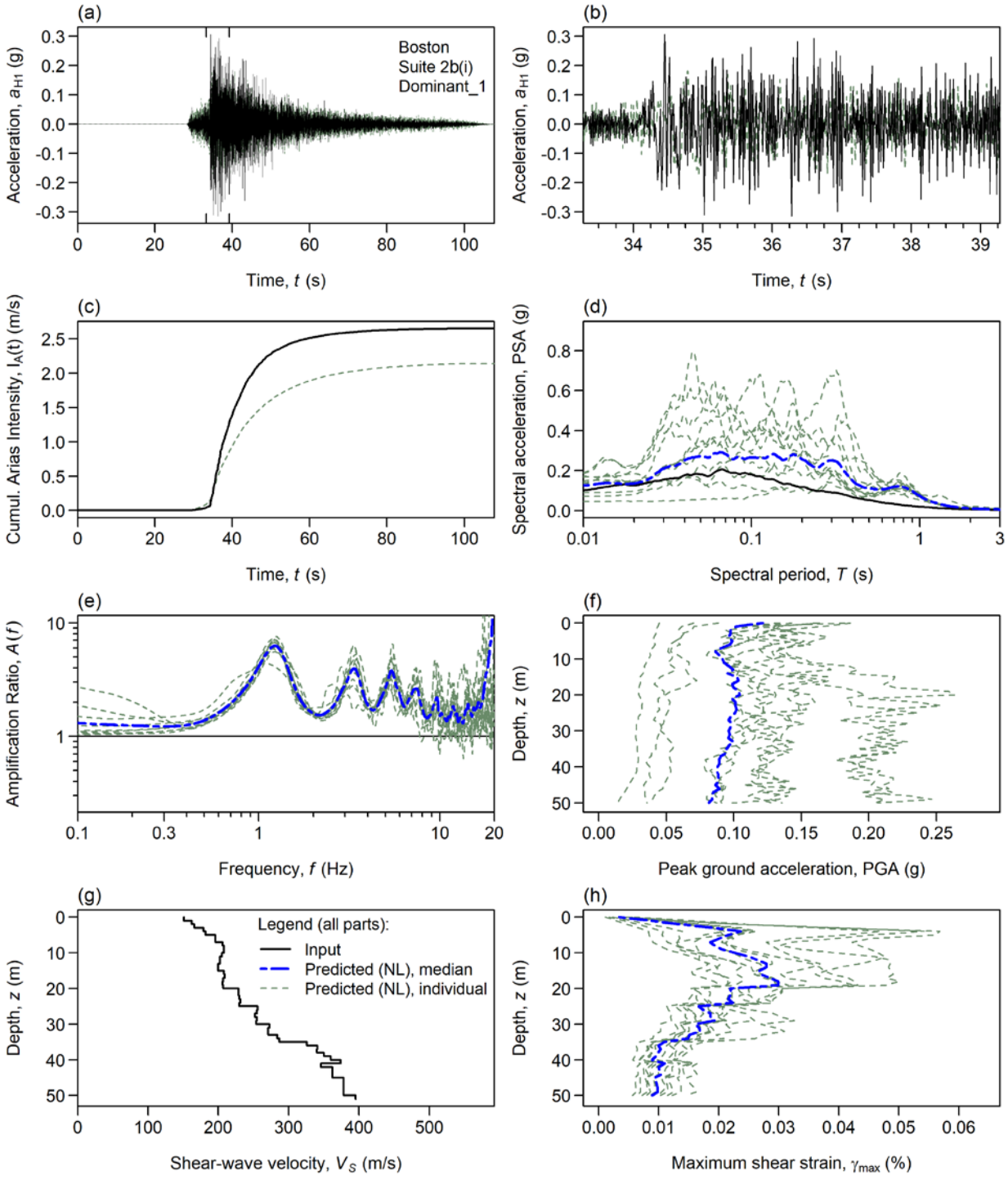

Figure S5. Detailed ground-motion plots for the NL analyses in Boston for the suite of ground motions obtained from the conditional spectra for a hazard level of 2% in 50 years corresponding to a spectral period of T = 1 s. For this suite, the input motions were selected for the dominant scenario from the deaggregation representing a near-source earthquake of moment magnitude **M** = 6.0 and source-to-site distance R_{rup} = 30 km [Suite 2b(i)].

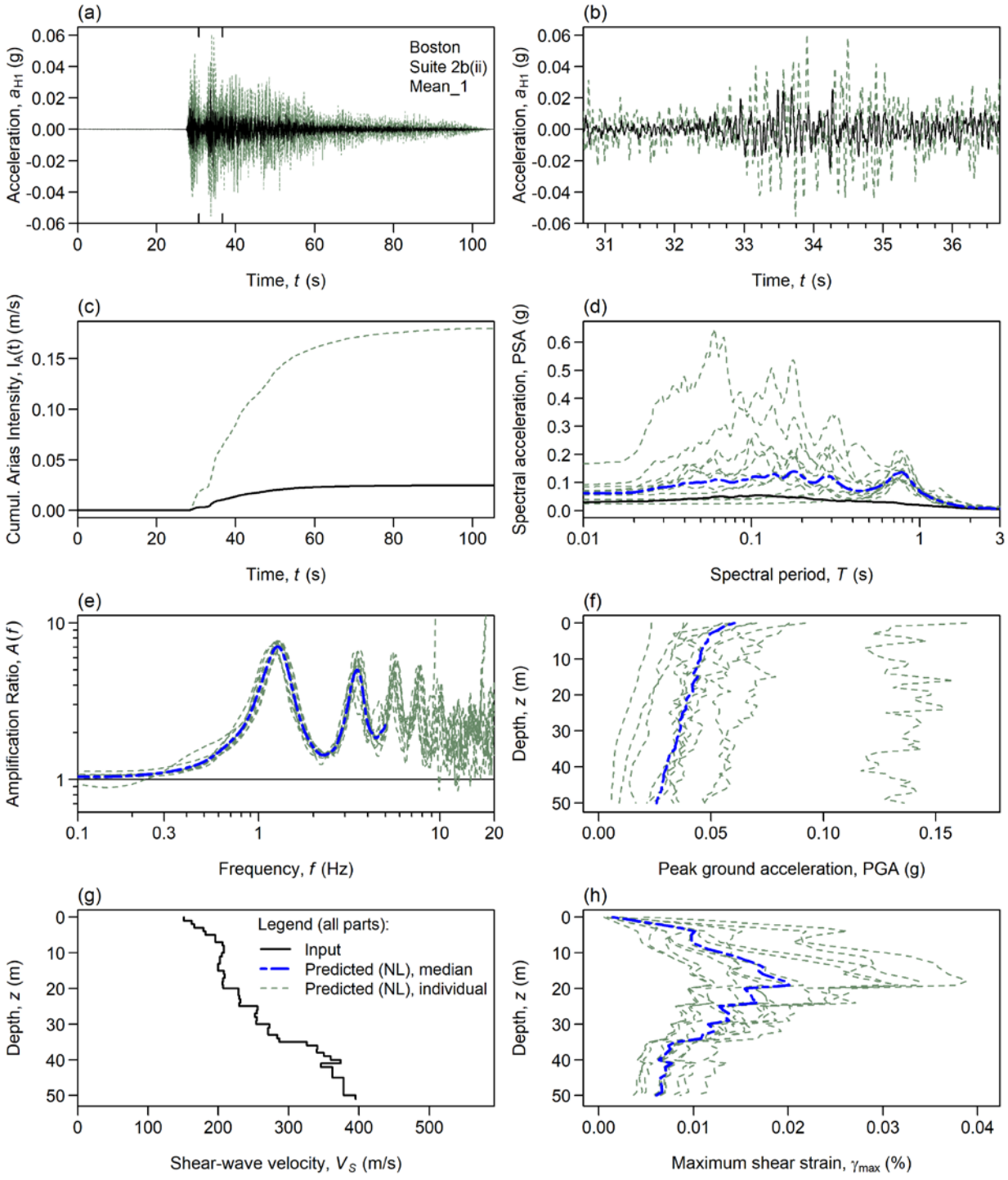

Figure S6. Detailed ground-motion plots for the NL analyses in Boston for the suite of ground motions obtained from the conditional spectra for a hazard level of 2% in 50 years corresponding to a spectral period of T = 1 s. For this suite, the input motions were selected for the mean M, R combination from the deaggregation: **M** = 6.22 and source-to-site distance R_{rup} = 149.21 km [Suite 2b(ii)].

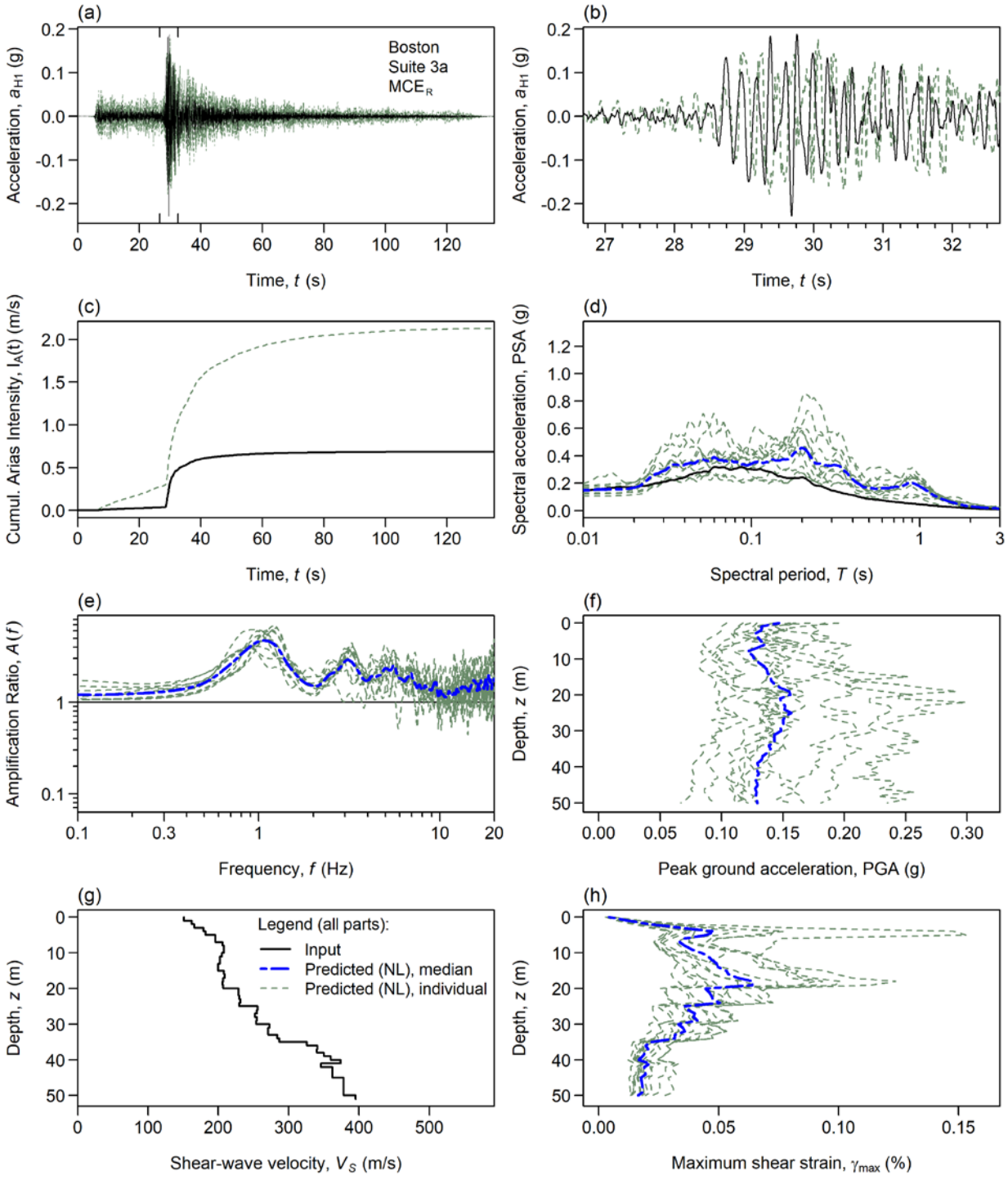

Figure S7. Detailed ground-motion plots for the NL analyses in Boston for the suite of ground motions obtained for the risk-targeted maximum considered earthquake (MCE_R) design spectrum [Suite 3a].

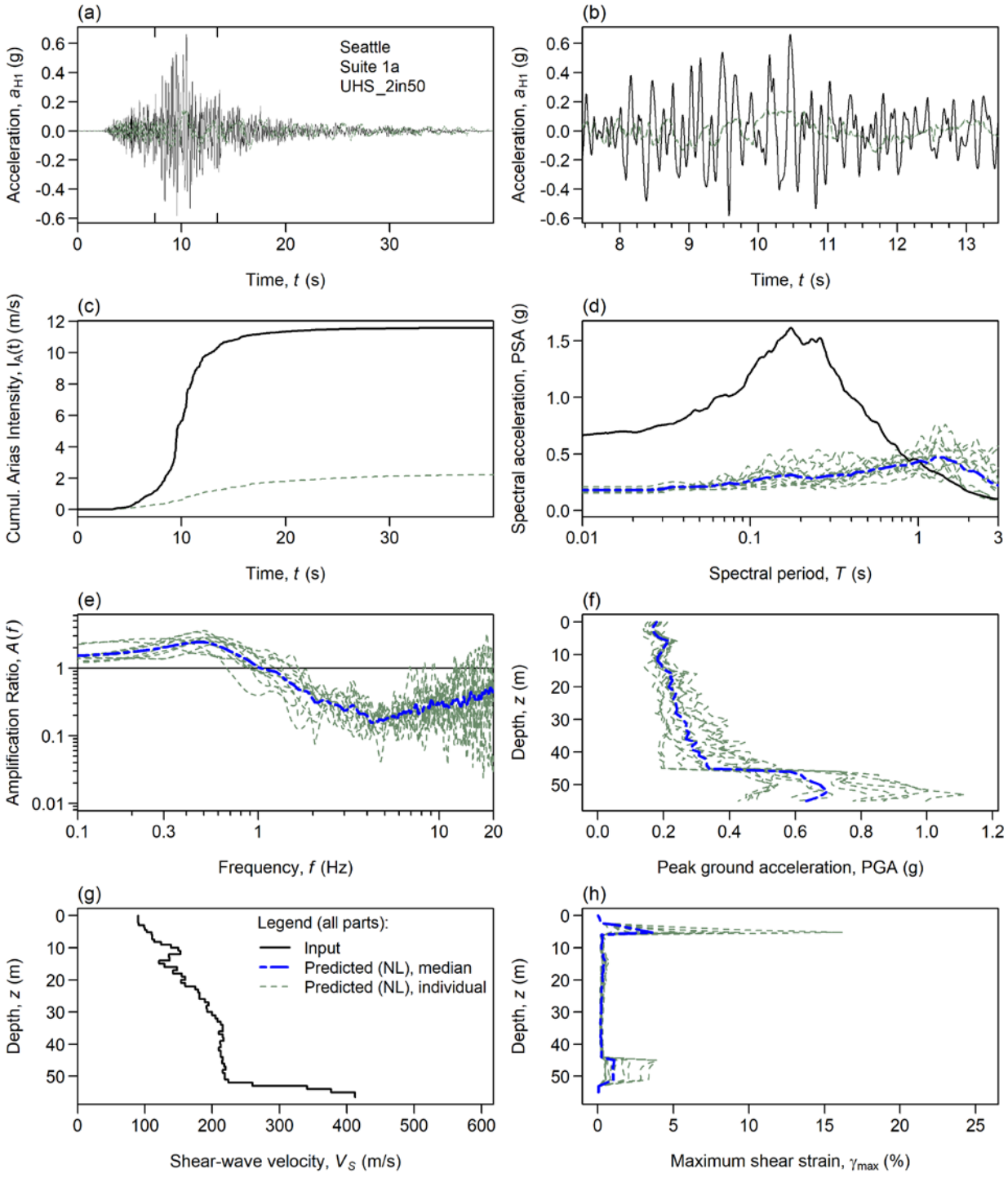

Figure S8. Detailed ground-motion plots for the NL analyses in Seattle for the suite of ground motions obtained for the uniform hazard spectrum for a 2% probability of exceedance in 50 years [Suite 1a].

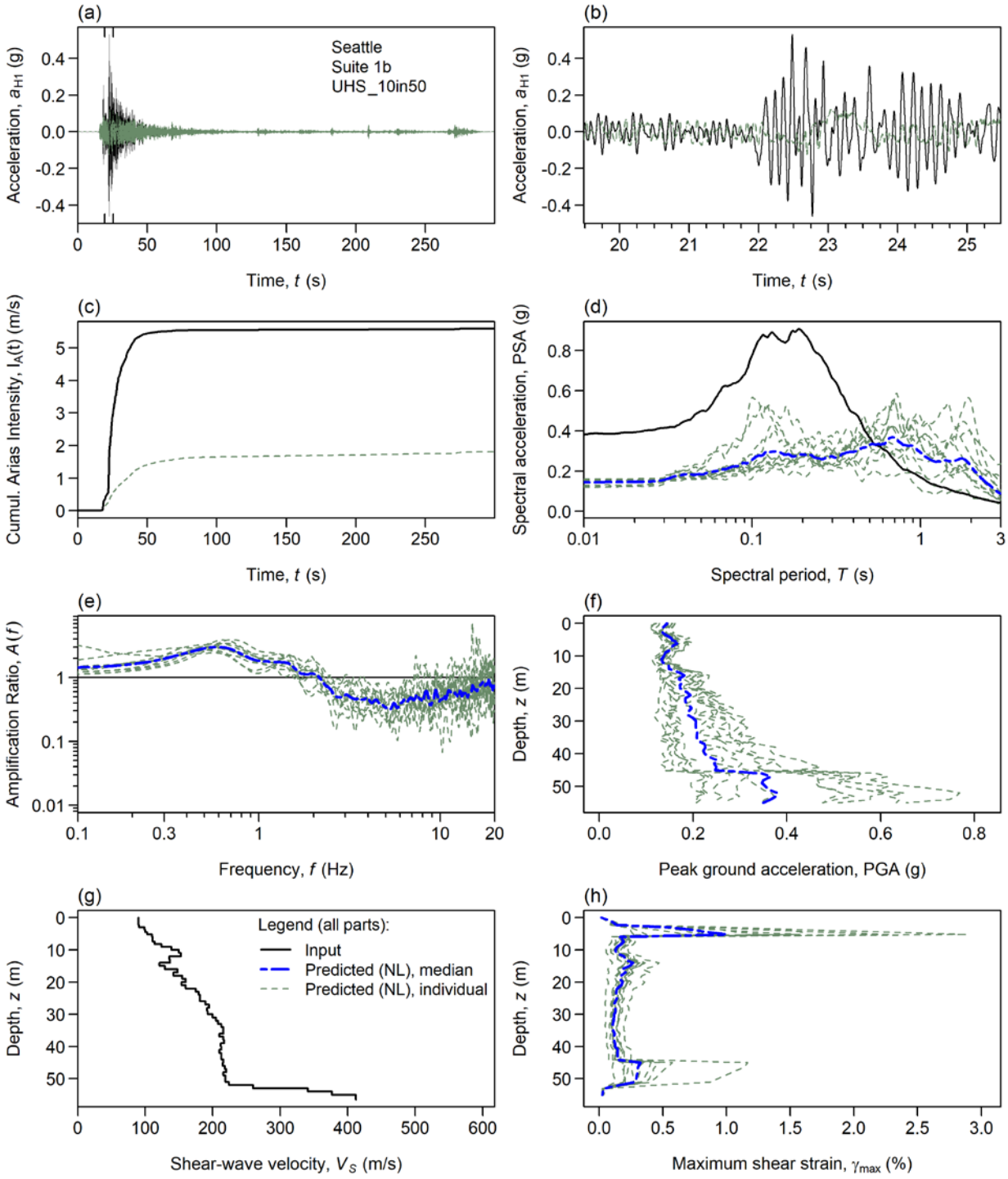

Figure S9. Detailed ground-motion plots for the NL analyses in Seattle for the suite of ground motions obtained for the uniform hazard spectrum for a 10% probability of exceedance in 50 years [Suite 1b].

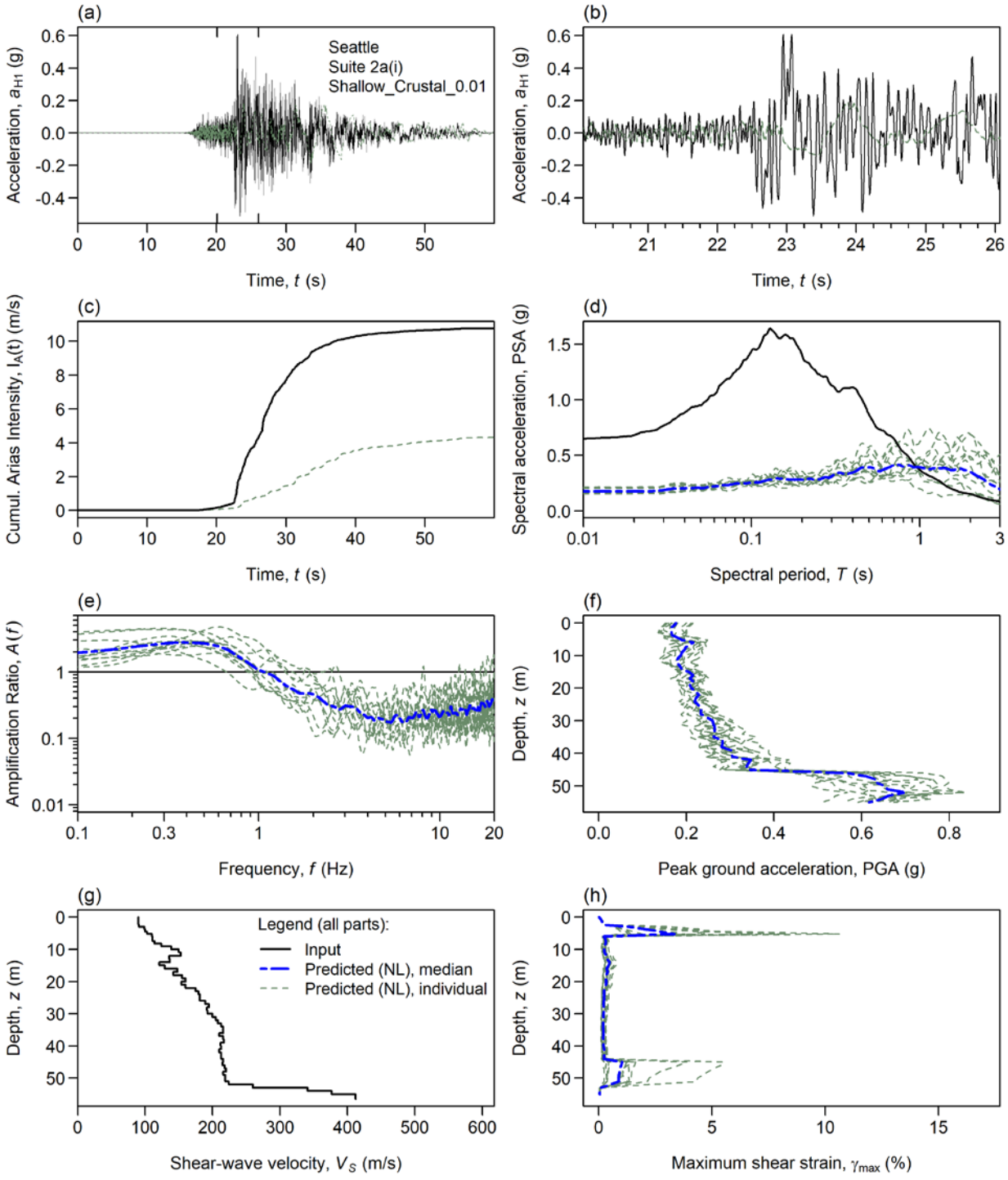

Figure S10. Detailed ground-motion plots for the NL analyses in Seattle obtained from the conditional spectra for a hazard level of 2% in 50 years corresponding to a spectral period of T = 0.01 s. For this suite (also shown in Figure 6.6), the input motions were selected for the shallow crustal earthquake dominant scenario from the deaggregation representing a near-source earthquake of moment magnitude **M** = 7.0 and source-to-site distance R_{rup} = 5 km [Suite 2a(i)].

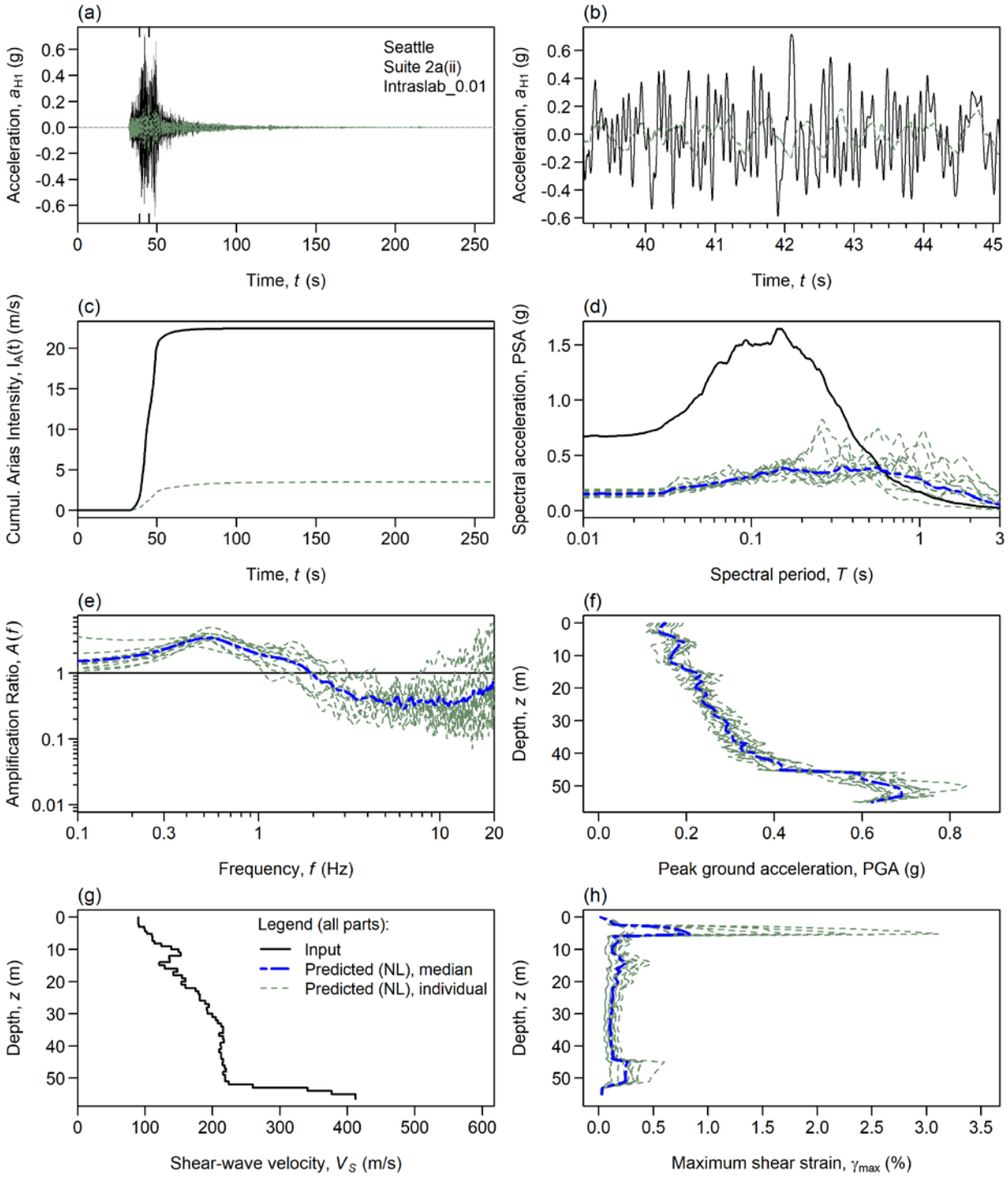

Figure S11. Detailed ground-motion plots for the NL analyses in Seattle obtained from the conditional spectra for a hazard level of 2% in 50 years corresponding to a spectral period of T = 0.01 s. For this suite, the input motions were selected for the subduction intraslab earthquake dominant scenario from the deaggregation representing an earthquake of moment magnitude **M** = 7.0 and source-to-site distance R_{rup} = 50 km [Suite 2a(ii)].

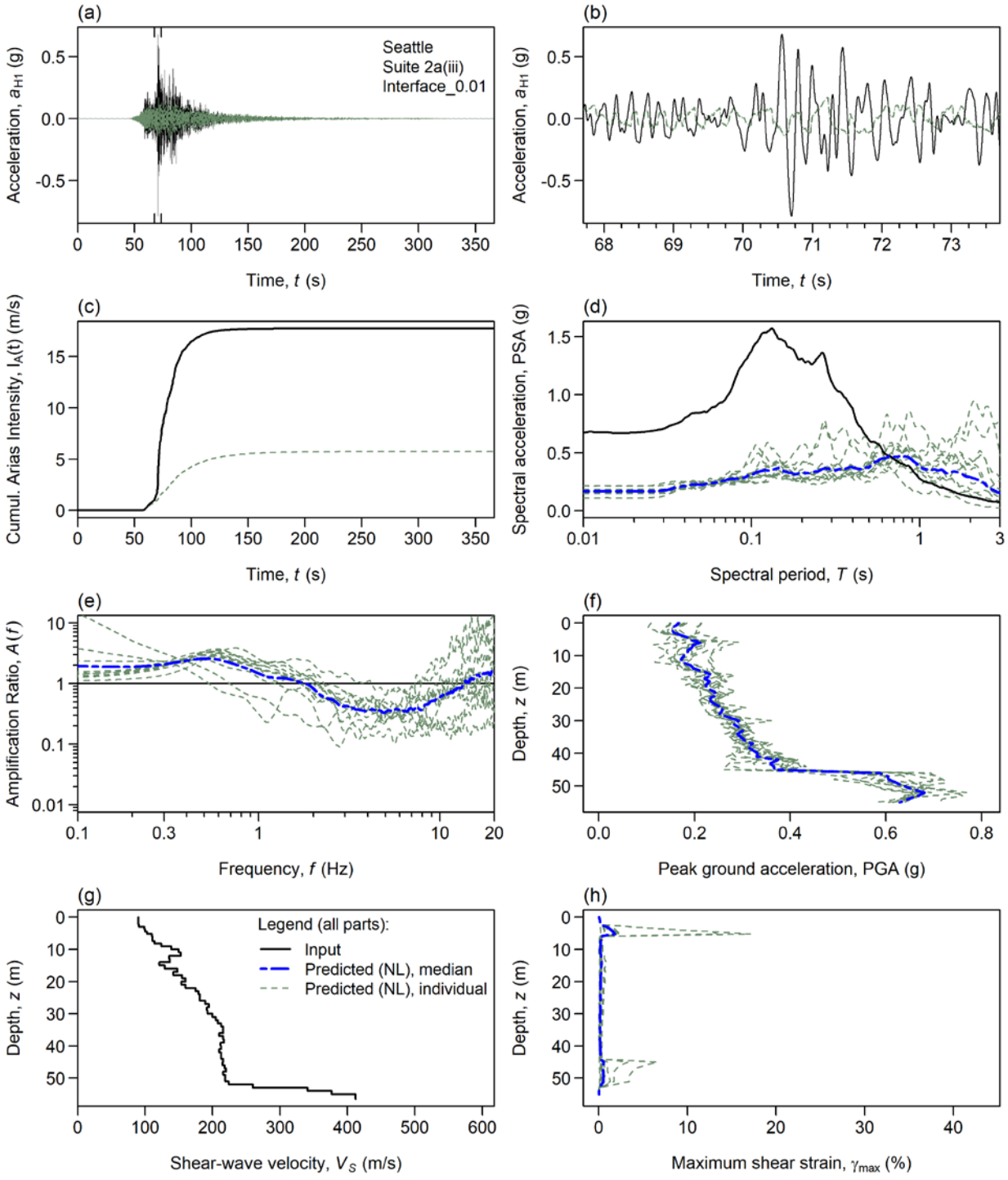

Figure S12. Detailed ground-motion plots for the NL analyses in Seattle obtained from the conditional spectra for a hazard level of 2% in 50 years corresponding to a spectral period of T = 0.01 s. For this suite, the input motions were selected for the subduction interface earthquake dominant scenario from the deaggregation representing an earthquake of moment magnitude **M** = 9.0 and source-to-site distance R_{rup} = 100 km [Suite 2a(iii)].

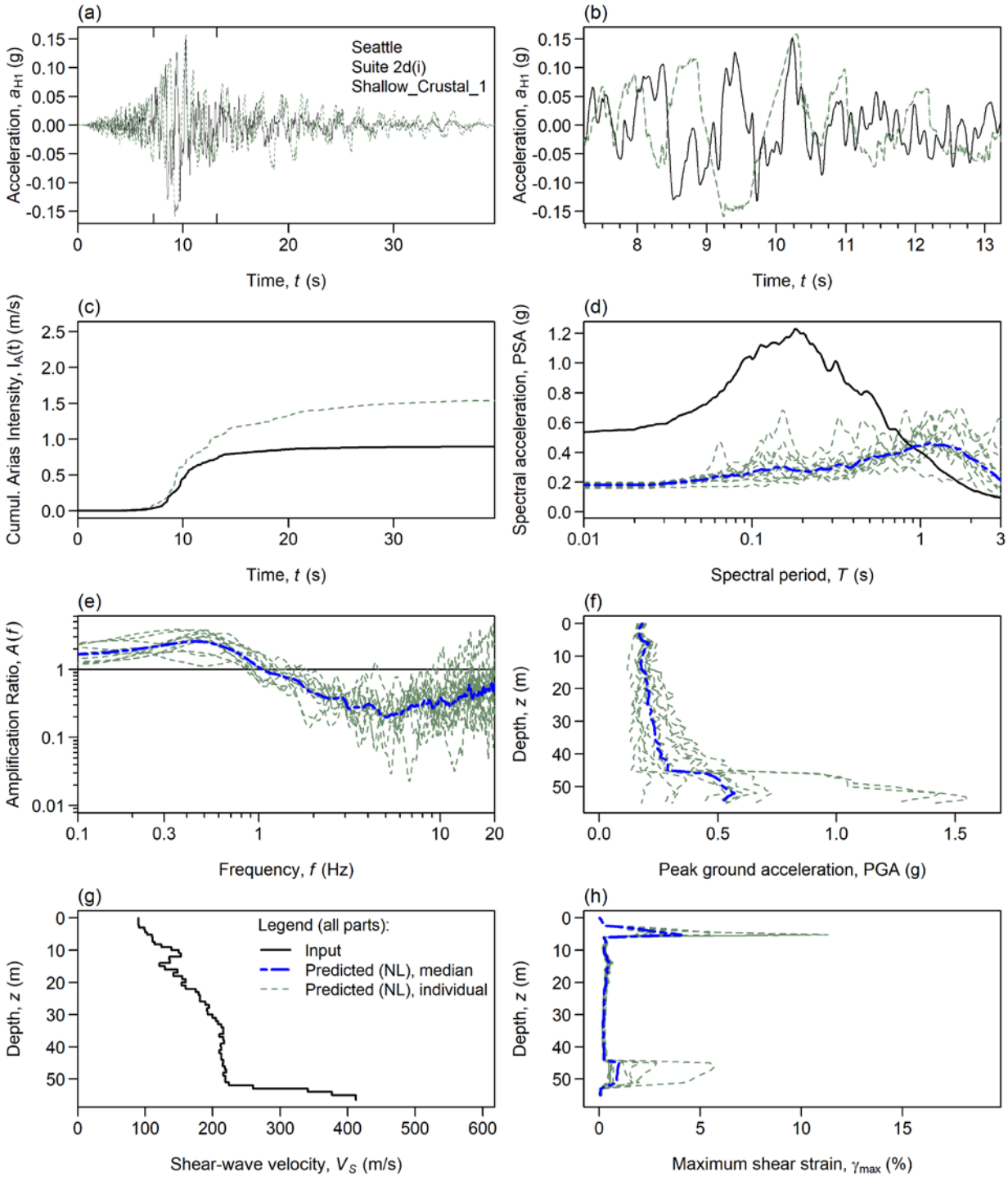

Figure S13. Detailed ground-motion plots for the NL analyses in Seattle obtained from the conditional spectra for a hazard level of 2% in 50 years corresponding to a spectral period of T = 1 s. For this suite, the input motions were selected for the shallow crustal earthquake dominant scenario from the deaggregation representing a near-source earthquake of moment magnitude **M** = 7.0 and source-to-site distance R_{rup} = 5 km [Suite 2d(i)].

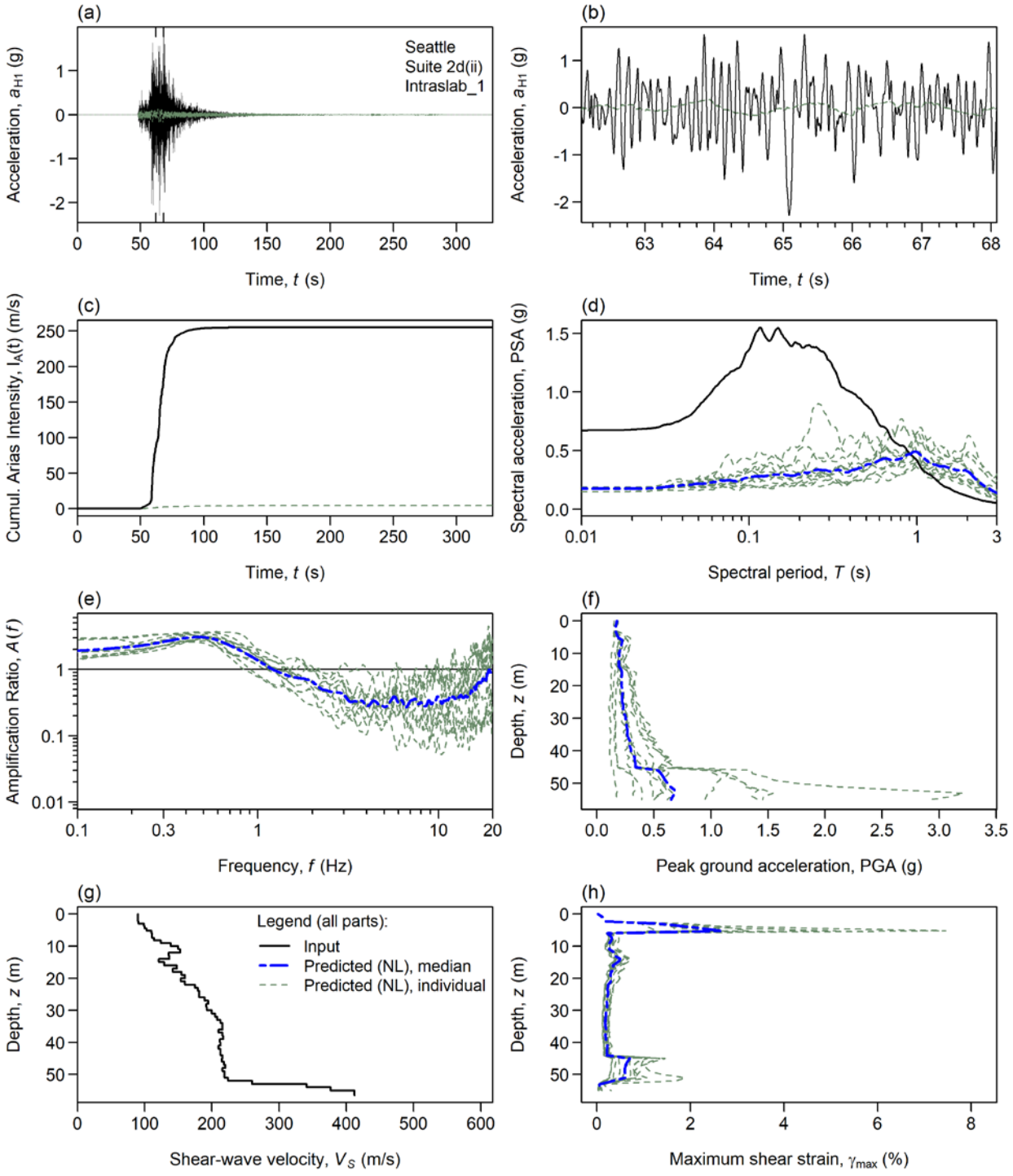

Figure S14. Detailed ground-motion plots for the NL analyses in Seattle obtained from the conditional spectra for a hazard level of 2% in 50 years corresponding to a spectral period of T = 1 s. For this suite, the input motions were selected for the subduction intraslab earthquake dominant scenario from the deaggregation representing an earthquake of moment magnitude **M** = 7.0 and source-to-site distance R_{rup} = 50 km [Suite 2d(ii)].

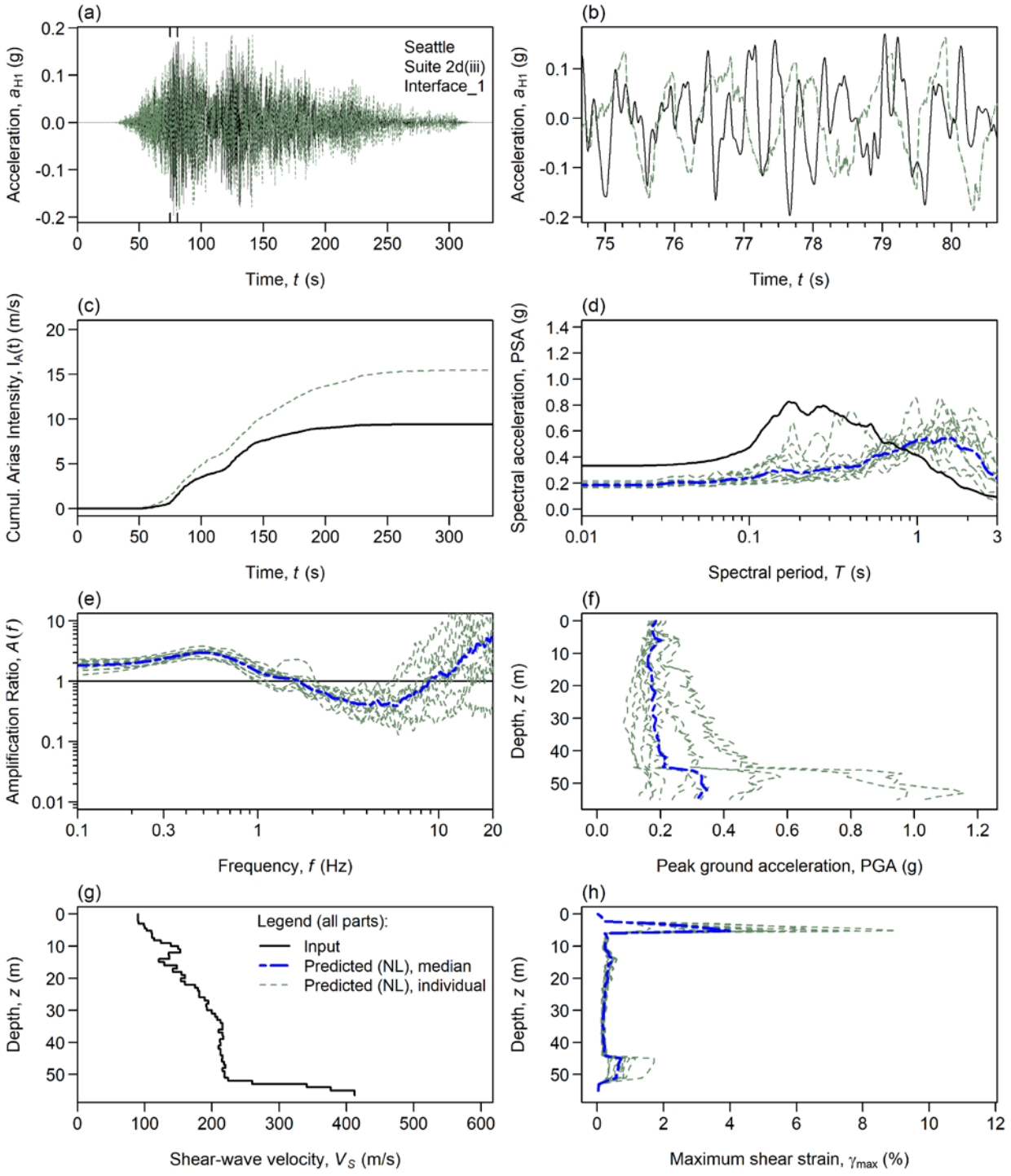

Figure S15. Detailed ground-motion plots for the NL analyses in Seattle obtained from the conditional spectra for a hazard level of 2% in 50 years corresponding to a spectral period of T = 1 s. For this suite, the input motions were selected for the subduction interface earthquake dominant scenario from the deaggregation, representing an earthquake of moment magnitude **M** = 9.0 and source-to-site distance R_{rup} = 100 km [Suite 2d(iii)].

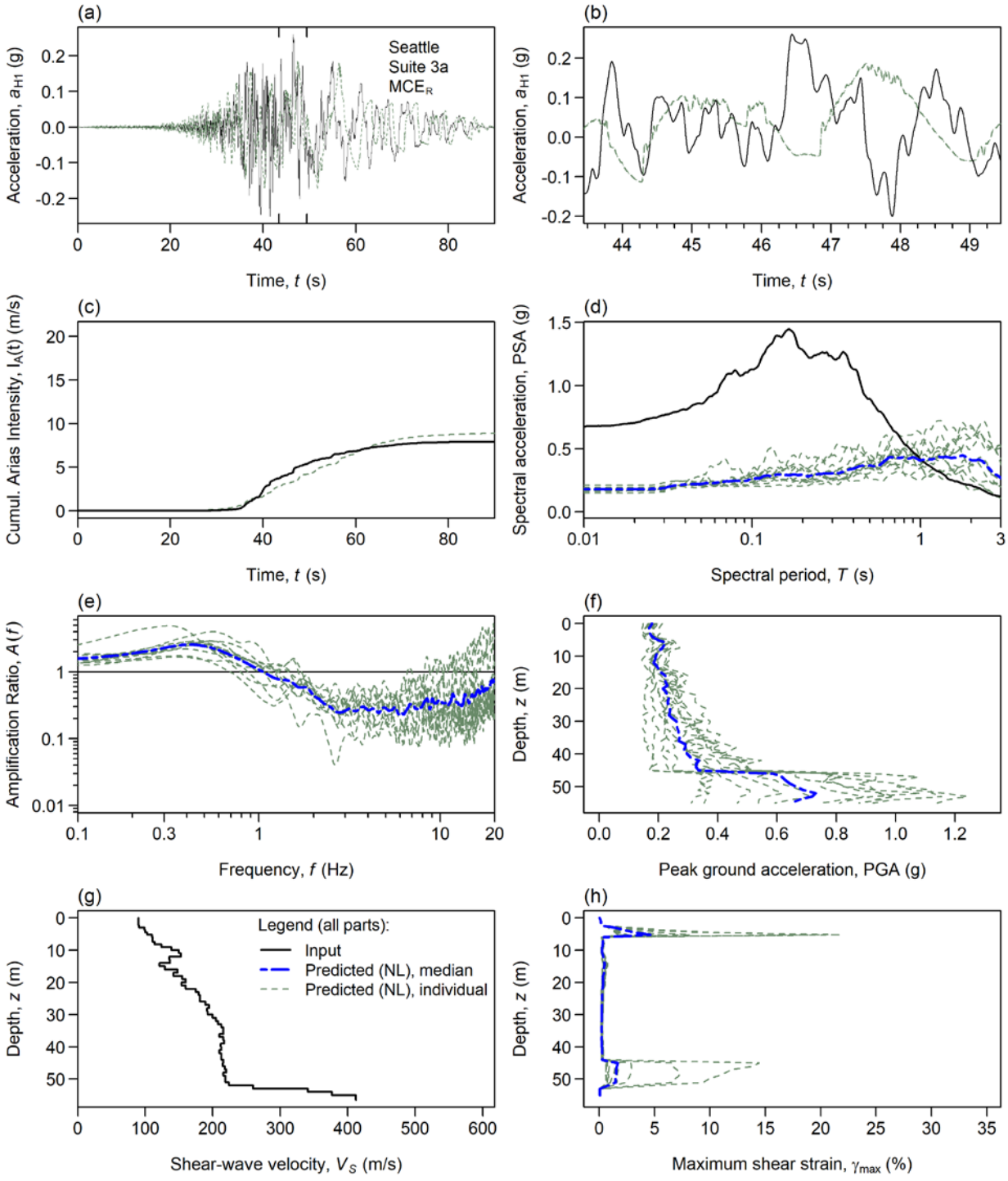

Figure S16. Detailed ground-motion plots for the NL analyses in Seattle for the suite of ground motions obtained for the risk-targeted maximum considered earthquake (MCE_R) design spectrum [Suite 3a].